Construction and Commissioning of a Setup to Study Ageing Phenomena in High Rate Gas Detectors

Dissertation
zur Erlangung des Doktorgrades
der Naturwissenschaften

vorgelegt beim Fachbereich Physik
der Johann Wolfgang Goethe-Universität
in Frankfurt am Main

von
ALHUSSAIN ABUHOZA
aus Damad, Saudi Arabia

Frankfurt am Main 2014
D30

vom Fachbereich Physik der Goethe-Universität
als Dissertation angenommen.

Dekan:	Prof. Dr. Rene Reifarth
Gutachter:	Prof. Dr. Christoph Blume
	Prof. Dr. Peter Senger
	Prof. Dr. Hans Rudolf Schmidt

Datum der Disputation: 01 April, 2014

DEDICATION

This dissertation is dedicated to my parents, my wife and my children who have supported me by their motivation and unconditional love

Contents

Abstract

In high-rate heavy-ion experiments, gaseous detectors encounter big challenges in terms of degradation of their performance due to a phenomenon dubbed ageing. In this thesis, a setup for high precision ageing studies has been constructed and commissioned at the GSI detector laboratory. The main objective is the study of ageing phenomena evoked by materials used to build gaseous detectors for the Compressed Baryonic Matter (CBM) experiment at the future Facility for Antiproton and Ion Research (FAIR). The precision of the measurement, e.g., of the gain of a gaseous detector, is a key element in ageing studies: it allows to perform the measurement at realistic rates in an acceptable time span. It is well known the accelerating ageing employing high intensity sources might produce misleading results. The primary objective is to build an apparatus which allows very accurate measurements and is thus sensitive to minute degradations in detector performance. The construction and commissioning of the setup has been carried out in two steps. During the first step of this work, a simpler setup which already existed in the detector laboratory of GSI had been utilised to define all conditions related to ageing studies. The outcome of these studies defined the properties and characteristics that must be met to build and operate a new, sophisticated and precise setup. The already existing setup consisted of two identical Multi Wire Proportional Chambers (MWPCs), a gas mixing station, an ^{55}Fe source, an x-ray generator, an outgassing box and stainless steel tubing. In a first step, the gain and electric field configuration of the MWPCs were simulated by a combination of a gas simulation ($Magboltz$) and electric field simulation program ($Garfield$). The performance and operating conditions of the chambers have been thoroughly characterised before utilising them in first preparatory ageing test. The main diagnostic parameter in ageing studies is the detector gain, thus it is mandatory for precise ageing studies to minimise the systematic and statistical variation of the pressure and temperature corrected gain. To achieve the required accuracy, several improvements of the chamber design and the gas system have been implemented. In addition, the temperature measurement has been optimised. During the preparatory tests, several ageing studies have been carried out. The ageing effect of seven materials and gases

have been carried out during these tests: RTV-3145, Ar/CO_2 gas, Durostone flushed with Ar/Isobutane gas, Vetronit G11, Vetronit G11 contaminated with Micro 3000 and Gerband 705. The results of these studies went into the design of the new sophisticated ageing setup. For example some tests revealed that there was, even after cleaning, a certain level of contamination with "ageing agents" in the existing setup, which made it imperative to ensure a very high level cleanness of all components during the construction of the setup. The curing period of some testing samples like glues or the gas flow rate were found to be very important factors that must be taken into account to obtain comparable results. Very important changes in the chamber design have been made, i.e., the aluminium-Kapton cathodes used in MWPCs have been replaced with multi-wire planes and the fibreglass housing of the chamber has been changed to metal.

The second step started with building the new setup which was designed based on the findings from the first step. The new ageing setup consists of three MWPCs, two moving platforms, an ^{55}Fe source, a copper-anode x-ray generator, two outgassing boxes, both flexible and rigid stainless steel tubes. Before fabrication of the chambers, simulations of their electric field and the gain have been done using $Magboltz$ and $Garfield$ programs. After that, the chambers were installed and tested. A 0.3% peak-to-peak residual variation of the corrected gain has been achieved. Finally, the complete setup has been operated with full functionality in no-ageing conditions during one week. This test revealed very stable gain in all three chambers. After that two materials (Gerban 705 and RTV-3145) have been inserted in the two outgassing boxes and tested. They revealed an ageing rate of about 0.3%/mC/cm and 3%/mC/cm respectively. The final test proves the stability and accuracy of the ageing measurements carried out with the ageing setup at the detector laboratory at GSI which is ready to conduct the envisaged systematic ageing studies.

Kurzfassung

In Schwerionenexperimenten mit hohen Teilchenraten nimmt die Effizienz von Gasdetektoren durch Alterungsphänomene mit der Zeit ab. In dieser Arbeit wurde im Detektorlabor der GSI ein Messaufbau für präzise Alterungsstudien von Gasdetektoren entwickelt und getestet. Das Hauptziel ist der Bau einer Apparatur zur Untersuchung von Alterungserscheinungen von Gasdetektoren durch Materialien, wie sie beim Bau für das Compressed Baryonic Matter-Experiment (CBM) an der zukünftigen Facility for Antiproton and Ion Research (FAIR) verwendet werden. Die Messgenauigkeit der hierfür relevante Größe, der Verstärkungsfaktor des Gasdetektors, ist ein Schlüsselelement in Alterungsstudien: sie erlaubt Messungen in einer akzeptablen Zeitspanne mit realistischen Teilchenraten durchzuführen. Es ist bekannt, dass der Einsatz von Quellen mit hoher Intensität zur beschleunigten Alterung, d.h. zu falschen Ergebnissen führen kann. Die Hauptaufgabe ist es, eine Vorrichtung zu bauen, die sehr genaue Messungen erlaubt und somit empfindlich genug ist um Verschlechterungen in der Detektorleistung ohne stark erhöhte Intensität der Bestrahlung zu registrieren. In der ersten Phase dieser Arbeit wurde ein einfacher Aufbau verwendet, der bereits am Detektorlabor vorhanden war. Das Ziel dieser vorbereitenden Untersuchungen war, die Eigenschaften und Merkmale zu definieren, die erfüllt sein müssen, um einen verbesserten Aufbau für hochpräzise Alterungsmessungen zu konstruieren und zu betreiben. Der bereits existierende Aufbau bestand aus zwei identischen Vieldrahtproportionalkammern (MWPCs), einer Gasmischstation, einer radioaktiven Röntgenquelle (^{55}Fe), einem Röntgengenerator, einer Ausgasbox und Gasleitungen aus Edelstahl. Der Gasverstärkungsfaktor und die elektrische Feldverteilung der MWPCs wurden mit dem Feldsimulationsprogramm "Garfield" und dem Gassimulationsprogram "Magboltz" im Vorfeld studiert. Die Betriebsbedingungen und die Effizienz der Detektoren wurden charakterisiert bevor sie für die ersten Alterungstests benutzt wurden. Die Hauptdiagnoseparameter bei Alterungsstudien ist der Gasverstärkungsfaktor. Daher ist es für genaue Studien notwendig die systematische und statistische Variation des druck- und temperaturkorrigierten Verstärkungsfaktors zu minimieren. Um die erforderliche Genauigkeit zu erreichen wurden mehrere Verbesserungen am Detektordesign und am Gassystem

vorgenommen. Außerdem wurde die Temperaturmessung optimiert. Während der Vorbereitungsphase wurden Alterungsuntersuchungen an diversen Materialien und Gasen durchgeführt: RTV-3145 (Silikon-Dichtmittel) in Ar/CO_2-Gas, mit Ar/Isobutan Gas gespültes Durostone, gereinigtes Vetronit G11, Vetronit G11 kontaminiert mit Micro 3000 (Kühlschmierstoff) und Aluminiumklebeband Gerband 705. Die Erfahrungen aus diesen Studien dienten als Grundlage für die Gestaltung des neuen Messaufbaus. Zum Beispiel zeigten einige Tests, dass das gasführende System bei Folgetests auch nach der Reinigung mit alterungsverursachenden Bestandteilen kontaminiert war. Daher ist ein hohen Reinheitsgrades aller gasführenden Komponenten bei der Konstruktion der Anlage zwingend zu berücksichtigen. Es stellte sich heraus, dass die benötigte Zeit zur Aushärtung mancher getesteter Klebstoffproben und die Zeit zur Stabilisierung der Glasflussrate ein wichtiger Faktor ist. Bedeutsame Veränderungen wurden beim Design des Detektors vorgenommen: die in den MWPCs als Kathoden verwendeten aluminiumbeschichteten Kaptonfolien wurden durch Drahtebenen und die Glasfasergehäuse wurden durch ein Aluminiumgehäuse ersetzt. Basierend auf den Ergebnissen der ersten Phase begann die zweite Phase der Arbeit mit der Konstruktion des neuen Messaufbaus. Dieser besteht aus drei MWPCs, zwei beweglichen Plattformen, einer ^{55}Fe-Quelle, einem Röntgengenerator, zwei Ausgasboxen und Gasleitungen aus Edelstahl. Auf Grundlage der Simulationen wurden die Detektoren aufgebaut und getestet. Zu Beginn eines Tests wurden die Spitze-Tal-Werte der Gasverstärkung des Referenzdetektors ohne Alterungseinflüsse zu 0,3% ermittelt. Schließlich wurde der komplette Messaufbau mit voller Funktionalität, d.h. alle drei Detektoren, ohne alterungsverursachende Umgebung für die Dauer von einer Woche in Betrieb genommen. Der Verstärkungsfaktor war für diesen Zeitraum in allen drei Detektoren stabil. Danach wurden zwei Materialien (Gerband 705 und RTV-3145) in je eine Ausgasbox eingebracht und getestet. Sie verursachten jeweils eine Alterungsrate von etwa 0,3%/mC/cm bzw. 3,0%/mC/cm. Die Resultate eines letzten Tests belegen die Stabilität und die Genauigkeit der Alterungsmessungen, die mit dem Aufbau durchgeführt werden können.

Chapter 1

Introduction

1.1 Overview

Deconfinement of Quarks and Gluons to form a Plasma (QGP) is expected during nuclear collisions at very high energies, either in nature or laboratories. This new form of matter can be characterised in terms of temperature and baryon chemical potential. (see the QCD diagram in Figure 1.1). Different regions of the QCD phase diagram can be probed by varying the collision energies.

The Compressed Baryonic Matter (CBM) experiment is one of the major pillars of the future Facility for Antiproton and Ion Research (FAIR) at Darmstadt, Germany. The CBM is foreseen to explore the QCD phase diagram in the region of high baryon densities. The fulfilment of the CBM physics goals requires operations at very high collision rates of up to about 10 MHz. At these collision rates, fast, rate capable, large area and highly granulate detectors are mandatory. According to the requirements of CBM and other particle physics experiments around the world, many generations of gaseous detectors have been developed with new geometries and different gases which gradually superseded slower detectors. Limitations of rate capability and detector granularity created the urgent need for the invention of Micro-Pattern Gas Detectors (MPGD) which offer the potential to develop detector systems with unprecedented spatial resolution, high rate capability, and large sensitive areas. The achievement of such desired qualities in these detectors faces several challenges. One of the most significant challenges is to obtain truly stable performance over the lifetime of the experiment in a high rate radiation environment [2].

Degradation of the performance or "ageing" of gaseous detector has been observed since

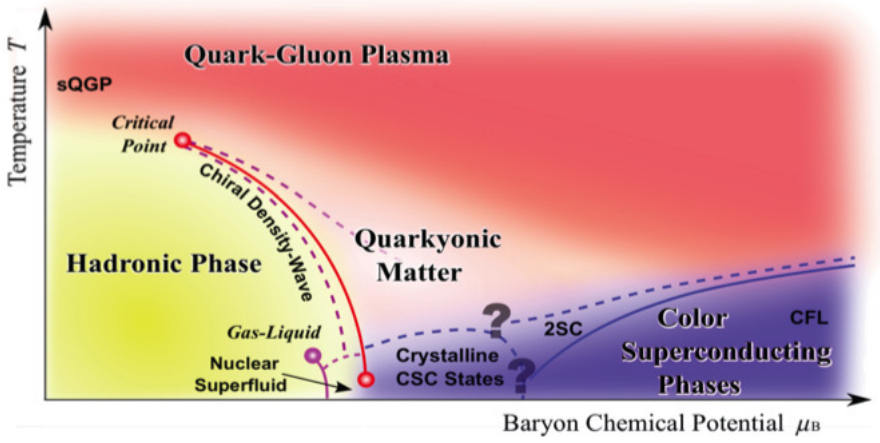

Figure 1.1: *Sketch of the phase diagram for strongly-interacting matter as a function of temperature (T) and baryon chemical potential (μ_B) . Picture is taken from Ref. [1].*

the start of their use in particle physics experiments [3]. This degradation manifests itself in several observables, such as gain loss, high dark current, efficiency loss, sparks and decreasing resolution. In most gaseous detectors, the detection process of particles is based on creating of electron and ion avalanches close to the detector electrodes. Several mechanisms in created avalanches are responsible for ageing in gaseous detectors. The ageing rate depends on many factors, such as the choice of construction materials, gas composition, gas quality, gas flow rate, particle rate and particle type. Therefore, the indications of gaseous detector ageing appeared in many experiments, thus greatly limiting the fulfilment of their purposes. Due to that, several studies have thoroughly investigated these manifestations of ageing in gaseous detectors and means to overcome them. Ageing studies carried out in laboratories usually have conditions that differ from those in real experiments. Therefore, these studies often fail to match with the results found in real experiments [4]. Consequently, it is desirable that these laboratory studies are held in conditions comparable to the real conditions as much as possible. Despite the attempts to mimic the real conditions, there remain large differences between the laboratory and real experimental conditions, such as the type of ionising particles, the size of detector, the area of irradiation, the gas system, irradiation intensity and detector gain. Therefore, it is important to perform the ageing laboratory studies using very precise apparatus, which is capable to sense any deterioration in the detector behaviour with high accuracy. Building an apparatus with high sensitivity is aimed to measure

the onset of ageing accurately in acceptable time periods with acceptable experimental error so that the detector electrodes used in ageing studies will collect a charge with rate comparable to that in the real experiments.
The objective of this PhD thesis is the construction and commissioning of an ageing test setup at the detector laboratory at GSI. It will be dedicated mainly to investigating the ageing properties of the materials used for the construction of gaseous detectors and studying ageing phenomena of gaseous detectors as well as monitoring the long-term behaviour of gaseous detectors, in particular those used in CBM.

1.2 Thesis structure

The physics goals and the detector system of the CBM experiment are briefly discussed in Chapter 2. In Chapter 3, defining the gaseous detector ageing, as well as sources, mechanisms and manifestations of ageing are discussed in detail. In addition, the gaseous detectors used in CBM are described. Construction and commissioning of an infrastructure dedicated to ageing studies have been carried out over two phases. In the first, several optimisations have been implemented over the design of the used detectors and the gas system. Based on the results of the first phase, the second phase has been operated more sophisticatedly and accurately. Details of these two phases are described in Chapter 4. Chapter 5 presents several ageing tests performed during the setup development. Summary and outlook of this work are presented in Chapter 6.

Chapter 2

The Compressed Baryonic Matter Experiment

The Compressed Baryonic Matter (CBM) experiment is one of the major scientific pillars of the future Facility for Antiproton and Ion Research (FAIR) at Darmstadt. It will be dedicated to investigating highly compressed nuclear matter [5]. Super dense matter can be generated in the laboratory by colliding heavy-ions accelerated to sufficient high energies. A hot and dense fireball will be generated in such collisions. In this fireball, a new form of matter, the Quark Gluon Plasma (QGP), might be created. After a very short time, the fireball will expand under its own pressure and will cool during the expansion. The individual quarks and gluons will start to recombine and form hadrons which fly away in all directions. During creation and expansion of the fireball different states of matter are expected, as illustrated in Figure 1.1. This diagram, named the Quantum ChromoDynamics (QCD) phase diagram, illustrates the possible phases of nuclear matter and their boundaries in a diagram of temperature (T) versus the baryon chemical potential (μ_B). At low μ_B, a smooth crossover is expected from the partonic to hadronic matter [6]. At relatively high net baryonic densities (μ_B) and lower temperatures, calculations expect a first order phase transition. The crossover and the first order phase transitions are separated by a critical point [7]. A new phase of matter called quarkyonic matter is proposed to exist beyond the first order phase transition at moderate temperatures [8]. Cold but compressed baryonic matter is believed to exist in astrophysical objects like neutron stars [9]. At such densities, baryons might dissolve into quarks and gluons. At even higher baryonic chemical potentials, correlated quark-quark pairs are predicted to form a colour superconductor as indicated in Figure 1.1.

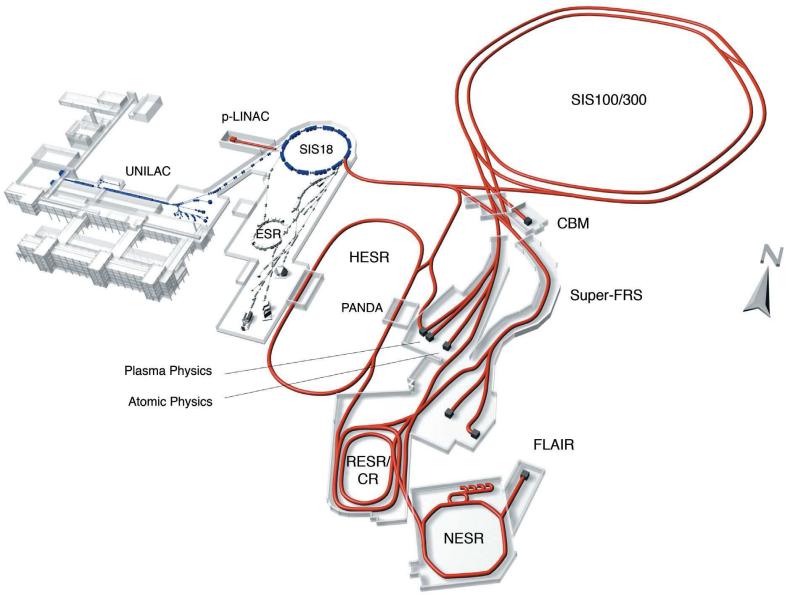

Figure 2.1: *Layout of the Facility for Antiproton and Ion Research (FAIR) [11].*

The main goal of the CBM experiment is to explore the QCD phase diagram in the regions of high baryonic densities and moderate temperatures. This includes the search for the critical point, the first order deconfinement phase transition from the hadronic matter to the partonic matter and the study of the equation-of-state of dense baryonic matter [10].

2.1 The FAIR facility

The Facility for Antiproton and Ion Research (FAIR) is a future facility at the GSI Helmholtz centre for heavy ion research in Darmstadt, Germany [11], as shown in Figure 2.1. It will have two superconducting synchrotrons (SIS100 and SIS300) which will deliver a variety of high intensity beams from protons to heavy nuclei. The beam intensities of about 10^{13} particles/sec for protons and 10^{9} particles/sec for Au-ions are foreseen. The SIS100 synchrotron with 100 Tm magnetic rigidity will provide proton beams with energies up to 29 GeV and Au beams up to 11 AGeV. The SIS300 synchrotron, with a magnetic rigidity of 300 Tm, will provide proton beams with energies up to 90 GeV and Au beams up to 35 AGeV.

2.2 CBM detector concept

The goals of the CBM research program requires the ability to measure multiplicities, phase-space distributions and flow of protons, pions, kaons, hyperons, hadronic resonances, light vector mesons, charmonium and open charm in heavy-ion collisions [11]. The proposed setup for the CBM experiment, sketched in Figure 2.2, includes two subsystems which are capable of measuring electrons (RICH) and muons (MuCH).
The main challenge of the CBM experiment is to identify both leptons and hadrons at event rates of up to 10 MHz. At such high rates, measurements can only be performed by fast and radiation resistant detectors and electronics. The main system of the CBM experiment consists of eight silicon layers placed inside a superconducting dipole magnet. The Silicon Tracking System (STS) will be used for track reconstruction and vertex detection in a wide range of particle momenta. The MVD is used for the identification of open charm mesons by a precise determination of the secondary vertices. The MVD consists of three layers of ultra-thin and highly-granulated Monolithic Active Silicon Pixel Sensors (MAPS). A Ring Imaging Cherenkov (RICH) detector together with a Transition Radiation Detector (TRD) will be used for electron identification in momenta up to 10 GeV/c [12]. In the place of the RICH detector, a system of carbon and iron absorbers and Muon tracking Chambers (MuCH) will be employed for muon measurement. A wall of multi-gap Resistive Plate Chambers (RPCs), located at a distance of 10 m downstream of the target, will be used for charged hadron identification by the time-of-flight (TOF) measurement. In order to measure direct photons and neutral mesons, an Electromagnetic Calorimeter (ECAL) will complement the setup. The Projectile Spectator Detector (PSD) will be employed to determine the collision centrality and the orientation of the reaction plane. These observables and their corresponding detection systems are listed in Table 2.1.

2.2.1 Dipole magnet

The superconducting dipole magnet will provide the bending power to the MVD and the STS. This magnetic field will bend the charge particle trajectories to determine the momenta. For good momentum resolution, a magnetic field integral of about 1 Tm is required. The magnet gap has a height of 140 cm and a width of 250 cm in order to accommodate the STS with a polar angle acceptance of $\pm 25^{o}$ and a horizontal acceptance of $\pm 30^{o}$ [13].

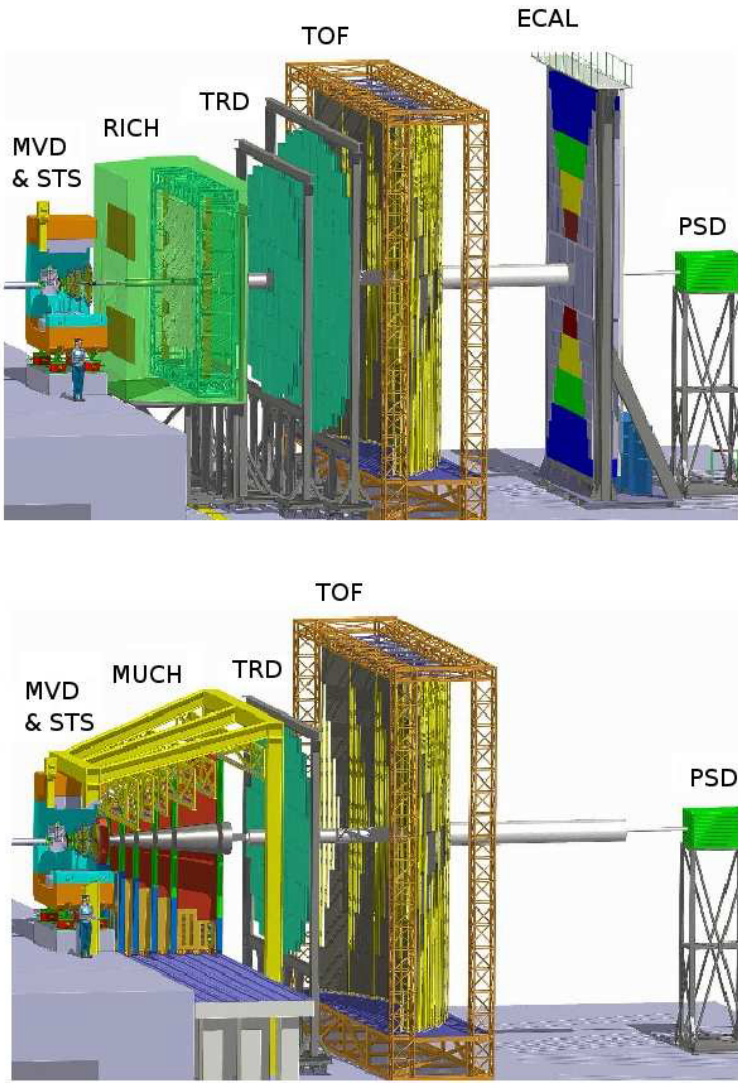

Figure 2.2: *The Compressed Baryonic Matter (CBM) experiment. The CBM setup consists of a dipole magnet, Silicon Tracking System and vertex determination (STS, MVD), a Ring Imaging Cherenkov detector (RICH) and Transition Radiation Detectors (TRD) for electron identification, Resistive Plate Chambers (RPC) for time-of-flight measurement, an Electromagnetic Calorimeter (ECAL) for photon identification, and a Projectile Spectator Detector (PSD) for centrality and reaction plane determination [11].*

Table 2.1: *Observables and required detectors in CBM. Detectors marked as (x) can be used to suppress background [11].*

Observables	MVD	STS	RICH	MuCh	TRD	RPC	ECAL	PSD
π, K, p		x	(x)		(x)	x		x
Hyperons		x			(x)	(x)		x
Open charm	x	x	(x)		(x)	(x)		x
Electrons	x	x	x		x	x		x
Muons		x		x		(x)		x
Photons							x	x

2.2.2 Micro-Vertex Detector (MVD)

A Micro-Vertex Detector (MVD) will be employed for the identification of D mesons via their weak hadronic decay into pions and kaons: $D^+ \longrightarrow k^-\pi^+\pi^+$, $D^- \longrightarrow k^+\pi^-\pi^-$ ($c\tau$=312 μm), $D^o \longrightarrow k^-\pi^+$ and $\overline{D^o} \longrightarrow k^+\pi^-$ ($c\tau$=123 μm).
The main purpose of MVD is to suppress the background of promptly emitted pions and kaons and determine the secondary decay vertices of D mesons with very high accuracy. A secondary vertex resolution of 50 μm along the beam axis is needed to identify open-charm particles. The radiation tolerance and readout speed considerations are the main R&D issues of detectors employed in the MVD. The sensor should survive a radiation dose of 10^{13} n_{eq}, which corresponds to 10^{12} minimum bias Au+Au collisions at 25 AGeV [14]. Monolithic Active Pixel Sensors (MAPS) can meet these requirements and obtain a spatial resolution of 3.5-6 μm with a pixel size between 18×18 μm^2 and 20×40 μm^2 and a material budget of only 0.05%X_0. The MVD consists of three MAPS layers located 5, 10 and 15 cm downstream of the target in a vacuum as shown in Figure 2.3(left) [15].

2.2.3 Silicon Tracking System (STS)

The silicon tracking system (STS) is considered to be the central component of the CBM experiment. Using a magnetic field to bend the trajectory of the charged particles, the STS layers will track and measure the momentum of the charged particles produced during the collision process. The STS, shown in Figure 2.3(right), consists of eight layers located at 30, 40, 50, 60, 70, 80, 90 and 100 cm distances from the target [16]. All the layers are made of low-mass double-sided silicon micro-strip detectors. The detector will be placed inside a dipole magnet with a bending power of about 1 Tm.

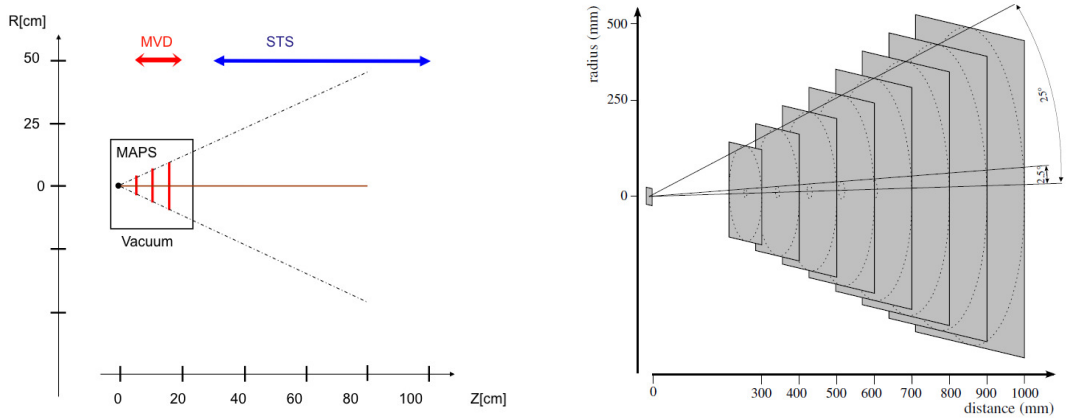

Figure 2.3: *Layout of the MVD layers (left), Layout of the STS tracking station covering the polar angles from 2.5° to 25° (right) [16].*

With this power of bending, the STS is envisaged to provide the required accuracy of the particle momentum measurement, which will be in the order of 1% at 2 GeV/c. All these measurements will be carried out at the expected collision rates up to 10^7 Hz [17], with a multiplicity of charged particles up to 700 per event within the detector acceptance [16]. Under these conditions of high rates and multiplicities, the main challenge the STS encounters is the achievement of the required tracking efficiency.

2.2.4 Dilepton identification systems

Since the leptons interact only electromagnetically with the particles in the collision region, any produced leptons in the fireball volume can leave it carrying undistorted information. Therefore, the dileptons produced in the fireball are promising probes for several physics investigations in CBM experiment. In this section, two tracking subsystems for dielectron(e^+e^-) and dimuon($\mu^+\mu^-$) will be discussed. The dielectron identification is the primary task of RICH and TRD while dimuons will be identified by MuCh.

2.2.4.1 Ring Imaging CHerenkov detector (RICH)

Cherenkov radiation is electromagnetic radiation (cone shape) emitted when a charged particle (such as an electron) passes through a medium at a speed greater than the velocity of light in that medium. The Ring Imaging Cherenkov detector (RICH) is a particle detector which allows to measure the particle velocity based on the angle of

the emitted cone. Measuring the particle speed by RICH detector and its momentum by magnetic bending will allow identification of its mass. In CBM, the RICH station will be dedicated for measurements of low mass vector mesons (ρ, ω and ϕ) via their decay into dielectrons. The RICH station consists of three main elements: a radiator, mirrors and a photodetector. The emitted light cone is reflected by the mirrors to a position sensitive photodetector (see Figure 2.4), which allows the reconstruction of the produced rings in order to measure the particle speed.

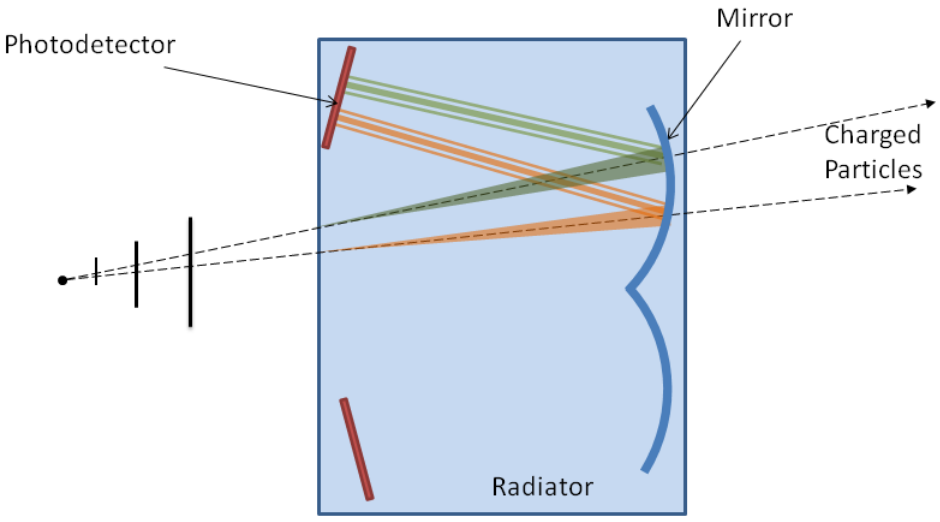

Figure 2.4: *Layout of dilelectron identification approach in RICH of CBM*

The RICH station in CBM will be located about 1.6 m downstream of the target. It will be composed of a 1.7 m long gas radiator (CO_2), two segmented mirror planes and two planes of photodetectors. It will be employed to identify electrons and to suppress pions with momenta up to 10 GeV/c. With the current setup of the CBM-RICH, a pion suppression factor on the order of 500-1000 can be achieved. This suppression factor is increased up to 10000 with TRD and RPC information [18].

2.2.4.2 Muon Chamber system (MuCh)

Measurements of J/ψ mesons are possible via their decay into dimuons. This approach is alternative to the dielectron measurements approach that has been discussed in Section 2.2.4.1. The concept of the Muon Chamber system (MuCh) at CBM, illustrated in Figure 2.5, is based on alternate layers of absorbers and detectors which serve for

hadron suppression and track reconstruction, respectively. The muon detection system

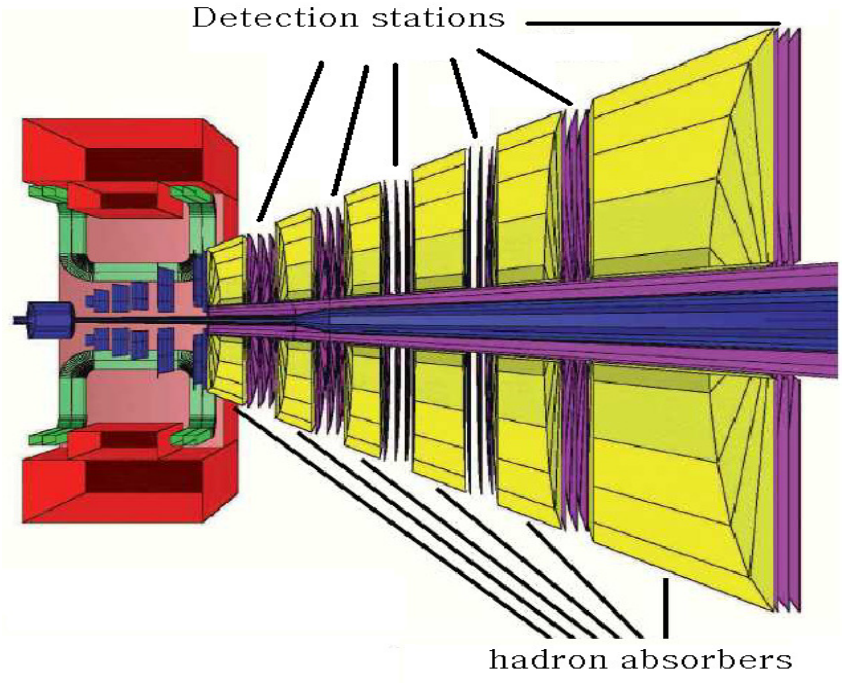

Figure 2.5: *The CBM muon detection system consisting of alternating layers of carbon and iron absorbers (yellow) and muon chambers (purple) [19].*

is designed to contain six detection stations in gaps of six segmented absorbers. The first layer will be located at 120 cm downstream from the target. The thicknesses of these absorbers are 60 cm of carbon and then 20 cm, 20 cm, 30 cm, 35 cm and 100 cm of iron, respectively from the target [20]. In this case, the total material budget would correspond to 13.4 times the nuclear interaction length. The total area covered by the muon chambers is about 70 m^2. The massive predicted particle rate in the first gap, which will be on the order of 4 MHz/cm^2 at central Au+Au collision of 25 AGeV energy, will be the main challenge for muon chambers and tracking algorithms. Therefore, the detector development concentrates on the design of fast and highly granulated gaseous detectors based on Gas Electron Multiplier (GEM) and straw tubes [11].

2.2.5 Transition Radiation Detector (TRD)

Transition radiation (TR) is a form of electromagnetic radiation emitted when a relativistic charged particle travels through an inhomogeneous medium, like crossing two materials with different dielectric constants ϵ. The intensity of this radiation is proportional to the relativistic gamma factor, $\gamma = E / m c^2$. These characteristics suggest

that one can use this effect to discriminate between particles that have similar energies but different masses. The transition radiation detector (TRD) is a device designed to distinguish electrons from heavier particles using transition radiation. It consists of a radiator, where the TR will be produced, and a gaseous detector, where the charged particle and TR will be measured. Figure 2.6 shows one of the schemes of TRD which consists of a radiator and a drift chamber. In CBM, a Transition Radiation Detector (TRD) will be dedicated for charged particle tracking and identification of electrons and positrons with p > 1.5 GeV/c ($\gamma > 1000$). In an integrated manner, TRD, RICH and the ECAL detector systems will be capable of providing sufficient electron identification for the measurements of charmonium and low-mass vector mesons. The TRD system will consist of three stations, each with three or four layers of TRDs. These stations will be located at distances of 5.0, 7.25, and 9.5 m from the target [11]. They cover a total active area of about 600 m^2. In the central part of the first station (5 m from the target), the expected particle rate is in the order of 100 kHz/cm^2 for 10 MHz minimum bias Au+Au collisions at 25 AGeV. Subsequently, fast and granular gaseous detectors such as Multi Wire Proportional Chamber (MWPC) will be under development and tolerance investigation.

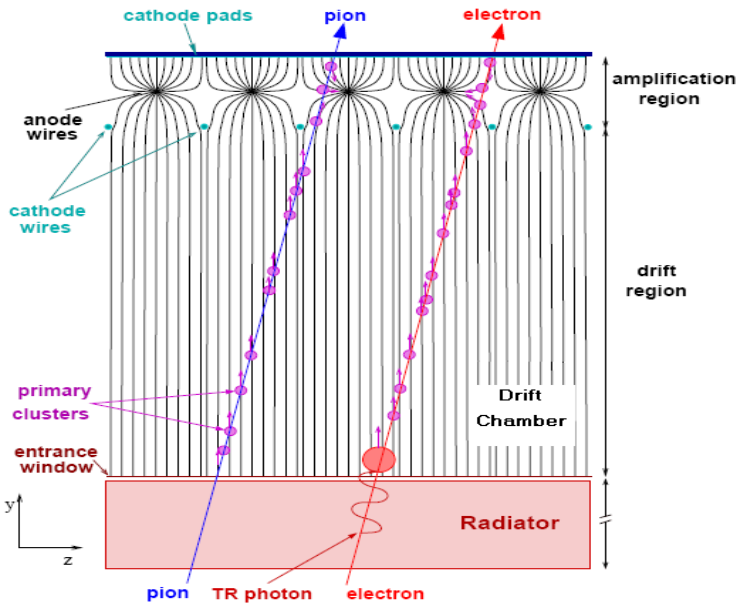

Figure 2.6: *Layout of a transition radiation detector consisting of a radiator and a drift chamber*

2.2.6 Time of flight measurements (TOF)

The time-of-flight (TOF) measurement can be used to identify charged particles. The particle identification depends on the measurement of the particle mass (m), which will be done with the time of flight measurement, and the particle momentum (p). In CBM, a wall of Resistive Plate Chambers (RPC) will be employed for the time-of-flight measurements. The TOF wall will be placed 6 and 10 m downstream of the target with SIS100 and SIS300 respectively since it will cover an active area of about 120 m^2 [11]. This wall consists of approximately 75,000 independent channels which will be envisaged to offer a time resolution of about 80 ps. A simulation, shown in Figure 2.7, illustrates the separation ability of TOF for pions, kaons and protons. In

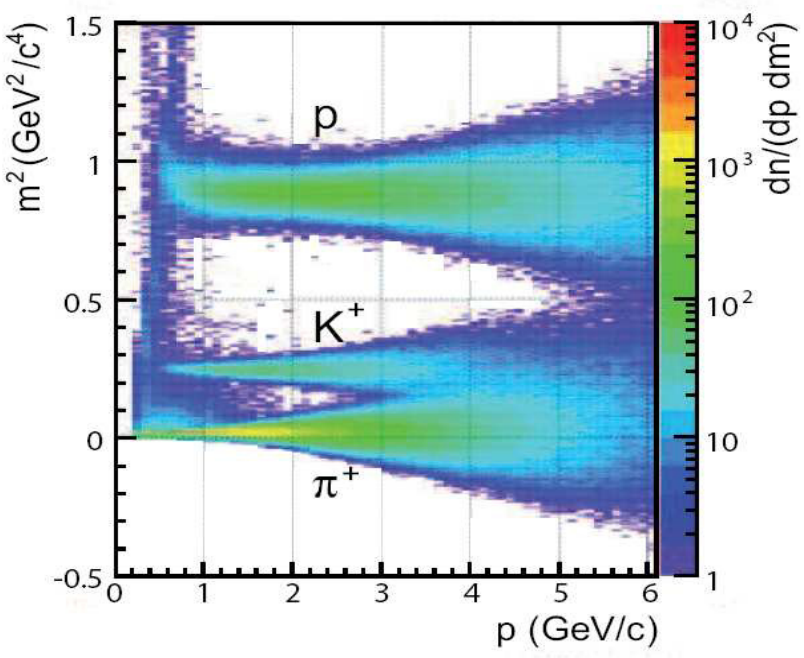

Figure 2.7: *Squared mass as a function of momentum of hadrons reconstructed by TOF in central Au+Au collisions at 25 AGeV beam energy [21].*

minimum bias Au+Au collision with a rate up to 10 MHz, the centre part of TOF should cope with a rate density on the order of 20 kHz/cm^2 [22]. Therefore, the RPCs developments will concentrate on high rate capability, low resistivity of the material and long-term stability.

2.2.7 Electromagnetic CALorimeter (ECAL)

Electromagnetic calorimeters are detectors for measuring the energy and the position of high-energy gamma rays or high-energy electrons and positrons [23]. A "shashlik" type calorimeter will be installed in CBM experiment to measure direct photons and neutral mesons (π^0, η) which decay into photons [11]. The ECAL will be composed of modules which consist of 140 layers of 1 mm lead and 1 mm scintillator, with cell sizes of 3 $\times$ 3 cm^2, 6 $\times$ 6 cm^2 and 12 $\times$ 12 cm^2. The shashlik modules can be arranged either as a wall or in a tower geometry with variable distances from the target.

2.2.8 Projectile Spectator Detector (PSD)

The Projectile Spectator Detector (PSD) will be used to determine the collision centrality and the orientation of the reaction plane. The PSD method is used to measure the number of non-interacting nucleons from a projectile nucleus in heavy ion collisions. The current PSD setup consists of 44 modules, each with 60 lead/scintillator layers with a surface of 20 $\times$ 20 cm^2. The scintillation light is read via wavelength shifting (WLS) fibres by Multi-Avalanche Photo-Diodes (MAPD) with an active area of 3$\times$3 mm^2 and a pixel density of 10^4/mm^2.

Chapter 3

Ageing of gaseous detectors

Heavy ion experiments have growing demands for fast, rate capable, large area and high granulated detectors. This has resulted in the development of many generations of gaseous detectors with new geometries and different gas mixtures. For example, Multi Wire Proportional Chamber (MWPC), drift chamber (DC), Time Projection Chamber (TPC), Ring-Imaging Cherenkov Counter (RICH) and Resistive Plate Chamber (RPC). Limitations of rate capability and the detector granularity created the urgent need for the invention of Micro-Pattern Gas Detectors (MPGD), such as Gas Electron Multiplier (GEM), Micro-Mesh Gaseous Structure (Micromegas) and other micro pattern detector schemes. This generation of gas detectors offers the potential to develop detector systems with unprecedented spatial resolution, high rate capability and large sensitive areas. The achievement of such desired qualities in these detectors faces several challenges. One of the most important challenges is to obtain stable performance over the lifetime of the experiment in a high rate radiation environment [2]. In many experiments which have employed gaseous detectors, the manifestations of ageing appeared in these detectors rapidly comparing to the envisaged live time, thus greatly limiting the fulfilment of their purposes. This has resulted in several studies deeply investigating manifestations of ageing in gaseous detectors and means to overcome them.

3.1 An overview on gaseous detector ageing

Ageing of gaseous detectors is defined as the degradation of their performance when they are exposed to ionising radiation. Several types of ageing phenomena in gaseous

detectors have been observed since the start of their use in particle physics experiments. At the CBM and all high rate experiments, ageing phenomena constitute one of the most complex and serious potential problems which could limit the lifetime of gaseous detectors. Long-term stable performance in high-intensity experiments not only requires the suitable selection of construction materials and gas mixtures, but also needs very specific and appropriate assembly procedures and quality checks during detector construction.

3.1.1 Avalanche propagation in proportional counters

The intended measurements determine the shape, dimensions, electric field configuration, signal time, appropriate gas and several other conditions of the gaseous detectors. In proportional counters, the result of a particle track is an avalanche of electrons and ions which will be ignited close to the anode. Many early studies investigated the energy distribution of electrons inside the plasma of these avalanches. From Ref. [24], the characteristic energy of electrons (ϵ_k) as a function of the electric field could be calculated as follows:

$$\epsilon_k = \frac{eED(E)}{w(E)} \tag{3.1}$$

where e is the electron charge, E is the electric field, D is the diffusion coefficient of electrons, and w is the drift velocity of electrons. Based on Equation 3.1, Figure 3.1 illustrates the characteristic energy of electrons as a function of the electric field at normal conditions. It is clear that the energy of electrons is based on the gas mixture, so the characteristic energy of electrons is in the order of 10 eV in pure argon at 2 kV/cm. The electron energies in the avalanche constitute one of the most important factors with respect to gaseous detector ageing, as will be discussed in the next section.

3.1.2 Molecular dissociation and polymerisation

The formation of molecular fragments is a prerequisite step for undesired polymerisation in gaseous detectors. This fragmentation could result either from electron or photon impact during avalanche development, since the electrons in the plasma of the avalanches have an energy not only sufficient to ionise new molecules, but to break

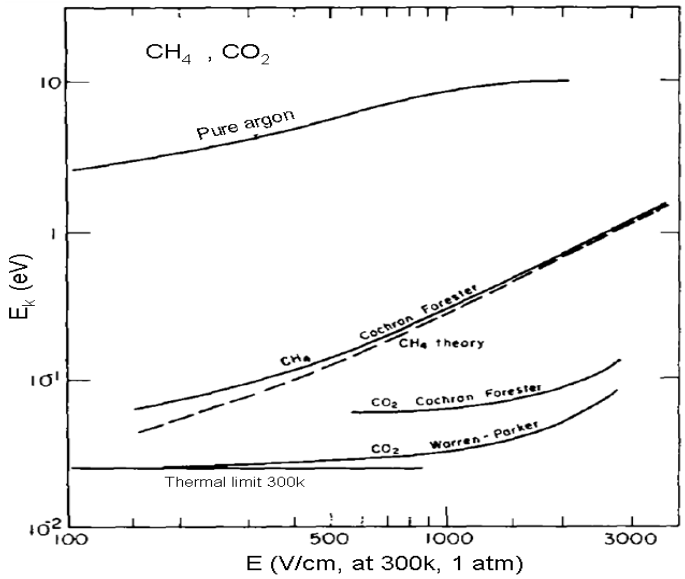

Figure 3.1: *Computed and measured ϵ_k for CH_4, CO_2 and pure argon as a function of electric field [24].*

typical molecular bonds [25]. Table 3.1 compares dissociation and ionisation energies of some gases used in gaseous detectors.

Table 3.1: *Dissociation and ionization energies [26]*

Compound	Dissociation by electron impact (eV)	Ionization energy (eV)
Ar	-	15.8
Xe	-	12.1
H_2	4.5	15.4
O_2	5.2	12.1
F_2	1.6	15.7
H-OH	5.2	12.6
0=CO	5.5	13.8
H-CH_3	4.6	12.6
CH_3-CH_3	3.9	11.5
CH_2=CH_2	7.5	10.5
H-CH(CH_3)OH (Ethanol)	4.0	10.5
F-CH_3	4.7	12.8
Cl-CCl_2F(Freon 11)	3.2	11.8

In many gases used in gaseous detectors and with the presence of pollutants that come with the gas flow, it would be easy to create active molecular fragments. As an example, a $-CH_2$: radical comes out from ($e^- + CH_4 \rightarrow -CH_2 + H_2 + e^-$). These radicals have a high tendency to polymerise in larger series of polymers, which in turn will deposit on the electrodes and ultimately insulate them. The existence of pollutant molecules may trigger or accelerate the polymerisation process [25].

In some cases, there are certain additives preventing polymerisation. For example, adding the following additives in plasma chemistry processes tends to eliminate the CH_2: radical by forming stable, volatile products, which impede the polymerisation process [25]

$CH_2 : +H_2 \rightarrow CH_4$,
$2CH_2 : +N_2 \rightarrow 2HCN + H_2$,
$CH_2 : +O_2 \rightarrow CO_2 + H_2$,
$CH_2 : +O_2 \rightarrow CO + H_2O$,
$CH_2 : +H_2O \rightarrow CO + 2H_2$,
$CH_2 : +CO_2 \rightarrow 2CO + H_2$,
$CH_2 : +CF_4 \rightarrow C_2H_2F_2$.

More generally, oxygen reacts with hydrocarbon radicals and the end-products of this reaction are volatile molecules such as CO, CO_2, H_2O and H_2, which are more stable, and can be removed by a sufficient gas flow. Furthermore, organic compounds with oxygen-containing groups -COOH, -CO-, -OCO-, -OH, -O-, -C=O, are generally reluctant to form polymers in a plasma environment [27].

3.1.3 Sources of gaseous detector ageing

Several ageing studies confirm that the ageing phenomena of gaseous detectors result from very complex processes. A number of these studies, whether in real experiments or in laboratories, revealed that there are many parameters to control the mechanisms that cause ageing in gaseous detectors. According to Reference [28], these mechanisms can be summarised as follows:

1. Polymerisation of the counting gas or the pollutants which come with the gas flow into the avalanche plasma. Picture 3.2 (left) shows an example of deposit growths on an aged wire used in a gas mixture of CO_2/isobutane.

2. Direct deposition of pollutants on the surface of electrodes and insulators which are transported by the gas flow and deposited due to electrostatic forces. These pollutants may arise due to one of three reasons:

   (a) Outgassed molecules come from organic materials in contact with the gas.

   (b) Pollutants come from the detector materials and the gas system under the effect of incompatible gases.

(c) Outgassed pollutants induced by the effect of ionising radiation on the detector materials.

3. Some initially neutral gases become reactive because of the species created around plasma region in the avalanche process. The created species are reactive enough to concurrently remove layers of some materials, damaging the detectors and polluting the counting gas. For example, Tetrafluoride radicals, on one hand, are capable of removing thin layers of deposits on coated wires. This capability might, on the other hand, become a serious problem when the radicals attack the assembly materials. Picture 3.2 (right) shows a corroded wire tested in a chamber filled with a gas mixture of $Ar/CF_4/CO_2$.

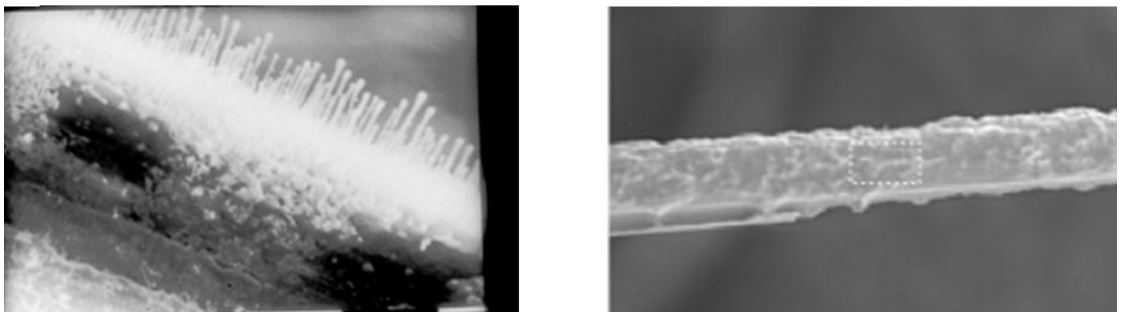

Figure 3.2: *left: Deposites on anode wire used in CO_2/isobutane [29]. right: A corroded wire used in $Ar/CF_4/CO_2$ [30].*

The contribution of materials and gases pollution to trigger ageing processes is shown schematically in Figure 3.3. The possibility of all these mechanisms to occur depends on a large number of factors. Gas flow, gas gain, detector geometry, electric field configuration, current density, incident particles, irradiation area and presence of additives play an influential role. In the end, if the ageing takes place, it will manifests itself by gain loss, high current, efficiency loss, sparks or decreasing resolution. Systematic investigation of the effects of these factors on the ageing rate of gaseous detectors is one of the goals of the ageing setup at the detector laboratory of GSI.

3.2 An overview on ageing studies

The current knowledge about the gaseous detector ageing is not sufficient to formulate a set of specific conditions to avoid deterioration of detectors exposed to high particle

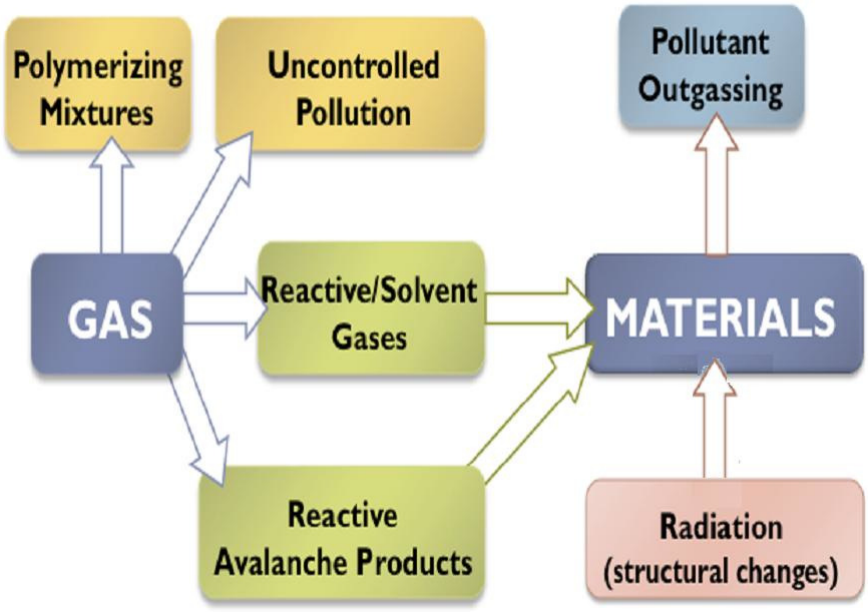

Figure 3.3: *Contribution of materials and gas to the ageing processes [28].*

rate. Experience from real experiments and ageing tests in laboratories allow to develop some general principles that may help, if not to prevent, to reduce the ageing effects [31].

3.2.1 Choice of gases

In heavy ion experiments, high luminosity poses a new challenge for counting gas mixtures in gaseous detectors. While a huge variety of gases has been successfully used for detectors in standard radiation level, only a limited choice of gases is available for the new high rate experiments like CBM. Among the mixtures demonstrated to tolerate such doses are Ar(Xe)/CO_2 and Ar(Xe)/CO_2/O_2. Since there is no well-established mechanism which could lead to the formation of anode deposits in these mixtures [32, 26]. However, the ageing performance in Ar(Xe)/CO_2 and Ar(Xe)/CO_2/O_2 is sensitive to hydrocarbon contamination and even to minor traces of silicon pollutants in the detector and the gas-system components [33, 34]. Years ago, CF_4 was proposed as the most attracting candidate for high-rate environments. This is primarily due to the high-drift velocity, high primary ionisation, low electron diffusion and resistance to ageing [35, 36]. A small addition of CF_4 to Ar/CO_2 in a high luminosity environment is very efficient to clean up Si-aged wires. The resulting balance between Si polymerisation and CF_4 etching processes was found to be very sensitive to the Si-source intensity and ionisation density [34]. Being transparent to UV photons, CF_4 presents serious gain

limitation in wire chambers due to the photoelectric emission from the cathode. In addition, Ar(Xe)/CF_4 mixtures have rather poor energy and spatial resolution due to the electron attachment processes in CF_4 [37]. The use of hydrocarbons (e.g. CH_4, C_2H_6) as quenching gas in proportional counters has been a rather popular choice because it gives an excellent energy resolution and small variations in gain. These advantages counteract its known tendency to polymerise [38] and the fact that it has been often found that this gas does not provide very long lifetimes [31].

3.2.2 Construction materials, adhesives and gas systems

The selection of construction materials of detectors, adhesives and the gas system components is very important for long-lived gaseous detectors in terms of radiation hardness and outgassing properties. In general, there is no good or bad material. A material is adequate or not for a particular type of detector and conditions of use [39]. Silicone has been systematically found coating aged chambers, although in many cases the origin of the pollutant has not been clearly identified. Probably the pollutant was part of the assembly materials or components in the gas system. Silicone can polymerise both with hydrocarbons and oxygen to form rather heavy polymers, thus not easily removable by the gas flow. Components used to build gas systems have to be selected with care to avoid unexpected pollution of an initially clean gas mixture. Selection of these materials should highly consider their low outgassing and to be chemically compatible with the gas mixture. However, a careful selection of joints still has to be made in terms of gas compatibility and outgassing. Strict cleanliness requirements usually are needed for components used for ultra high purity applications.

3.2.3 Detector assembly procedures

Contaminates during assembly can cause fail the best detector. As a general rule, the assembly area must be isolated from other manufacturing areas and usually following clean room standards. Another major source of contamination is the personnel. The people in the production should know the reason why something must be done in a specific manner; hence careful and exhaustive training is needed. Examples of contamination are street clothing; hair, make-up, fingernail and fingerprints are source of oil and particulates and many creams and cosmetics contain silicones. The assembly process has to be well specified and stable. It should be rechecked periodically and

only include proved improvements result of a careful observation of the process. A good assembly process includes procedures about cleanliness of assembly components and its verification [39].

3.2.4 Ageing rate and experimental variables

Recent experimental results from hadron beams show a strong dependence of the detector lifetime upon basic macroscopic variables: ionisation density, irradiation rate, particle type and energy, high voltage (gas gain), size of the irradiated area and gas flow. These data emphasise the importance to study the radiation hardness of the prototype detector under conditions as close as possible to the real environment. Presently, we do not know the relationship between the microscopic and the macroscopic variables we can control. Therefore, it is difficult to truly understand any ageing measurements quantitatively from the physics point of view. At best, we can describe it qualitatively and measure some systematic dependencies [31].

3.3 CBM gaseous detectors

Different gaseous detectors will be employed in CBM based on their characteristics and agreement with the CBM goals. GEMs are currently under R&D to be installed behind the first, second and third hadron absorbers in the muon tracking system whilst Straw Tubes (ST) modules will be used in the fourth and the fifth gaps [20]. MWPCs are under testing to be used in the TRD layers for the tracking of charged particles and electron identification. For time-of-flight measurement, MRPCs are being developed.

3.3.1 Gas Electron Multiplier in MuCH

The Gas Electron Multiplier (GEM) (Figure 3.4), introduced in 1996 by F. Sauli, is a type of gaseous ionisation detector used in nuclear and particle physics. Proportional gaseous detectors collect the electrons released by ionising particles and subsequently guide them toward a high electric field region, then initiating an electron avalanche. In typical GEMs, the high electric field region is configured in 30-50 micrometer diameter holes etched by a photolithography and acid process through 50-70 micrometer thick Kapton foil clad in copper on both sides. A GEM detector has many features which

make it a promising detector to play a main role in the dimuons tracking system (MuCh) of CBM. Amongst the challenges facing the GEM in CBM is the very high particle rate leading to a very high radiation dose, in particular at the layers close to the target. The expected particle rate at central Au+Au collision of 25 AGeV energy is about $4\times10^6/\text{cm}^2\cdot$sec in the first gap of MuCh system of CBM. Figure 3.5[20] illustrates the expected rate density per central Au-Au event at 25 AGeV in detector gaps from 1 to 6 of MuCh station. Depending on the expected rate value and definition of detector gain, the accumulated charge (Q) per 1 cm^2 of the detector surface can be calculated as follows:

$$\text{Q} = e \cdot n \cdot r \cdot G \cdot t \tag{3.2}$$

where e is the electron charge, n is the mean number of ion pairs released in 1 cm of a minimum ionising particle (MIP) track, r is the particle rate per 1 cm^2, G is the detector gain, and t is the exposure time. Calculated through 3 mm drift gap of the first layer of GEM-MuCh station, Figure 3.6 (left axis) illustrates the estimated accumulated charge as a function of detector operation years of the CBM run. Table 3.2 summarises the values of variables used in this calculation. These large values of the expected accumulated charges raise big concerns in term of their lifetime.

Table 3.2: *Values of e-ion pairs, particle rate, gain, gas composition and the accumulated charge rate in three gaseous detectors used in CBM.*

Chamber	gas composition	n (ion-pair/cm)	r (Hz)/cm^2	G	Accumulated charge rate C/cm^2/year
GEM-MuCh	Ar-CO_2 (70-30%)	93	4×10^6	5×10^4	32
MWPC-TRD	Xe-CO_2 (85-15%)	275	1×10^5	5×10^4	1.2
ST-MuCh	Ar-CO_2 (70-30%)	93	4×10^4	5×10^4	0.16

3.3.2 Multi-Wire Proportional Chamber in TRD

The multi-wire proportional chamber (MWPC) invented and developed by Georges Charpak in 1968 is one of the proportional counters which has played and is still playing an important role in high energy physics. The TRD system of CBM contains three stations located at distances of 5, 7.25 and 9.5 m downstream from the target with three or four layers each. All these layers will be based on MWPCs. The expected

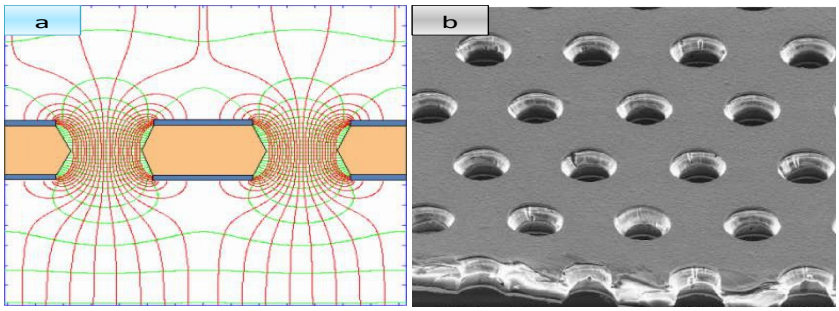

Figure 3.4: *a) Electric field lines and hole structure in a GEM amplification cell. b) Electron microscope view of a GEM foil etched on a copper-clad and thick polymer foil [2].*

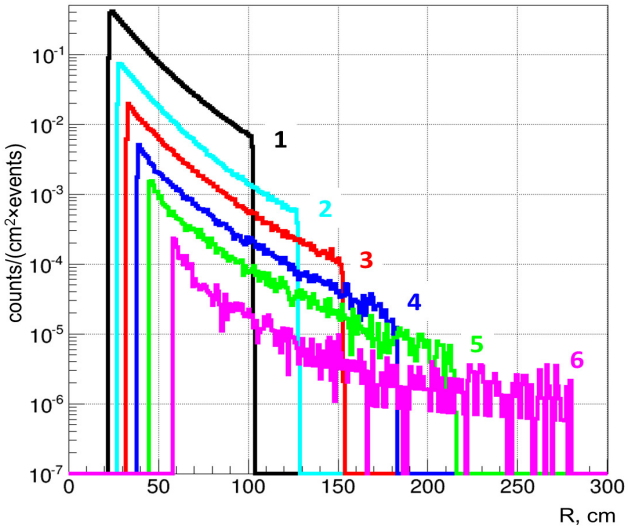

Figure 3.5: *Simulation of particle density of a central Au-Au collision at 25 AGeV at the six gaps of MuCh as a function of radial distance from the beam axis [20]*

rate at the first TRD layer is in the order of $1\times10^5/\mathrm{cm}^2\cdot\mathrm{sec}$ [40]. The right black axis in Figure 3.6 shows the estimated charge per cm^2 of its surface to be collected in 1 cm of MIP track in the first TRD layer during ten years.

3.3.3 Straw Tubes in MuCH

Straw tubes (ST) are basically proportional chambers fabricated with an anode wire taut along the centre of a small tube. Usually, several layers of straw tubes are used for tracking purposes as shown in Figure 3.7. In CBM, two tracking stations of straw tubes are planned to be employed in the fourth and the fifth gaps of MuCh[20]. Based on the simulation of particle density in Figure 3.5 (blue(4) and green(5) curves) and

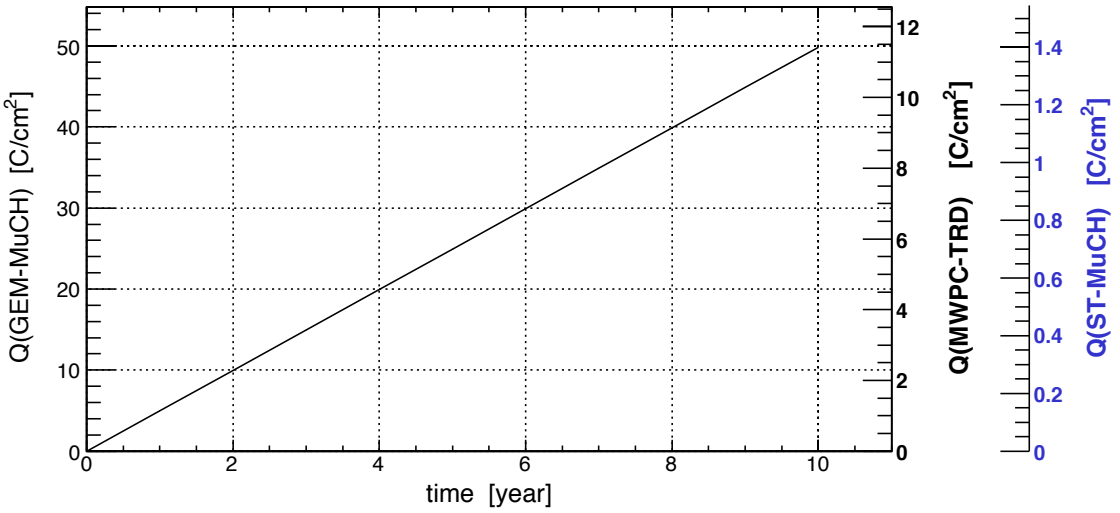

Figure 3.6: *Predicted accumulated charge in the first layer of GEM-MuCH (left axis), MWPC-TRD (right-black axis) and ST (right-blue axis) as a function of operation years of CBM.*

parameters in Table 3.2, the estimated accumulated charge could be calculated from Equation 3.2 as illustrated in the right blue axis of Figure 3.6. The charge calculation supposes 6 mm of diameter of the straws.

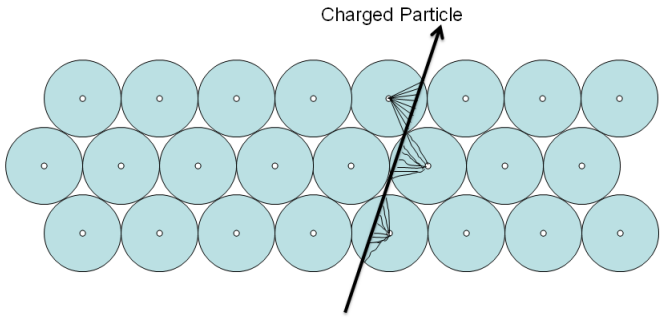

Figure 3.7: *Scheme of ST layers used for tracking purposes.*

3.3.4 Resistive Plate Chamber in TOF

In high energy physics, the resistive plate chamber (RPC) is one of the widely used gaseous detectors for large areas. The single gap RPC, first developed by R. Santonico

and R. Cardarelli, is a charged particle detector consisting of a gas gap between two parallel plate electrodes in high voltage between 7 and 12 kV. These plates are made of resistive materials such as Bakelite or glass. The innermost part of the Multipage RPCs employed in the TOF station of CBM is expected to work at a rate up to 20 kHz/cm^2 [22].

From the previous discussions of all these gaseous detectors, it is clear that considerations should be kept greatly in mind in terms of ageing and long-term operation. Accordingly, stability studies should be performed for the detector under similar conditions of those in real experiments.

Chapter 4

Ageing setup

Several ageing studies raise a number of concerns which suggest the laboratory studies of ageing should mimic realistic conditions as much as possible. However, despite the attempts to mimic the real conditions, there remain large differences between the laboratory and real experimental conditions, such as type of ionising particles, size of the detector, area of irradiation, gas system, irradiation intensity and detector gain. Thus, for performing laboratory studies related to ageing, it is important to perform very precise measurements capable of sensing any degradation in the detector behaviour with high accuracy. The objective is to build an apparatus with high sensitivity that allows to measure the onset of ageing accurately in an acceptable time period. Thus, the ageing investigations can be carried out at a rate of charge accumulation that matches with the real experiments.

In order to address this issue, an infrastructure has been set up at the detector laboratory at GSI dedicated primarily to investigate the ageing properties of the materials used for the construction of gaseous detectors. Moreover, it can also be used for monitoring the performances of gaseous detectors, in particular those used in CBM. Construction and commissioning of this infrastructure have been carried out over two steps. In the first step, using an existing setup, several characterisations and optimisations were implemented for the design of detectors and gas systems. Based on the findings from this step, a new ageing setup was designed with the objective to reach the required sensitivity of ageing measurements. In this chapter, the details of all these characterisations and optimisations tests, designing, building and commissioning of the ageing setup will be presented.

4.1 Preparation and characterisation tests

At the beginning of this project, an existing setup in the detector laboratory of GSI has been utilised to identify all influential parameters related to the ageing tests, then to select the properties and characteristics that must be met to build and operate the new ageing setup.

4.1.1 Components of the preparation setup

According to test procedure which will be discussed below, the scheme of the existing setup consisted of two identical Multi Wire Proportional Chambers (MWPCs), an X-ray generator with copper anode, an ^{55}Fe source and an outgassing box. Figure 4.1 shows the arrangement of such components and the gas system which contains flexible and rigid steel tubes. In this section, the test approach and the descriptions of all the setup components will be presented.

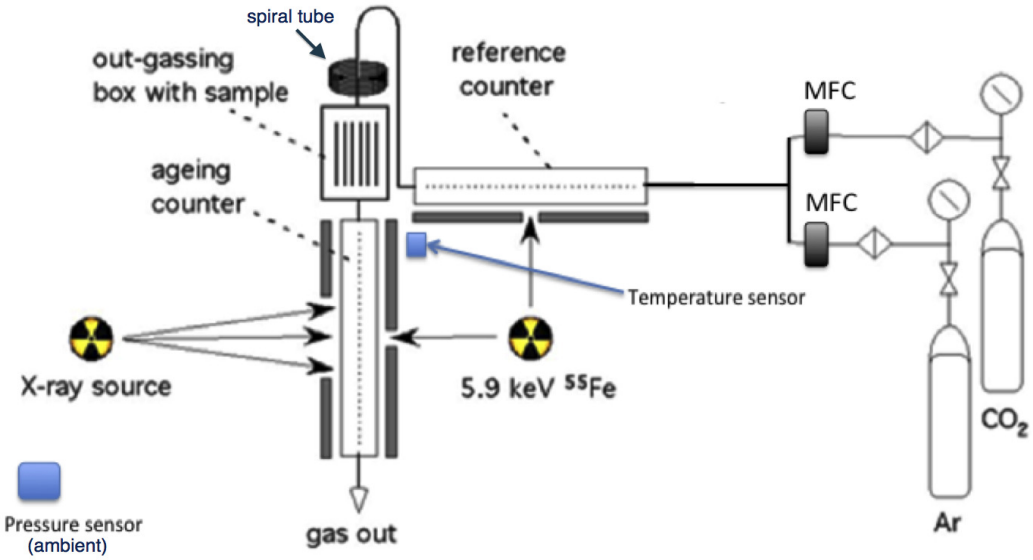

Figure 4.1: *Scheme of the existing setup in the detector laboratory of GSI.*

4.1.2 Gas mixture

The counting gas plays the main role for several properties of gaseous detectors, such as gain, resolution, drift time and detector lifetime. A gas mixture of Argon (Ar) and CO_2 has been selected, because a number of prior studies have revealed that this mixture

does not adversely affect the detector in terms of ageing. One of the main reasons is that this gas does not polymerise like hydrocarbon gases [25]. Furthermore, the selected ratio of 80% Argon and 20% CO_2 allows to operate the chambers at high gain [31]. It is important in ageing studies to consider all parameters of the selected gas, which are important to estimate the accumulated charge. Table 4.1 illustrates some properties of Argon and CO_2 gases, such as energy of ion pair production (w), energy loss (dE/dx) and the number of ion pairs per unit length (n_T) in a track of Minimum Ionisation Particles (MIP). In a mixture of two gases (gas-1 and gas-2), the total number of ion pairs (N) released by a deposited energy (E) is calculated as follows:

$$N = \frac{E}{w_1} \cdot f_1 + \frac{E}{w_2} \cdot f_2 \tag{4.1}$$

where f_1 and f_2 are the fractions of gas-1 and gas-2 respectively.

Table 4.1: *Properties of Argon and CO_2 at atmospheric pressure for MIP [41].*

Gas	w (eV/i.p.)	dE/dx (keV/cm)	n_T (i.p./cm)
Ar	26	2.44	94
CO_2	33	3.01	91

4.1.3 ^{55}Fe Source

Measurement of the chamber gain likely requires a mono-energetic source. The single peak of the mono-energetic source allows to monitor the gain variation precisely. ^{55}Fe is a radioactive isotope of iron with a nucleus containing 29 neutrons and 26 protons. Its half-life is 2.74 years by electron capture process. The energies of its emitted photons are so similar ($k_{\alpha 1}$=5.89875 keV, $k_{\alpha 2}$=5.88765 keV and k_{β}=6.49045 keV) that it is often considered a mono-energetic photon source with 5.9 keV. Using Equation 4.1 and values listed in Table 4.1, the total number of ion pairs released by a 5.9 keV photon is 217 when a gas mixture of Ar-CO_2 (80-20%) is used. The lower plot of Figure 4.2 shows ^{55}Fe spectrum registered by a MWPC. Two peaks are clearly observed in this spectrum, since the main peak corresponds to a full deposition of 5.9 keV whereas the small peak (escape peak) corresponds to ∼2.7keV where a fluorescence photon escapes the sensitive volume.

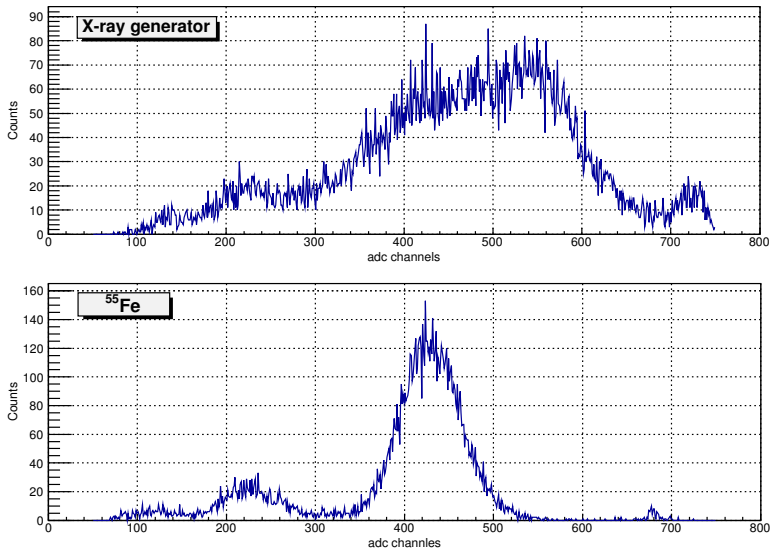

Figure 4.2: *The full spectrum of X-ray generator (upper) and spectrum of Iron source (lower) obtained by MWPC.*

4.1.4 X-ray Generator

Accelerated ageing tests at laboratories necessitate high rate photon or charged particle sources [34, 42, 43]. For these high rate exposures, the ageing setup of GSI uses an X-ray generator based on a copper anode. Its beam intensity could be varied by altering the tube accelerating voltage and/or filament current, thereby it provides a wide range of energies as shown in the upper plot of Figure 4.2 and rates. There are two distinct features to the spectrum. First, the smooth distribution results from electrons being decelerated in the anode material. This deceleration process produces radiation that is called bremsstrahlung as shown in the upper plot of Figure 4.2. The second feature is the existence of the characteristic peak of the anode material.

4.1.5 ADC and preamplifier calibration

If there are no precise modules to measure the very low currents, the value of chamber gain becomes very important to estimate the collected charge during the avalanche and thus to calculate the accumulated charge per unit length of electrodes. Due to that, a calibration of the preamplifier and the ADC has been implemented to measure the effective gain in three steps:

1. Using a pulser, the relationship between input charge (Q) of a charge sensitive preamplifier and the output pulse height (P.H.) was calibrated as:

$$Q(fC) = -3.44(fC) + 1.852(fC/mV) \times P.H.(mV) \tag{4.2}$$

2. Known height of pulses generated by the pulser was used to define the corresponding channel number of the ADC (Chs. No.) practically.

$$P.H.(mV) = -0.5(mV) + 0.28(mV) \times Chs.No. \tag{4.3}$$

3. The effective gain (G) is defined as the ratio of the total charge of an avalanche to the primary charge generated by the incident particle, which is equal to e×217 for 5.9 keV photons.

$$G = \frac{Q}{e \times 217} \tag{4.4}$$

From that, the gain is derived from this calibration as follows:

$$G = -125.6 + 14.96 \times Chs.No. \tag{4.5}$$

4.1.6 Ageing detectors

There are several factors affecting the ageing of gaseous detectors as detailed in Section 3.1.3. Thus, studies of those factors in detail require a large number of fresh detectors, which are usually suitable only for a single use. Therefore, it is preferable to employ detectors which are relatively inexpensive, easy to be manufactured as well as assembled and having appropriate properties for ageing tests. As a result of such considerations, the MWPC is a compatible solution employed for this purpose. First of all, chamber simulation has been implemented, accordingly it has been fabricated. Simulation, fabrication and characterisation tests will be presented in this section in detail.

4.1.6.1 Detector design

Based on chamber gain, the rate of charge accumulation is an important parameter in ageing studies. Due to that, a simulation of a typical MWPC has been performed to configure the desired gain. This simulation has been performed by a combination of the gas simulation program (*Magboltz*) [44] and the electric field simulation program (*Garfield*) [45]. The simulated chamber consists of a multi-wire plane (anode) at 1500 volt and two metallic plates (cathodes) at zero volt. They are separated by 3 mm gap on both sides (Figure 4.3 left). The anode plane has wires of 20 μm diameter and 3 mm spacing. The simulation reveals that the expected detector gain is in order of 8600 for Ar/CO_2 (80/20). Figures 4.3 illustrates, the simulation of the electrode configuration (left) and a closer view of ion drift lines around three wires in the centre area of the chamber(right).

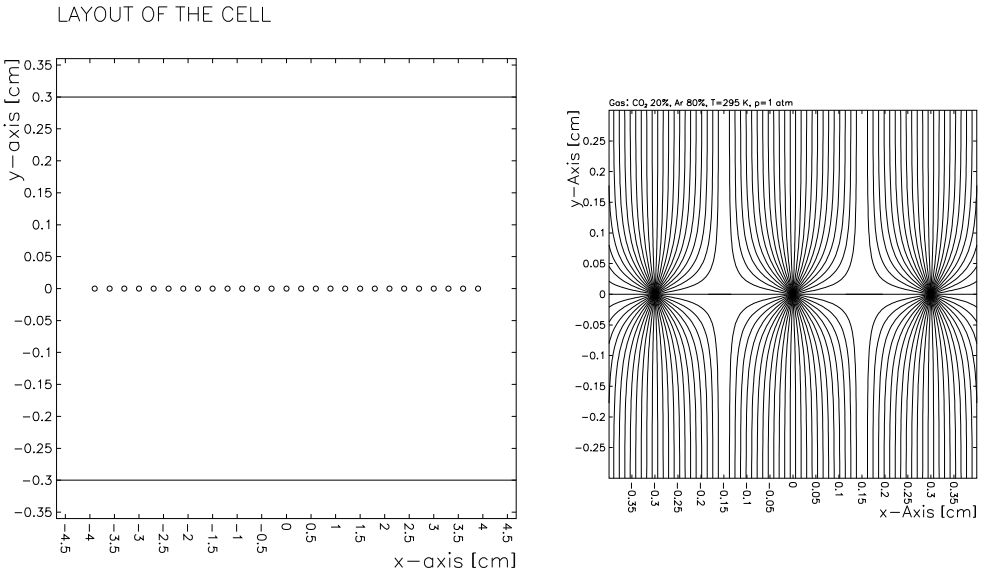

Figure 4.3: *Electrode configuration of the MWPC (left), drift lines around three wires in the centre area of the chamber (right)*

The MWPC anodes are fabricated of gold-plated tungsten wires of 20 μm diameter and 3 mm spacing. The two cathode planes are made of 25 μm thick aluminium-coated Kapton foils separated by 3 mm from the anode plane as illustrated in the lower plot of Figure 4.4. Frames made of fibreglass, termed G10, hold the chamber components, so they have windows with dimensions of 6 $\times$ 8 cm. Left and right pictures in Figure 4.4 show, respectively, the final chamber layout and components scheme.

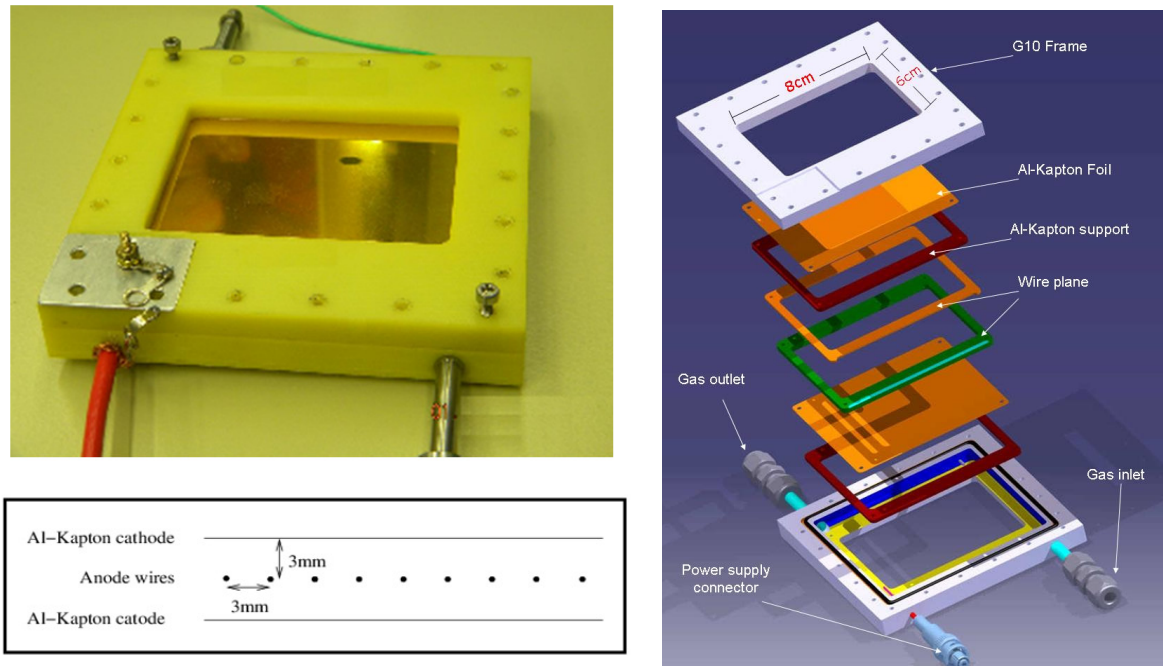

Figure 4.4: *An assembled chamber (upper-left), anode wire spacing and the drift gap (lower-left) and a sketch of the MWPC components (right),*

4.1.6.2 Characterisation tests

Many characterisation tests were carried out before utilising the MWPC in ageing tests. Figure 4.5 illustrates a signal processing through a single amplification electronic channel connected to the whole anode plane in each chamber. The pulse is amplified by a charge sensitive preamplifier, then it is processed by a fan in-fan out module into two outputs. One of these is proceeded to an ADC which registers the pulse height in a computer utilising the LabView program. Simultaneously, the other is used to measure the particle rate by a scaler. After many attempts to shield the detector and its associated electronics against noise, the spectrum of ^{55}Fe and X-ray generator were sampled as shown in Figure 4.2, with energy resolution ($\triangle E_{FWHM}/E$) $\sim$17% in the case of ^{55}Fe, when it collimated by 1 mm diameter aperture. Using a 1 mm diameter collimator allows the X-rays to pass through and irradiate a small spot of the chamber. Employing the calibration carried out in Section 4.1.5, the chamber gain has been measured as a function of applied voltage as illustrated in the left plot of Figure 4.6. It is clear from this figure that the obtained gain is 8600 only when anode voltage is $\sim$1700 volt, unlike the simulation which calculated a gain of 8600 in 1500 volt. This difference is attributed to two causes; a leak in the gas system which means more

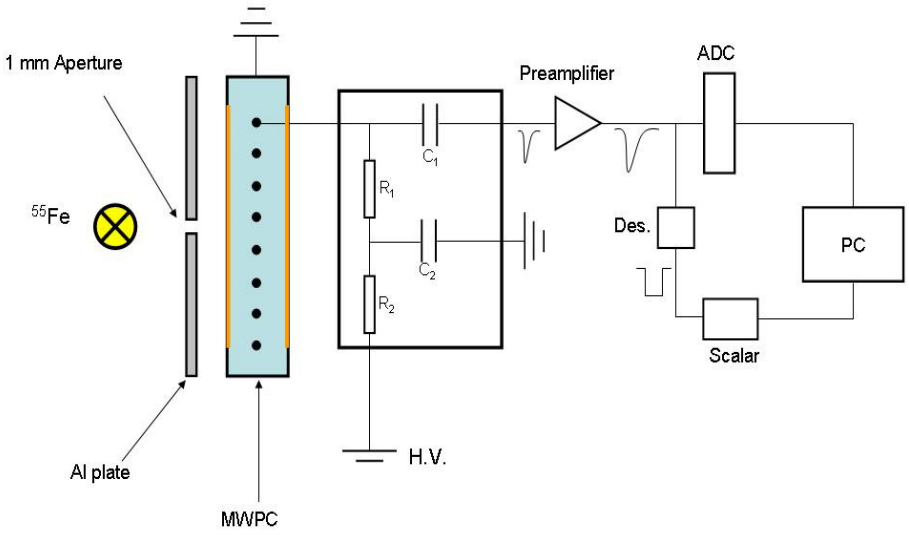

Figure 4.5: *Scheme of pulse processing*

electron attachment and/or the gap between anode and cathode is practically more than 3 mm. The wider anode-cathode gap the lower gain as described in next section by Diethorn's formula (Equation 4.7) [46]. The space charge effect is produced by residual ions around the anodes. The electrons multiplied in avalanches are quickly collected to the anodes. On the other hand, the ions remain in the gas gain region for long period because the drift velocity of the ions is significantly lower than that of electrons. The electric field is distorted by these remaining ions [47]. Space charge effect is an important factor in high rate chambers due to its effect on the energy distribution in the hot plasma created in avalanches. The impact of this effect has been measured by varying the particle rate of the iron source using different number of thin aluminium foils. The right plot in Figure 4.6 illustrates the chamber gain as a function of particle rate, as it loses about 4% of its gain when the particle rate increases to 120 kHz.

4.1.7 Test approach

Test approach in this study was proposed depending on approaches used in many former ageing studies [48, 29]. In ageing tests, detector gain is the most important parameter, accordingly detector performance is being diagnosed by continuous measurement of its gain.

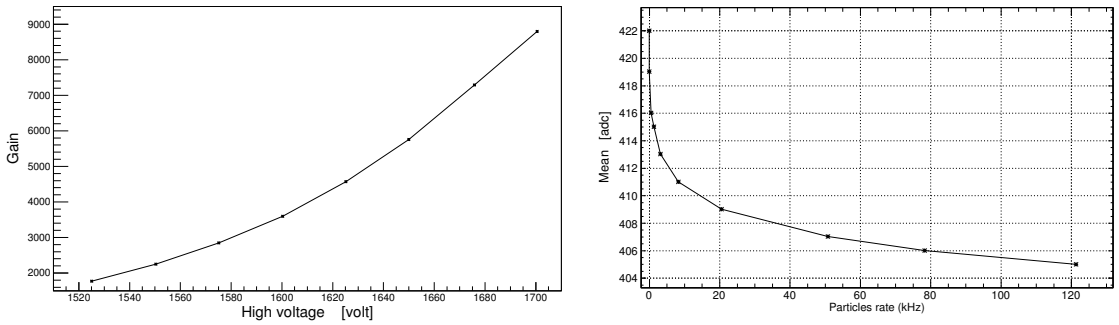

Figure 4.6: *Gain as a function of anode voltage in a MWPC (left) and mean of pulse height as a function of particle rate (right)*

4.1.7.1 Test procedure

Test procedure was set to mix argon and carbon dioxide by a station consisting of two Mass Flow Controllers (MFC). Then, this mixture is flowed with a specific rate toward two chambers in a serial line. In the case of testing the ageing effect of a specific material, a box containing this material (called outgassing box) will be inserted in between the two chambers, as shown in Figure 4.1. With this scheme, measurement steps were set to irradiate the contaminated chamber, called the ageing chamber, over a specific period by photons coming from the X-ray generator. Following that, the generator will be switched off automatically, and consequently, the mean of pulse height of the ^{55}Fe spectrum will be registered in the ageing chamber then in the reference chamber. Reference chamber is used for gain normalisation of the ageing chamber. These steps are repeated until the required charge is accumulated in the ageing chamber. During the complete process, the data (mean of pulse height, counting rate, current, resolution, ambient parameters) of the ageing and reference chambers are continuously recorded. After accumulating the desired charge for the test, the ageing is specified by a parameter called ageing rate (R) which is defined as follows [26]:

$$R = -\frac{1}{G_0}\frac{\Delta G}{\Delta Q} \tag{4.6}$$

where G_0 is the initial gas gain, defined by the mean of pulse height of the main peak of the iron spectrum, ΔG is the loss of gas gain over the test period, and ΔQ is the corresponding charge collected per unit length of the irradiated wires.

4.1.7.2 Gain normalisation

The accuracy of ageing measurements depends on the precision of gain measurement. In the MWPC there are four factors affecting its gain in addition to permanent ageing if any:

1. Variation of the gas density.
2. Variation of the gas composition.
3. Variation of electrode potentials.
4. Modification of chamber geometry .

Diethorn's formula [46] describes the influence of these factors on the gain value (G):

$$G = \left(\frac{V}{r_a ln\left(\frac{r_c}{r_a}\right) E_{min} \frac{\rho}{\rho_o}} \right)^{\frac{Vln2}{ln\left(\frac{r_c}{r_a}\right)\triangle V}} \tag{4.7}$$

where r_a is the wire radius, r_c depends on geometrical parameters such as wire pitch and gap size, $\triangle$V is the potential drop during an avalanche, E_{min} is the minimum electric field to start the avalanche, ρ is the gas density, ρ_0 is the gas density at which E_{min} has been measured and V is the value of voltage difference between anode and cathode. Once the chamber geometry and the applied voltage are constant, this formula could be approximately reduced to:

$$G = k \cdot \left(\frac{T}{p}\right)^{\alpha} \tag{4.8}$$

where T is the gas temperature, p is the gas pressure, k and α are constants. From the latter formula, gain variation as a function of gas density could be estimated as shown in Figure 4.7.
Therefore, the effect of gas density variation can be removed by:

1. *ρ-corrected Gain*: in this method, the gas density effect could be removed by the calculation of the mean from Equation 4.8. Afterward, the normalised gain is defined by the ratio of measured mean of pulse height to the calculated mean, as follows:

$$Normalised\ Gain = \frac{measured\ mean}{calculated\ mean} \tag{4.9}$$

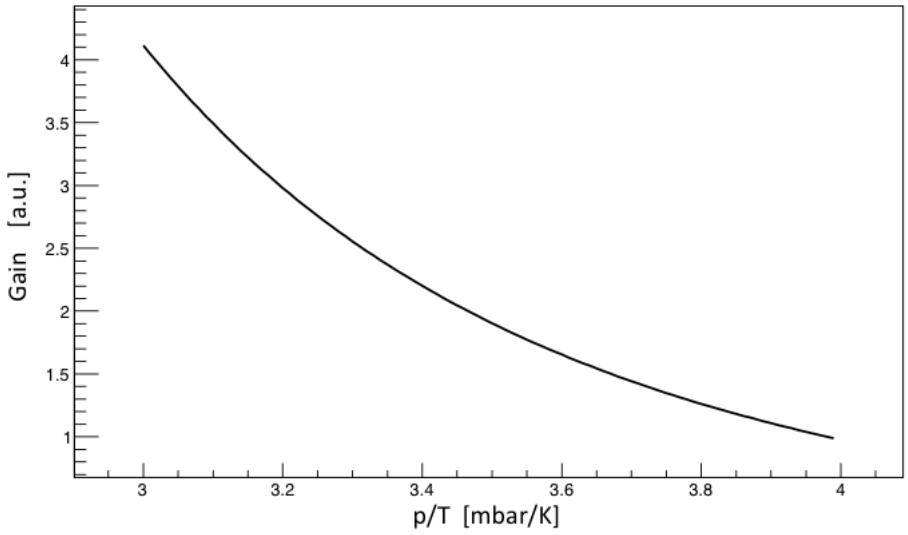

Figure 4.7: *Variation of gas gain in a MWPC as a function of gas density in stable applied voltage and chamber geometry.*

This method does not necessitate a reference chamber but requires precise measurement of gas temperature and pressure. Moreover, every new test (in particular, new spot of ^{55}Fe in the chamber) requires individual derivative of k and α. They could be derived by measuring the mean of pulse height in different ambient temperature and pressure, thus at different gas density. Then, they are derived by fitting this experimental data of the mean of pule height on Equation 4.8.

2. *Gain Ratio*: this method of normalisation requires two chambers in identical conditions. Since the density variation effect could be removed, by definition the normalised gain is as follows:

$$Normalised\ Gain = \frac{mean\ of\ pulse\ height\ of\ ageing\ chamber}{mean\ of\ pulse\ height\ of\ reference\ chamber} \tag{4.10}$$

On one hand, the advantage of such a method is that the precise measurements of the ambient conditions, like the temperature and the pressure, are not required. But on the other hand, one must guarantee that no variation of the gas density or composition occurs in the time between recording the mean of pulse height of these two chambers.

4.1.8 Optimisation of gain measurement

It is of utmost importance for our objectives to obtain a stable gain measurements with statistical and systematic variation of the normalised gain as low as possible. The low variation of normalised gain at standard conditions allows distinguishing of any permanent gain degradation when using contaminated setup with any material under investigation. This desired accuracy makes the ageing investigations possible with lower irradiation intensity and in a reasonable time scale. In the pursuit of that mandatory precision, many stability tests have been performed. Thus, several improvements of the apparatus have been implemented, which include chamber design, chamber cathodes, schema of gas lines and gas mixing approach.

4.1.8.1 Effect of cathode curvature

The first test was performed to examine the stability of gain measurement, using the test procedure outlined in Section 4.1.7.1, but with no contamination material in the outgassing box. The mean of pulse height was being registered during 10 days. The upper two plots of Figure 4.8 illustrate gain of ageing chamber (left plot) and reference (right) as a function of gas density during the entire 10 days, in which the gas density was fluctuating due to rising and dropping of the ambient temperature and pressure. The high variation of chamber gain was measured in both chambers which clearly does not resemble the expected stable behaviour illustrated in Figure 4.7. Accordingly, one can easily understand that this fluctuation was neither related to gas density variation nor to a permanent ageing, which makes it difficult to filter out the onset of permanent ageing. Therefore, the gas mixing station (station-1) was suspected to be the cause of such instability, since the ambient parameters were assumed to have an effect on the mixing station that causes a variation of gas composition. Consequently, a second test was performed with other mixing station (station-2) which contains other MFCs. The similar unstable gain behaviour was observed, as shown in the middle two plots of Figure 4.8, which means that the instability cause still existed even after replacing the MFCs. The next step was to use a premixed gas bottle instead of a mixing station. After two days of using premixed gas, both chambers revealed the same undesired fluctuation of gain, as shown in the lower two plots of Figure 4.8. Based on the above, the cause of this fluctuation was assumed to be that the windows of MWPC were functioning at the same time as cathodes and as gas sealing. Due to that, the variation

of ambient pressure reconfigures the drift gap and thus the electric field as well, hence the gain fluctuates differently in the two chambers, as it is clear from the gain ratio shown in Figure 4.9. Figure 4.10 shows a simple illustration of how the drift gap (d) will be changed due to cathode curvature.

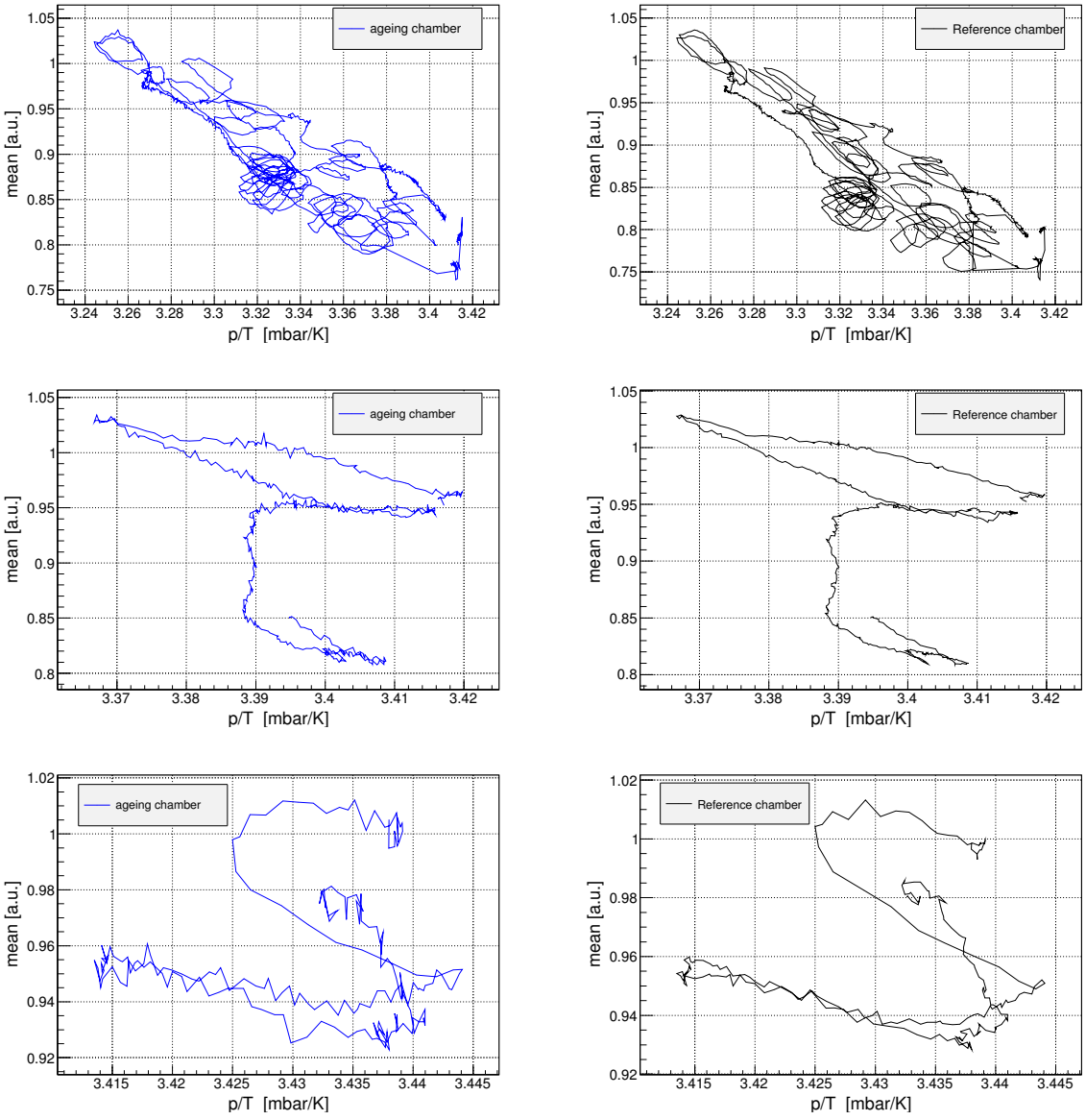

Figure 4.8: *Detector gain of ageing chamber(left) and reference chamber(right) as a function of gas density during three independent tests, using mixing station-1(upper), mixing station-2(middle) and premixed gas(lower)*

The upper plot in Figure 4.9 illustrates the gain ratio (black curve) and the corresponding temperature (red) as a function of time during the first test of the above three tests

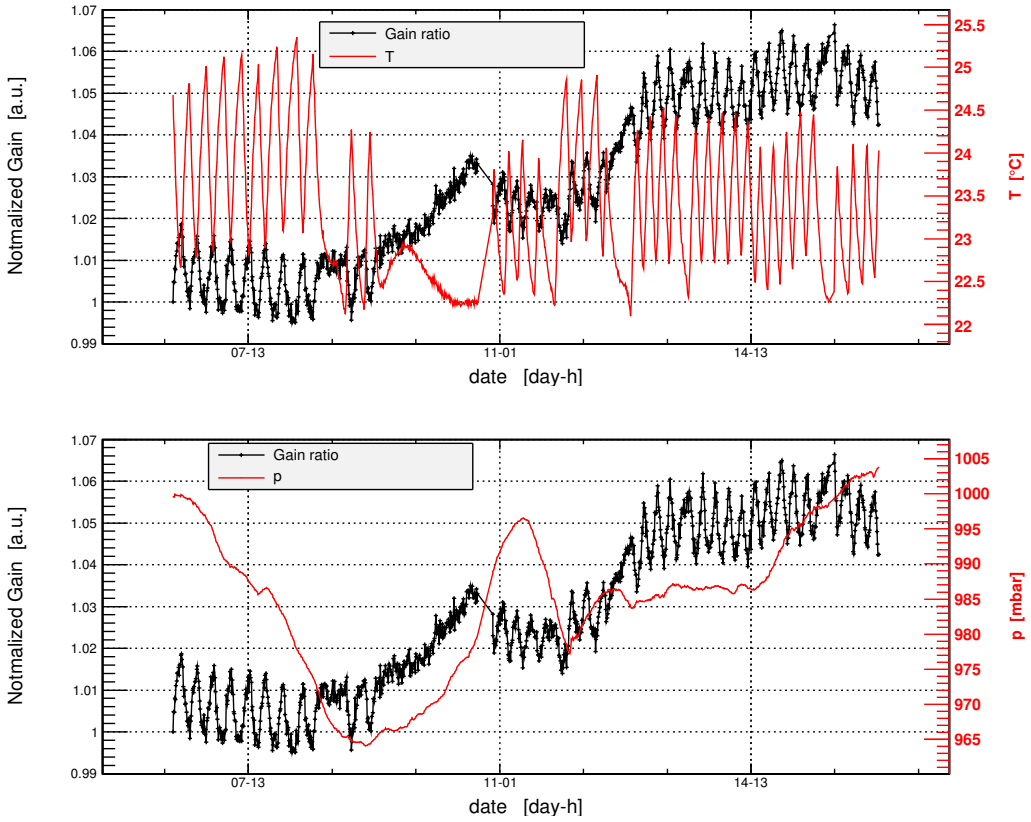

Figure 4.9: *upper: The gain ratio of unmodified chamber (left axis) and the corresponding temperature (right axis) as a function of time. lower: The gain ratio of unmodified chamber (left axis) and the corresponding pressure (right axis) as a function of time.*

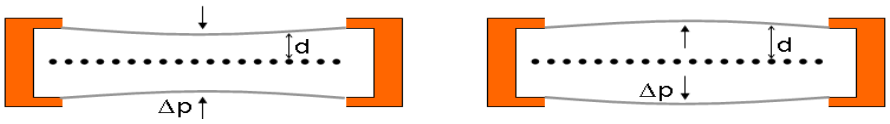

Figure 4.10: *Curvature of chamber windows (cathodes) due to variation of ambient pressure*

while the lower plot illustrates the gain ratio (black curve) and the corresponding pressure (red). It is obvious that the residual instability of the gain ratio, which was about 7% peak-to-peak, correlates not only to the pressure variation but to the temperature as well. Therefore, the subsequent logical steps were to modify the chamber design to avoid any cathode curvature, after that to examine the temperature variation effect.

4.1.8.2 Separating the functions of cathodes and gas tightening foils

From the previous test, a remedy was proposed to add two outer windows and make two small holes in the corners of the inner windows. Figure 4.11 illustrates the design of a modified and an unmodified chamber. In effect, the idea was to separate the functions of the outer windows (sealing the device) and inner cathode electrodes (defining electrostatic geometry). In the manner of previous tests, a new test was carried out for two chambers simultaneously, one of them has four windows (modified design), while the other has only two windows (unmodified design). The chamber gain was monitored during more than 10 days. Figure 4.12 compares the gain behaviour of the modified chamber(left) to unmodified (right) as a function of gas density, which shows clearly that a significant improvement of gain stability was achieved after this modification. The left plot of this figure (modified chamber) shows how chamber gain behaves nearly like the calculated gain in Figure 4.7. Figure 4.13 shows how the peak-to-peak fluctuation of the normalised gain was ∼2% in the modified chamber as compared to 8% of the unmodified chamber. This improvement allows the identification of any continuous drop of normalised gain more than 2% of its initial value caused by a permanent ageing. As a result of this achievement in gain stability, all chambers in the next tests were modified to the new design.

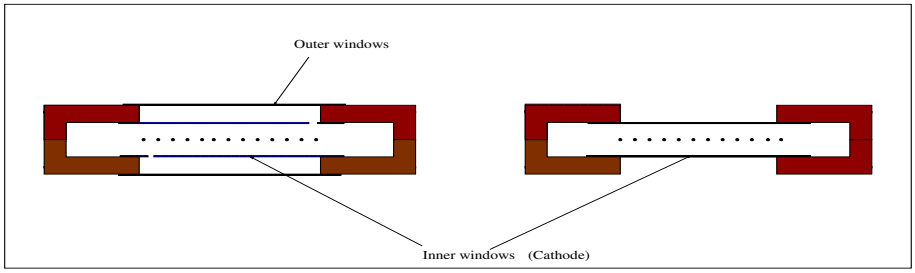

Figure 4.11: *Modified chamber with additional windows(left) compared to the unmodified chamber(right).*

4.1.8.3 Effects of power supply modules

After the achieved improvements discussed above, a new test using two modified chambers was carried out to verify the gain stability. The result of this test, illustrated in Figure 4.14, shows a clear decline in gain ratio at the first forty hours (left plot), where the right plot explains how this decline is correlated to a different variation of anode voltage of the two chambers since the anode voltage of the reference chamber

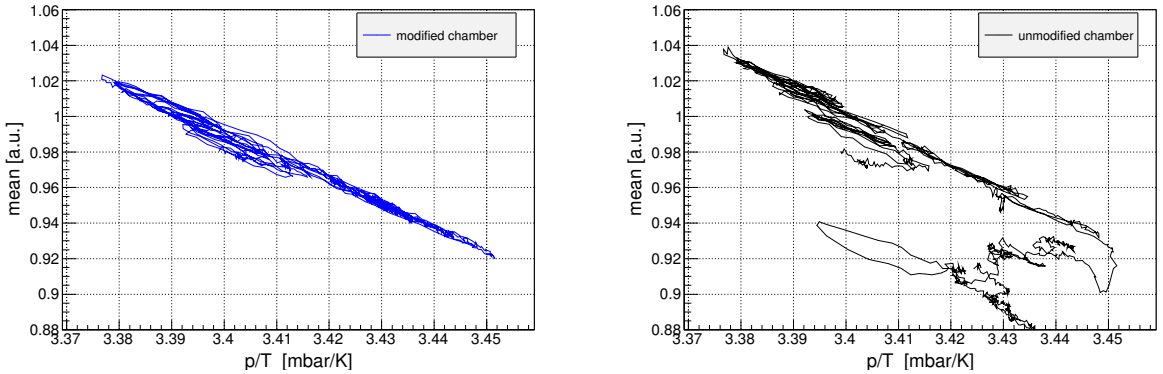

Figure 4.12: *Mean of pulse height of modified (left) and unmodified (right) chambers as a function of gas density.*

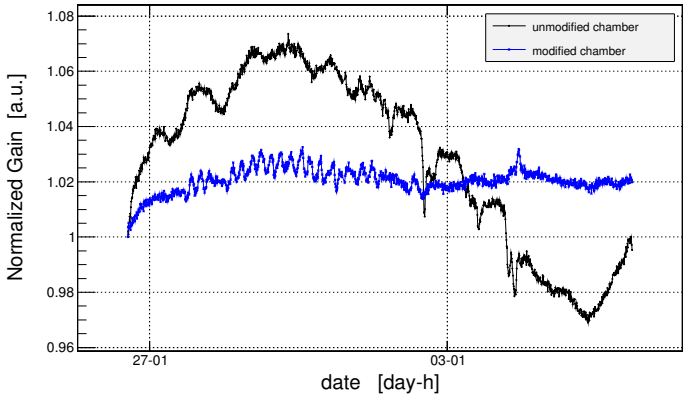

Figure 4.13: *Normalised gain of modified (blue) and unmodified (black) chambers as a function of operation time.*

was increasing by ∼0.4 volt, whilst at the same time it was almost stable for the ageing chamber. This variation of anode voltage is attributable to different effect of the lab conditions on the power modules. As a result of this test, it was reasoned that it is better to use a single module with a divider instead of the two. Consequently, gain stability was examined using one module and a divider in a new test. In this test, gain ratio was not affected by raising the anode voltage ∼2 volt, as is evident in Figure 4.15, since the left plot shows that the gain variation is only about 0.6 % peak-to-peak while raising the anode voltages by about 2 volt. Due to this, it was decided to use a divider in all upcoming tests.

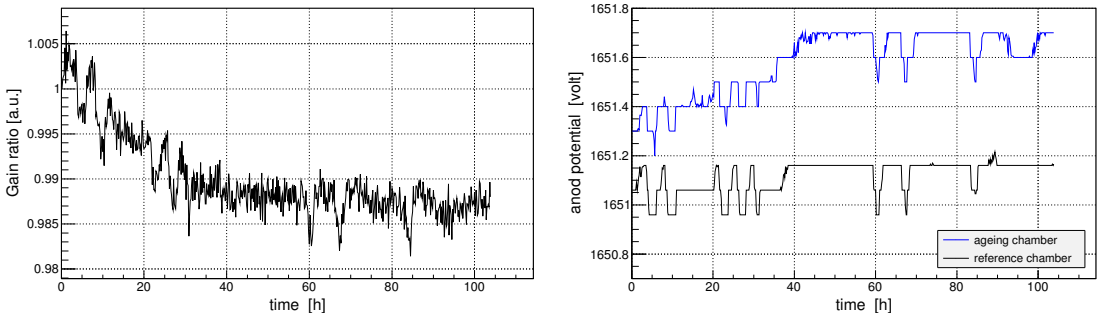

Figure 4.14: *Decline of gain ratio as a function of time (left) and anode voltage of two chambers (right) using two power modules.*

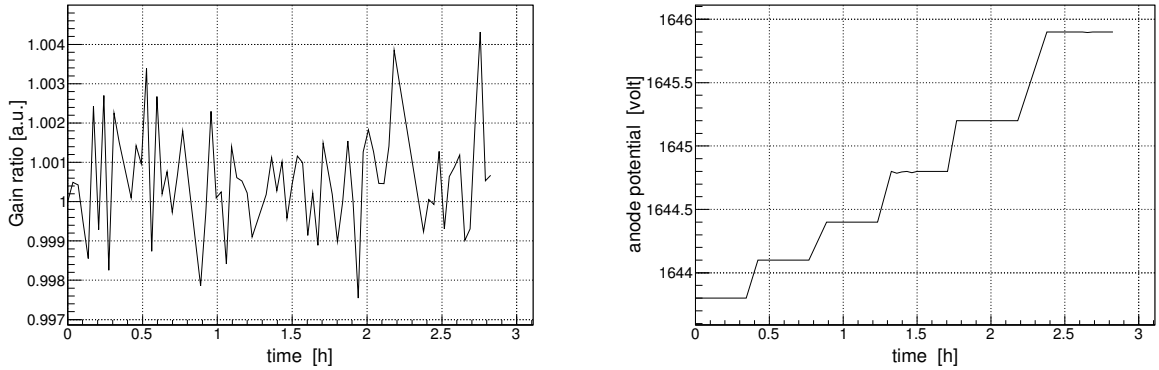

Figure 4.15: *Gain ratio (left) and common anode voltage of two chambers (right) as function of time*

4.1.8.4 "Hysteresis" effect of temperature variation

After the modifications of chamber design and power supply discussed in the above two sub-section, two tests were carried out to verify gain stability and to examine the residual effect of ambient conditions. The setup sketched in Figure 4.1 was used in these two tests, each using two chambers as in all previous tests, but with no material in the outgassing box and no irradiation by X-ray generator. Resulted gain revealed clear "hysteresis" effect on the gain during gas density fluctuation as illustrated in Figure 4.16, whilst Figure 4.17 shows the normalised gain (ρ-corrected gain) of all four chambers as a function of the operating hours. The black and blue curves represent the normalised gain of reference and the ageing chamber respectively, and the red curve represents the corresponding temperature. A clear correlation is present between the temperature variation and the big jumps in the normalised gain, which were in some cases $\sim$2%. Figure 4.18 states that the temperature variation effected even the gain

ratio of the two chambers in both tests, which means there was an effect reaching one chamber before the other. This "hysteresis" was attributed to two causes:

1. The temperature variation effects the mass flow controllers (MFC) which in turn changes the gas mixture composition, but depending on the tube length from the MFC to the chambers, this change of gas composition is reached at a specific time after registering the temperature.

2. The quick rise or drop of temperature reaches the sensor before the gas inside the chamber, since the sensor was pointed outside the chamber at about 2 cm from the chamber and was not isolated from the air.

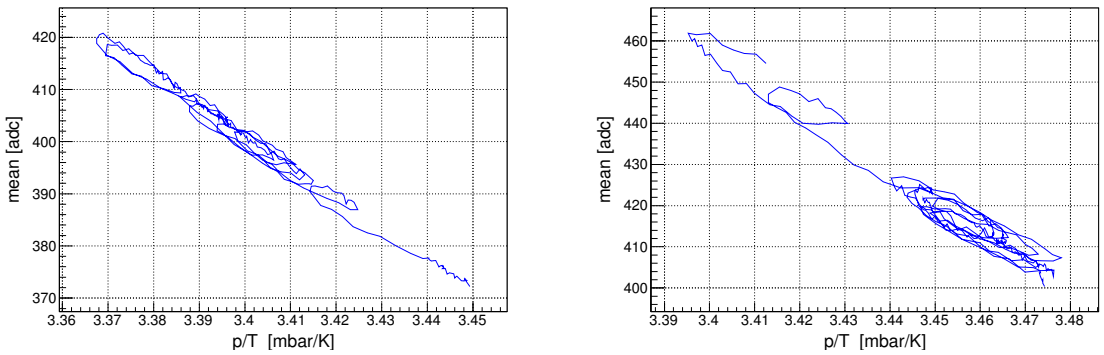

Figure 4.16: *"Hysteresis" effect of the temperature variation on the chamber gain at two chambers using two mixing station.*

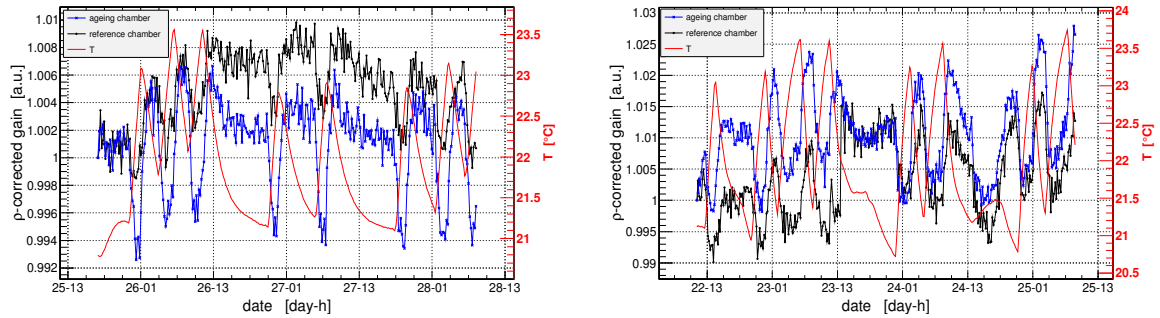

Figure 4.17: *Normalised gain of ageing and reference chambers (left axis) and the associated temperature (right axis) as a function of time for two individual tests using two mixing stations.*

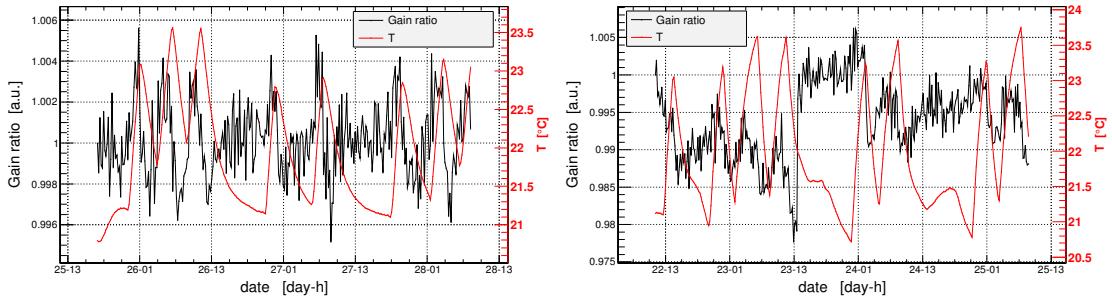

Figure 4.18: *Gain ratio (left axis) and the associated temperature (right axis) for two individual tests using two mixing stations*

4.1.8.5 Temperature dependence of Mass Flow Controller (MFC)

A clear correlation between the residual instability of the normalised gain and the lab temperature was observed, as discussed in Section 4.1.8.4. Due to that, the effect of the lab temperature variation on the behaviour of the MFCs was investigated. This test was performed with the same procedure discussed in Section 4.1.7.1 in two steps utilising a setup shown in Figure 4.19. In the first, the gas was flowing from chamber 2(Ch2) to chamber 1(Ch1), whilst it was in the opposite direction during the second step. The setup was running under these conditions:

1. Gas flow rate was 92.5 ml/min.
2. Volume of both chambers and tubes in between them was about 340 cm^3.
3. The gas needed around 2.4 min to transfer from the MFCs to the first chamber in the gas line.
4. The gas required around 4.2 mins to transfer from the first chamber to the second.
5. The mean of pulse height of ^{55}Fe spectrum was read during 1 min for CH1, then 1 min for CH2, then 10 mins without reading and so on.
6. The surrounding of MFCs were being heated periodically for 2 hours by a heater every 4 hours.

Figure 4.20 shows clear dependency of gain variation on the temperature as recorded by a sensor in the vicinity of the MFCs. The upper three plots show temperature variation (a) and the corresponding effect on gain of CH-1 and CH-2 (b and c) as a

function of time during 40 hours. Temperature was fluctuated by switching the heater on for 2 hours and off for 2 hours. Plots d, e and f show a closer view of the upper plots which illustrate clearly the gain drop of both chambers corresponding to temperature increase and vice versa. This drop was about 1.6% corresponding to about 1.1 ^{o}C. Gain variation was attributed to the temperature effect on the MFCs behaviour, which in turn varied the quencher (CO_2) concentration. During step 1, the gas was flowing from Ch2 to Ch1. Due to that, the change of gas composition reaches first Ch2 and then Ch1 definitely after more than 1 min. Therefore the gain of Ch2 will vary before the gain of Ch1. Figure 4.21 shows the correlation between the onset of the temperature change (red) and the highest tips in the gain ratio (black). This effect was verified even after reversing the flow direction.

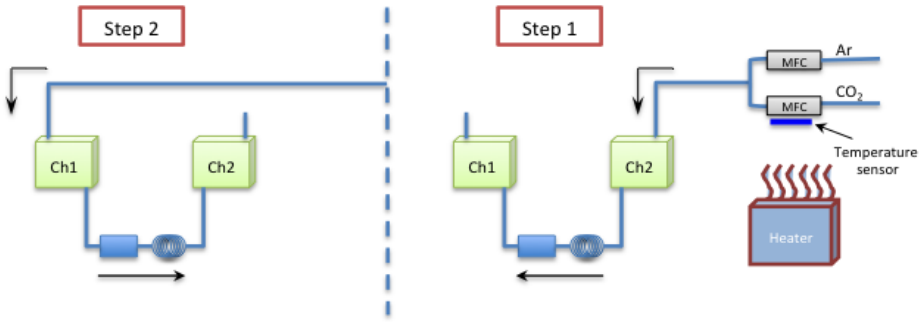

Figure 4.19: *Setup scheme and the gas flow direction during test of temperature effect on the MFCs.*

As a result of this clear effect of temperature on the behaviour of MFCs, two solutions were proposed to overcome it:

1. **Prolong the time constant of the gas concentration change**: A cylinder of 5 l volume was inserted in the gas line upstream from the chambers to extend the time of the gas composition change. Improvement from this modification of the gas line scheme was investigated during about 60 hours. Figure 4.22 (left) illustrates big spikes in the gain ratio associated with temperature variation (right) during the first 15 hours of this test, whilst the effect of the cylinder on the gain ratio is clear in the rest of the test period. Despite the slight improvement, there was a variation about 1.5% peak-to-peak of the gain ratio.

2. **Premix gas bottle**: Due to the above, a premixed gas bottle of Ar/CO_2 (80/20) was used. The stability of the normalised gain was improved to a value better

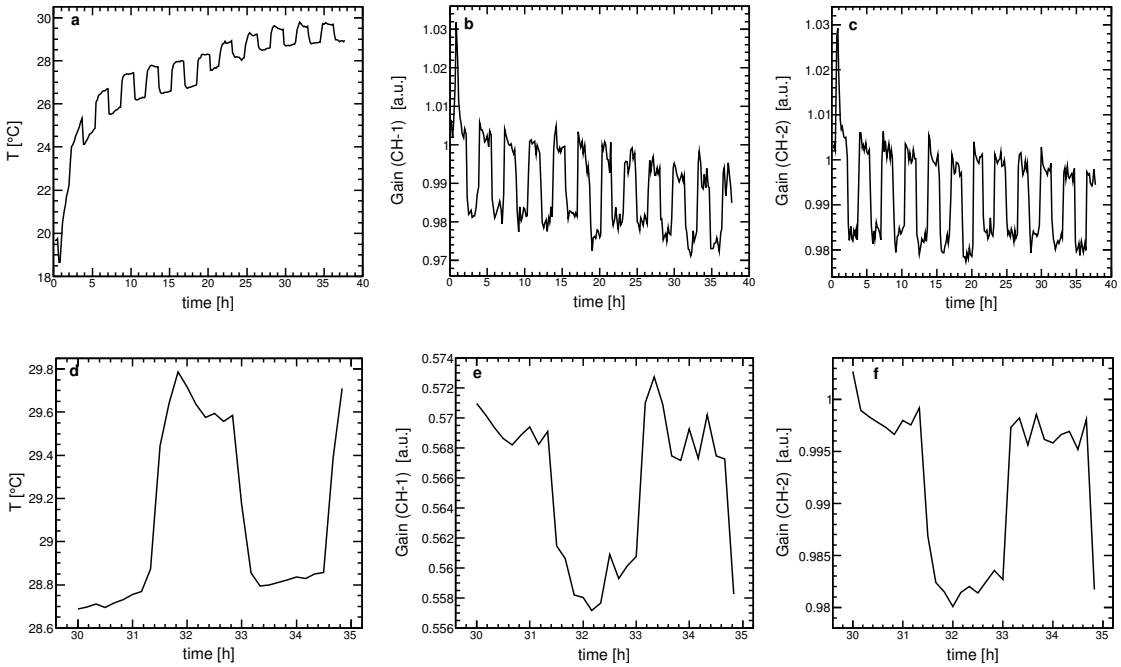

Figure 4.20: *Temperature of MFCs surrounding (a), gain variation of chamber 1(b) and chamber 2(c) as a function of time. d,e and f are close-up view of a,b and c respectively.*

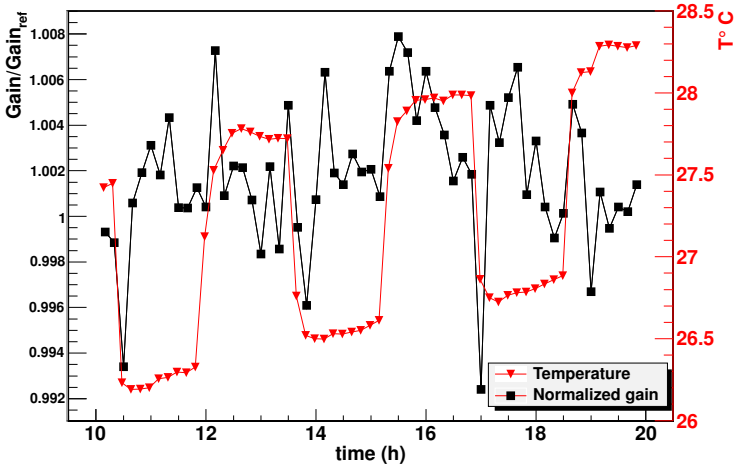

Figure 4.21: *Effect of the temperature variation of the MFCs vicinity (red) on the gain ratio(black)*

than 0.6% peak-to-peak variation during 80 hours and RMS of about 0.0016 as shown in Figure 4.23.

As a result, a premixed gas bottle instead of gas mixing station was decided on.

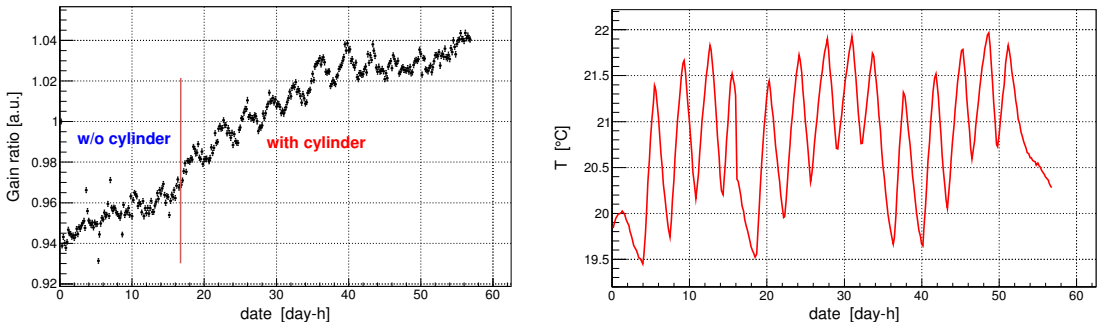

Figure 4.22: *Variation of the normalised gain with and w/o cylinder as a function of time(left) and the corresponding temperature variation(right)*

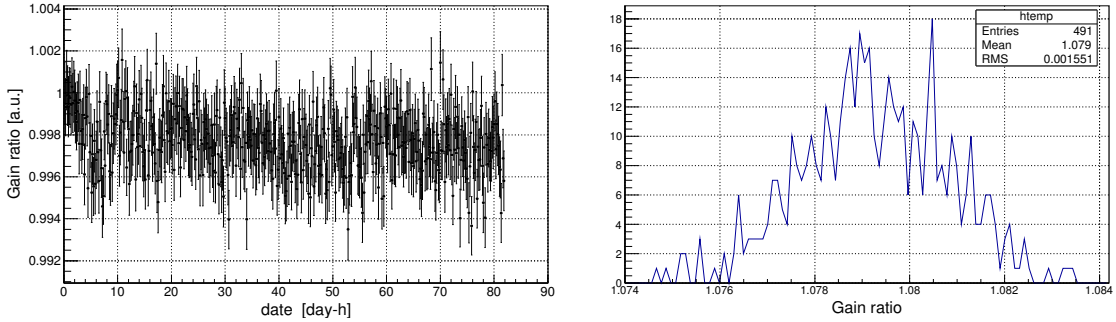

Figure 4.23: *Variation of the normalised gain (left) during 80 hours and its projection (right) using premixed gas.*

After the decision to use a premixed gas bottle and to avoid the inequality of gas pressure in the two chambers, it was preferable to modify the gas scheme from one line to two individual lines (namely two chambers in parallel), so the setup became as Figure 4.24

4.1.8.6 Effect of temperature measurement on normalised gain

After the optimisation of the setup stability obtained in previous tests, the effect of precision of temperature measurement was investigated. A new test, with a procedure similar to that used in section 4.1.8.4, was carried out to verify the "hysteresis" effect of the temperature variation. Accordingly, it was performed in the same setup sketched in Figure 4.1, except for the use of a premixed gas bottle and a heater to vary the temperature in the lab. Clear improvement of setup performance, in terms of "hysteresis" effect of temperature variation, can be read by comparing Figure 4.25 after using a premixed gas bottle opposed to before in Figure 4.16. Despite this improvement,

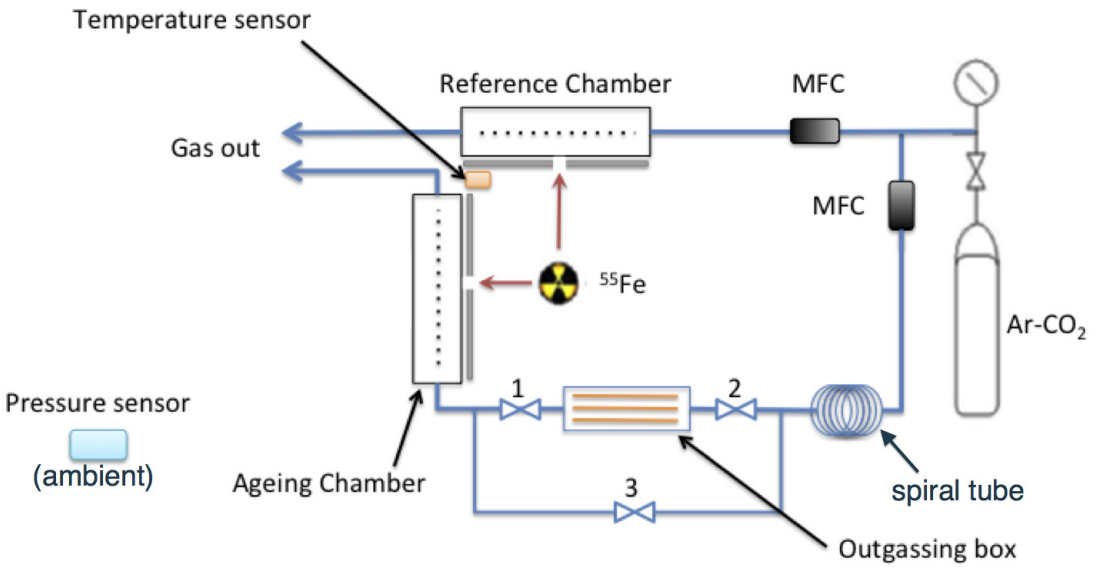

Figure 4.24: *Setup scheme with two parallel gas lines and premixed gas bottle.*

there was little effect. About 0.6% variation of the normalised gain (both ρ-corrected gain and gain ratio) appeared systematically with the temperature variation as shown in Figure 4.26. As it was supposed before, the little residual effect is explained that the temperature sensor not registering the real gas temperature, because it is not in contact with the gas and not isolated from the surrounding air.
Two solutions had to be inserted in the new setup. The first was to modify the chamber by inserting the sensor inside it while the second was to modify the chamber material housing from fibreglass to metal, then to attach the temperature sensor to the exterior. The second solution was taken to avoid any negative effect of inserting the sensor inside the chamber.

4.1.8.7 Ageing of the Al-kapton cathode

When the detector is exposed to the X-rays radiation, over about 1 week using 500kHz, clear signs of itching of the aluminium layer always appear on the cathode foils. They appear in lines perfectly parallel to the wire anode and exactly in the irradiated area. Figure 4.27 shows clear etching lines in the aluminium layer of a cathode being irradiated during two weeks in clean setup. Appearance of such an effect raised a great concern resulting in avoiding the use of the Al-kapton foils as cathode and replacing them with wire planes, as will be explained during building the new ageing setup.

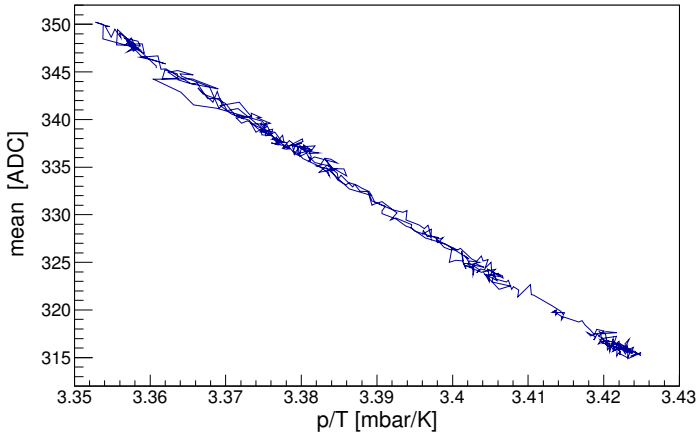

Figure 4.25: *Peak position of iron spectrum in MWPC as a function of gas density using a premixed gas bottle.*

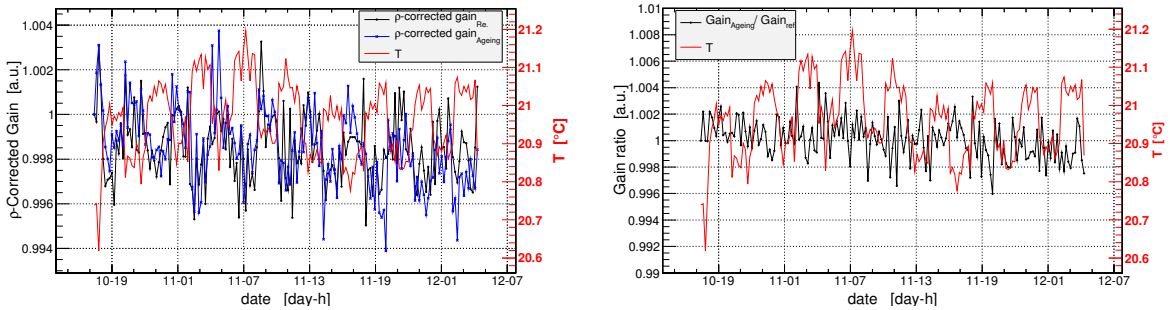

Figure 4.26: *left: Normalised gain (ρ-corrected gain) of two chambers as a function of time (left axis) and the corresponding temperature (right axis) using premixed gas. right: Gain ratio of ageing and reference chamber as a function of time.*

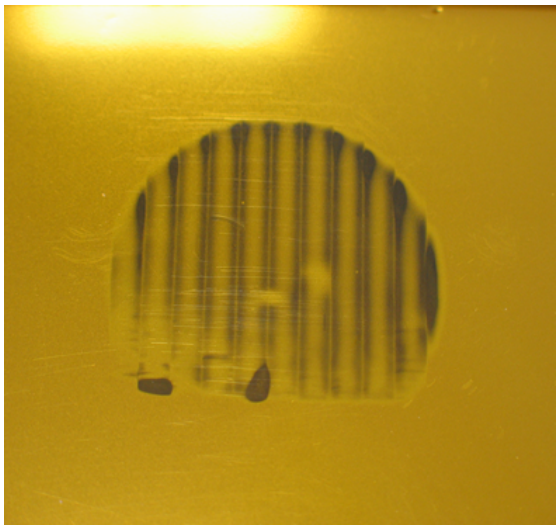

Figure 4.27: *Etching in the Aluminium layer of a cathode exposed to X-ray.*

4.2 Assembly and commissioning of a fully automised ageing setup

As previously mentioned, the main goal of this project is to construct and commission a sophisticated apparatus aimed to study precisely the ageing in gaseous detectors. In order to obtain that, several studies were implemented by an existing setup and resulted in many improvements and recommendations. Based on those recommendations, the envisaged apparatus was constructed. Thereafter many tests were carried out to commission it according to the prospective goals. The setup, the operation and all the tests that have been carried out will be presented below.

4.2.1 Components of the setup

Based on the studies done with the previous setup, a new optimised setup has been built. All setup components were assembled in a box with dimensions of $110 \times 130 \times 83$ cm, at 110 cm above the lab floor. Its walls are made of steel sheets connected by aluminium pillars. The upper picture in Figure 4.28 shows the complete setup, including the rack of the data acquisition and control system whereas the lower picture shows a closer view of its components. Figure 4.29 shows a sketch of the overhead view of the components inside the box. For long-term studies, the setup was converted into an automatic moving setup with a larger number of test chambers. All parts of the setup are new and used for the first time, such as flexible and rigid gas pipelines, chambers and the outgassing box, as well as each detector was provided with an attached temperature sensor. The detectors were altered utilising aluminium instead of fibreglass. Two moving platforms have been inserted; one is carrying the chambers whereas the other is carrying an aluminium collimator plate which has three apertures: 1 mm, 1 mm and 3 cm diameter. Using these two platforms, the ageing setup has been designed to operate three chambers. One of them is assigned as a reference (CH-0) and the other two as ageing test chambers (CH-1, CH-2); each has an individual gas line.

4.2.2 Gas system

The new ageing setup has been equipped with three gas lines which include new tubes and connectors used for the first time after the production. The counting gas in this system as illustrated in Figure 4.30 will be in contact with: Detector Lab (D.L.) global

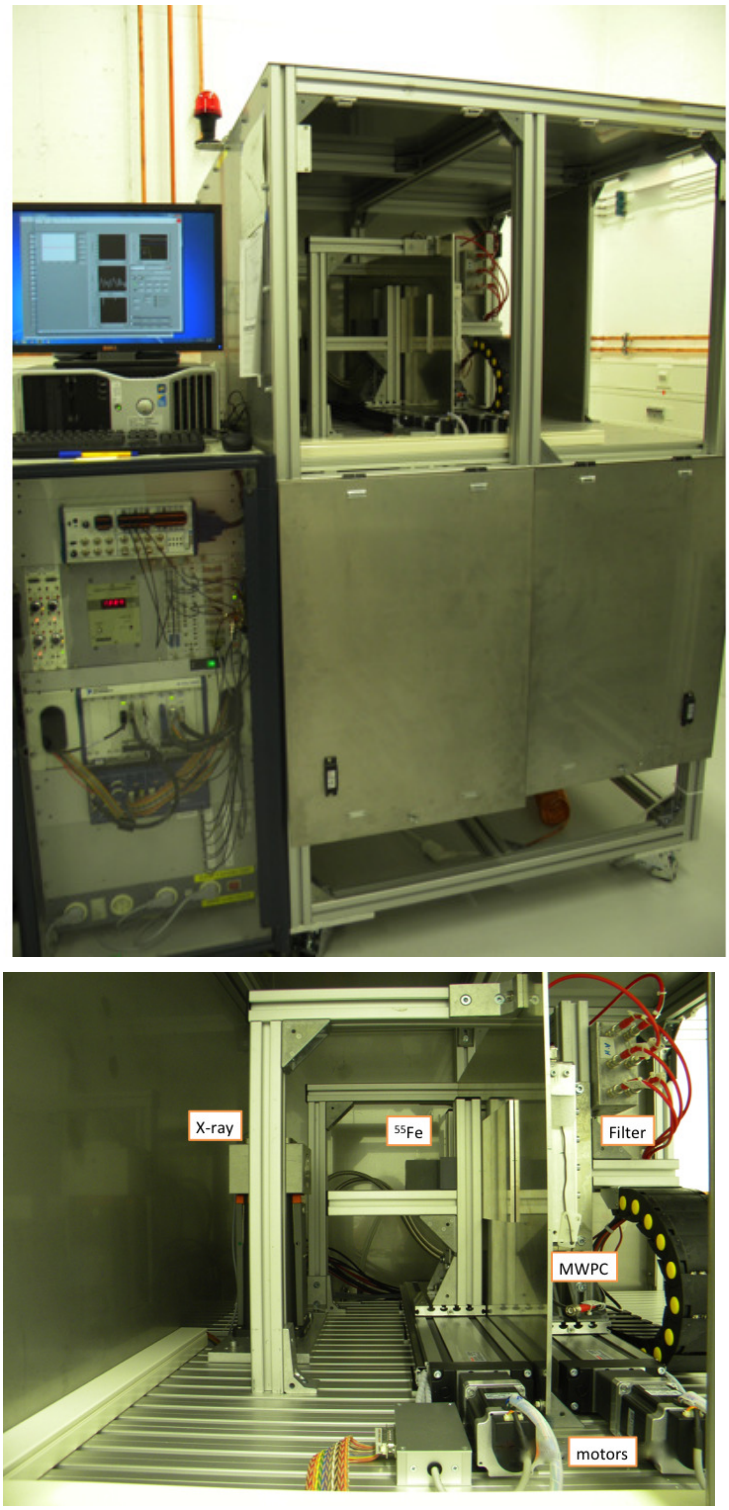

Figure 4.28: *(upper) The whole box of the setup and the associated data acquisition system. (lower) Closer view of the setup components.*

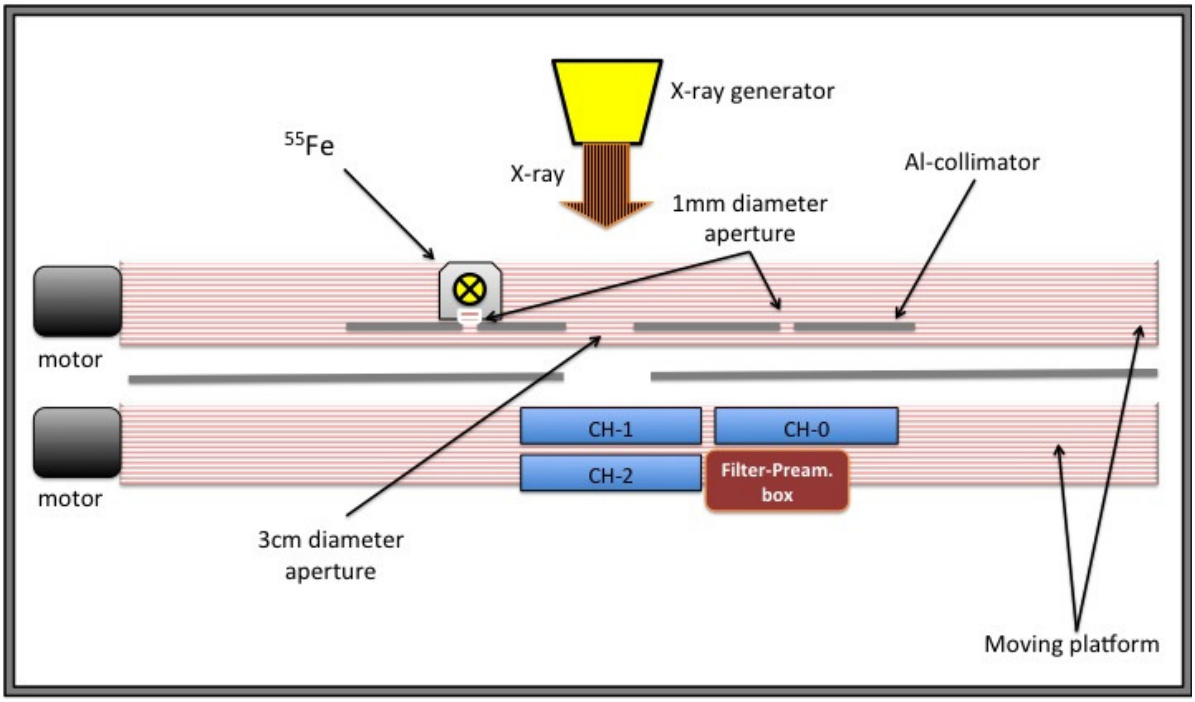

Figure 4.29: *A sketch of the overhead view of the components inside the box.*

gas-line, Mass Flow Controller (MFC), rigid steel tubes inside the lab, flexible steel tubes and an outgassing box in two lines.

Study of ageing influence of a material requires an outgassing system. The outgassing system is one which drives the gas to flush a specific material then transfer its contamination to the detector. The design of such a system should consider the exposed area of the material, avoid of rubber sealing and the ease of inserting and removing the material. At this setup, the outgassing system contains six microscope slides (2.5×7.5 cm) coated with the material to be tested as shown in Part 1 of Figure 4.31. These slides are inserted in parallel inside a holder as shown at Parts 2 (front view) and 3 (side view). Then the holder is inserted into a copper-sealed cylinder. Figures 4.31, 4 and 5 illustrate a sketch and real picture respectively of the final layout of the system.

4.2.3 Data acquisition and control system

The setup has been equipped with a data acquisition and control system in line with the desired measurements so it incorporates multiple functions. The data acquisition and control system based on National Instruments (NI) PXIe-1062Q chassis which equipped with six modules, as shown in Figure 4.32. The NI PXIe-1062Q chassis is linked to

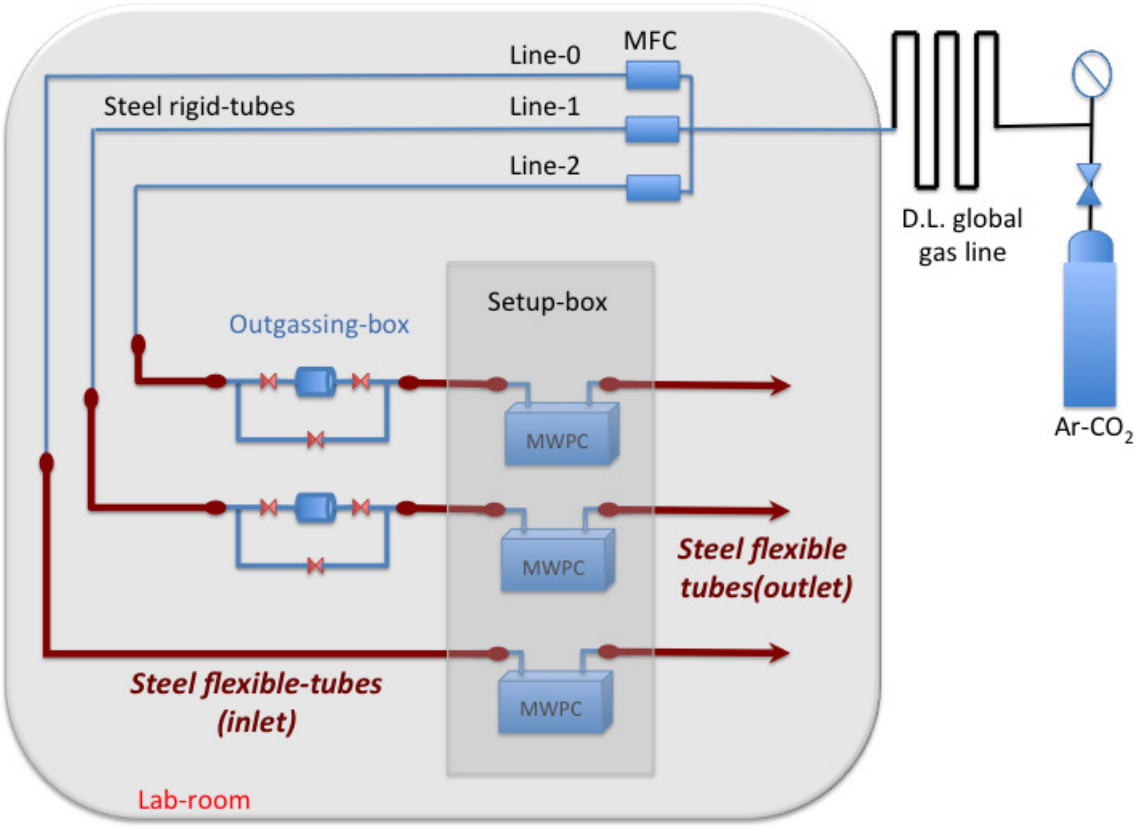

Figure 4.30: *The gas system of the new setup*

a desktop computer via a PXI-8360 module to control the system and document the data. The module PXI 7330 is used to control the stepper motor. The signal coming from the whole anode plane in each chamber is processed through a single amplification electronic channel using a charge sensitive preamplifier, then it is routed into two inputs. One is proceeded to the ADC NI PXI 5105 module to record the pulse height whereas the second is fed directly into GSI CF 8001 discriminator then to the level adapter GSI LA 8010 then via NI BNC-2121 connector to the NI PXI 6602 counter for the particle rate measurement. Simultaneously, the NI PXI-8512 module registers the potential and the current of the chamber anodes and cathodes while the NI PXI-6229 module registers the analog input signals coming from the temperature, pressure and oxygen sensors and controls the x-ray generator. The anodes and cathodes are supplied with high voltage by two power supply modules (NHQ 244M) using a filter.

Operating all these hardware needs a compatible software. Accordingly, a Lab-View code, running under Windows, has been prepared to operate all these functions. It has

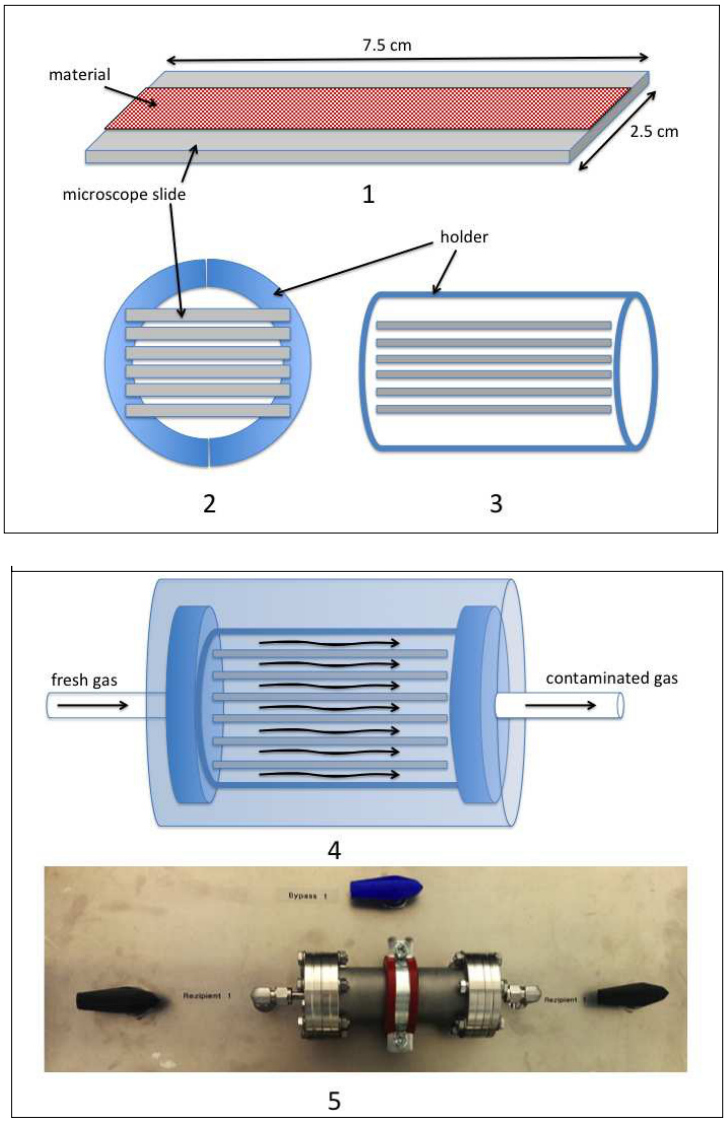

Figure 4.31: *Microscope slides painted with the material under test (1). Front and side view of a slide holder (2,3). View of gas stream in contact with the material under test inside the outgassing box (4) and the final exterior of the outgassing box (5)*

been designed to be modified depending on the measurement mode and to present a live measurement of the chamber gain and current, particle rate, temperature, pressure, oxygen concentration and X-ray generator voltage and current. Data are stored in the ASCII format.

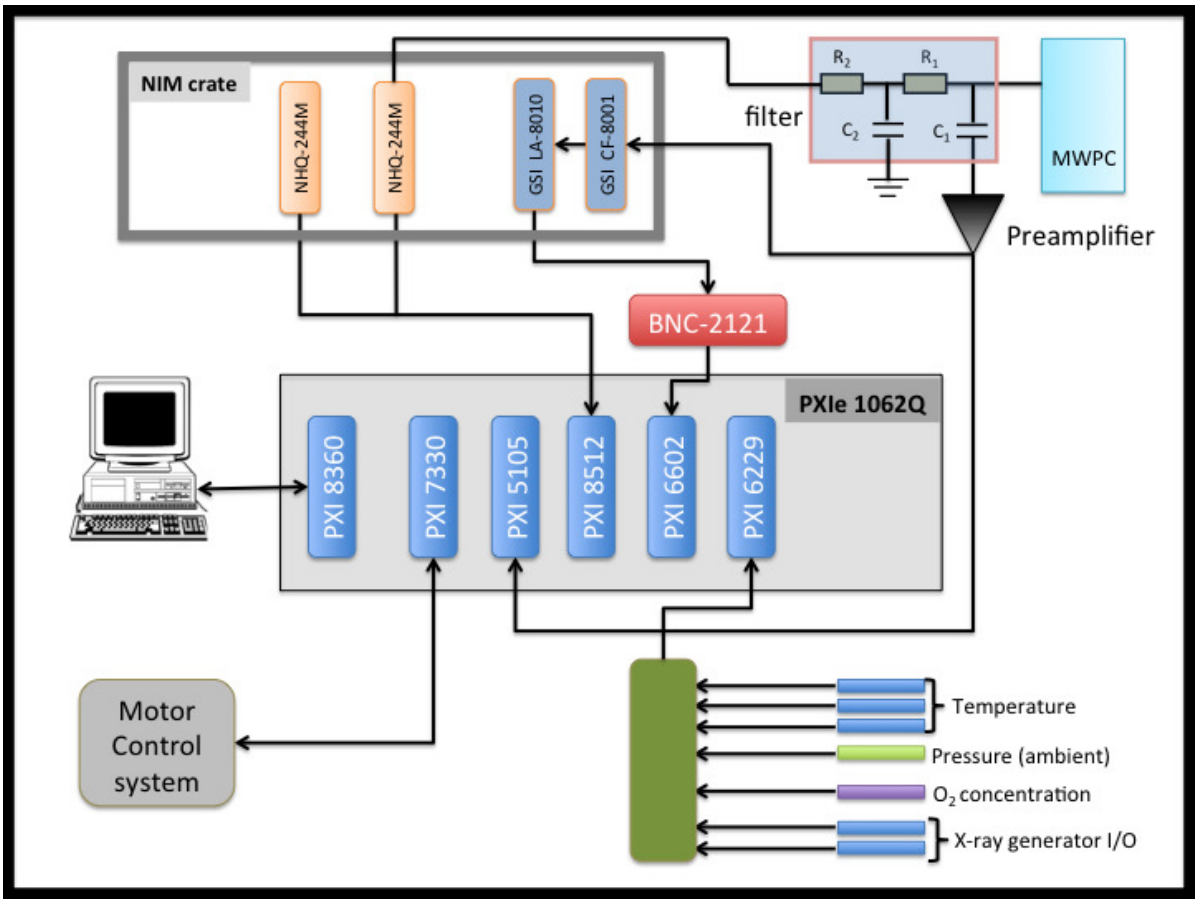

Figure 4.32: *Data acquisition and control system in the setup*

4.2.4 Ageing detectors

Based on the experience gained from the tests carried out in the old setup, the MWPCs have been built in a different style. The aluminised-Kapton cathode has been replaced with a wire plane, and the housing is made of aluminium instead of fibreglass. Firstly, simulation has been performed by GARFIELD program. Accordingly, an optimised chamber has been produced and assembled. After that, characterisation tests have been performed before utilising it in ageing tests. In this section, simulations, fabrication and characterisation tests will be presented in detail.

4.2.4.1 Detector design

Different configurations of anode and cathode wires have been simulated by a combination of the gas simulation program (*Magboltz*) and the electric field simulation program (*Garfield*). The simulated chamber is always filled with Ar-CO_2 gas of 80-20% ratio,

using two cathode planes and one anode plane in-between, as in Figure 4.33. In these simulations, electric field contour, ion drift lines and gas gain have been calculated for different pitches and diameters of cathode wires, and for different electrode potentials. Firstly, simulations have been performed using, in all of them, +1500 volt for anode plane and -200 volt for cathode. The wires of the anode plane have 20 μm diameter and 3 mm pitch, whereas the cathode wires have two different diameters, each in three different pitches. Table 4.2 summarises the electrode configurations and the output gain of these simulations. It is clear from both curves in Figure 4.34 that the wider the

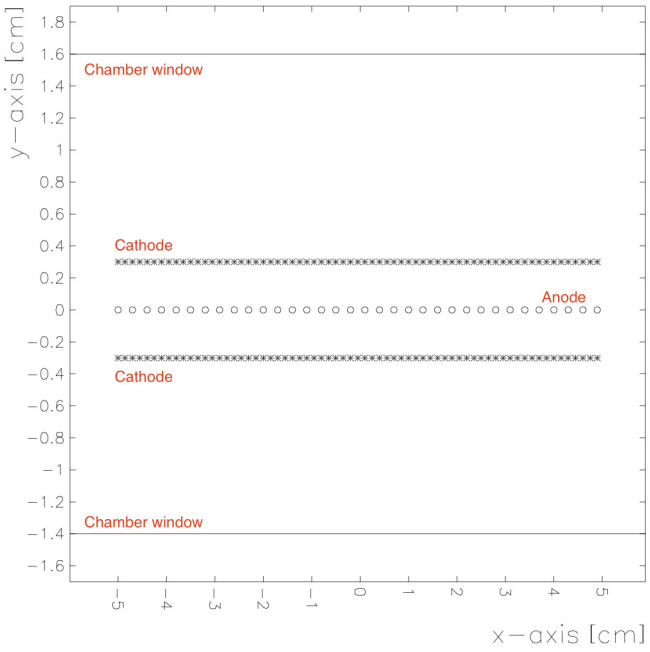

Figure 4.33: *Electrode configuration of a MWPC made for the ageing setup.*

pitch the lower the gain and a higher gain is obtained when using a diameter of 75μm than when using 20μm.

Plots 1, 2 and 3 of Figure 4.35 show the ion drift lines in the centre area of the chamber created with cathode wire pitches of 3, 1.5 and 0.75 mm respectively and 20μm diameter for all. While plots 4, 5 and 6 show the lines using cathode wire pitches of 3, 1.5 and 0.75 mm respectively when using 75μm diameter. By comparing the density of the drift lines that reflects the electric field strength, one can see that the electric field is higher when using a smaller pitch, which explains the higher obtained gain. The fifth configuration in Table 4.2 has been selected to be used in the chambers of the setup. This selection was due to two reasons; the first, because it is preferable in ageing studies to use a higher gain to accumulate more charge in less time, the second is that the

Table 4.2: *Electrode configuration values and calculated gain.*

	Anode			Cathode				
simulation	diameter (μm)	Pitch (mm)	Potential (volt)	diameter (μm)	Pitch (mm)	Potential (volt)	Drift gap (mm)	Gain
1	20	3	+1500	20	3	-200	3	420
2	20	3	+1500	20	1.5	-200	3	1550
3	20	3	+1500	20	0.75	-200	3	3430
4	20	3	+1500	75	3	-200	3	840
5	20	3	+1500	75	1.5	-200	3	2600
6	20	3	+1500	75	0.75	-200	3	4660

rigidity of wire frames limits the use of a high number of wires (high tension). Based on the previous, further simulations have been done for the selected configuration in different electrode potentials. Figure 4.36 shows the calculated gain as a function of electrode potential differences in four different sets (0, -100, -200 and -300 volt) of the cathode potential. Looking at this figure, a different set of the cathode potential does not produce a significant difference of gain.

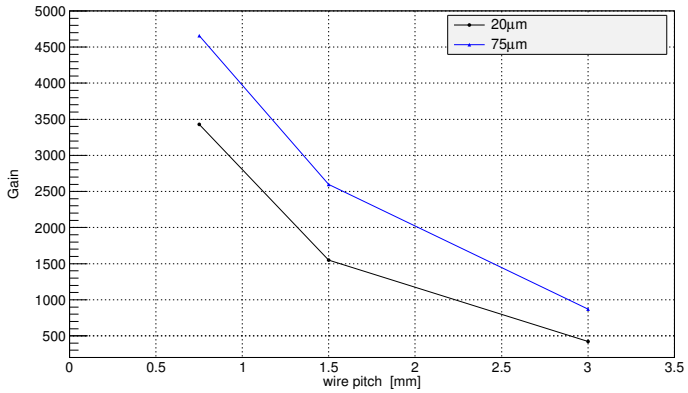

Figure 4.34: *Simulated gain, of a MWPC, as a function of cathode wire pitch for two different diameters, 75µm (blue) and 20µm(black).*

4.2.4.2 Detector fabrication

Based on the results obtained by the simulation, a multi wire proportional chamber (MWPC) has been fabricated with an anode plane of gold-plated tungsten wires of 20 μm diameter and 3 mm spacing. Two cathode planes have been made of copper-plated beryllium wires of 75 μm diameter and 1.5 mm spacing. The gap between the electrode planes is 3 mm as illustrated in sketch 4.33. The box made of aluminium with dimensions of 20×20×3 cm^3 holds the chamber components. It has windows

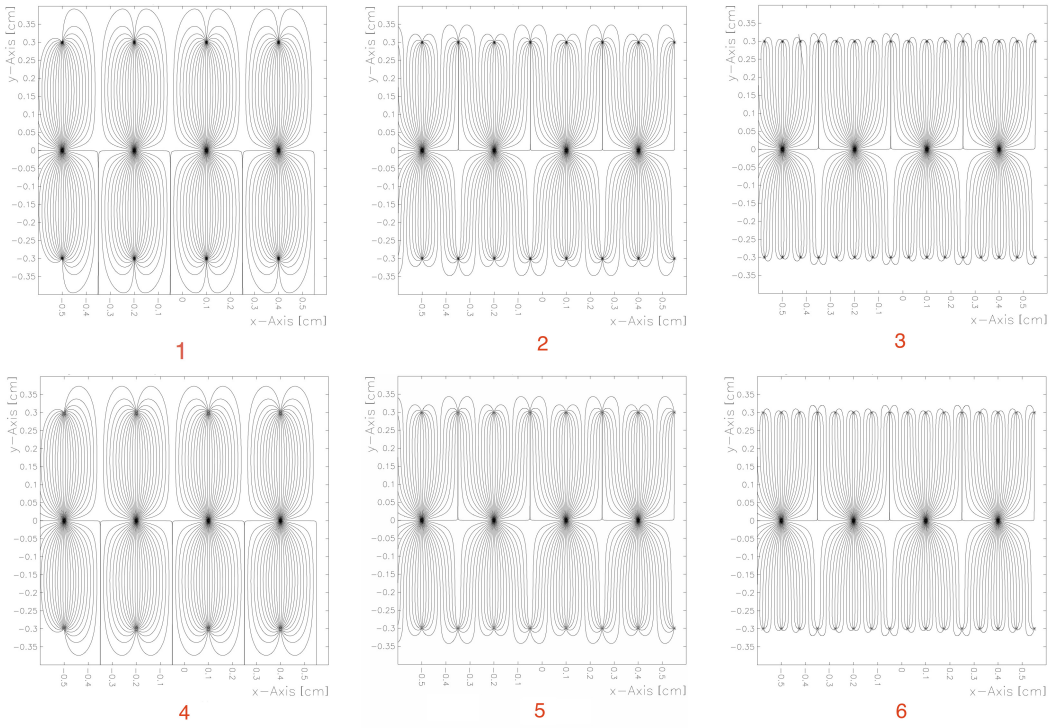

Figure 4.35: *Simulation of the drift lines in the centre area of a MWPC in different diameter and pitch of cathode wires. 1, 2 and 3 for 3, 1.5, and 0.75 mm pitch respectively with 20µm diameter of cathode wire. 4, 5 and 6 for 3, 1.5, and 0.75 mm pitch respectively with 75µm diameter of cathode wire.*

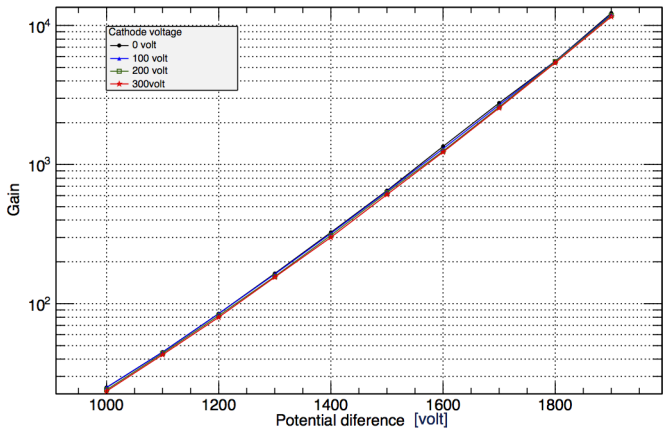

Figure 4.36: *Simulated gain as a function of potential difference in a MWPC.*

with dimensions of 10×10 cm^2 onto a 10×10 cm^2 active area. In addition to this new configuration of the MWPC electrodes, the prior electrode configuration of the old setup that uses aluminised-Kapton foils has been fabricated in the new metal housing

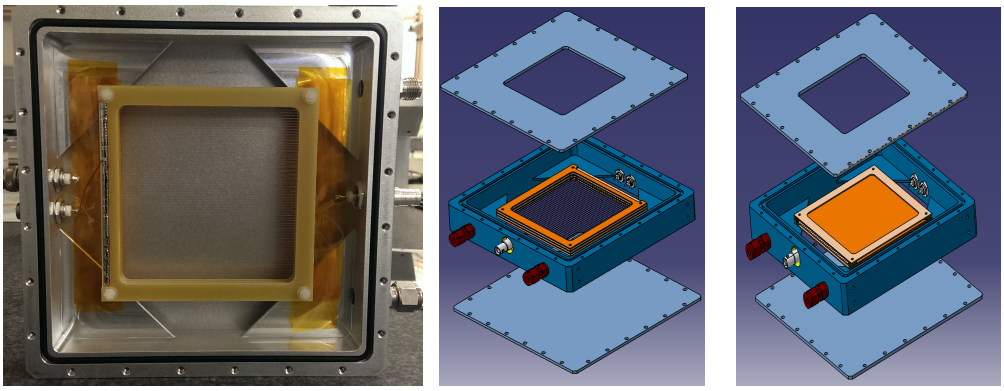

Figure 4.37: *(left): Final layout of a wire cathode MWPC in the setup. (middle and right): Drawings of wire and foil cathode of MWPC respectively.*

for some tests as it will be discussed in Section 4.2.6. Right and middle drawings in Figure 4.37 show the two versions of MWPC in new housing while the left picture shows the final layout of the wire-cathode version.

4.2.4.3 Characterisation tests

Characterisation tests have been carried out before utilising the MWPC in ageing tests. Using the ADC-preamplifier calibration implemented at the old setup, the chamber gain and resolution have been measured as a function of potential difference of electrode in five sets of cathode voltage. It is evident from the left plot of Figure 4.38 there is no

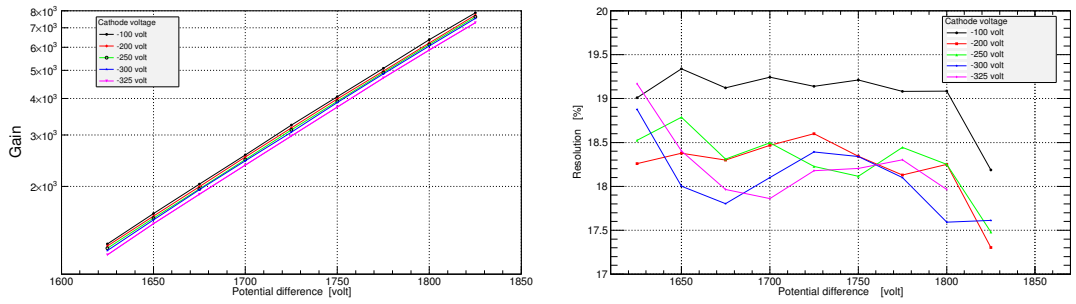

Figure 4.38: *Measured gas gain (left) and resolution (right) as a function of electrode potential difference in a MWPC for five different cathode voltages.*

significant difference of their gain. The measured gain matched well with the simulation in Figure 4.34. However, better resolution has been obtained as when using a higher set as with the blue and pink curves of the right plot. Based on these measurements, cathode voltage of -300 volt has been selected for all future measurements. After

selecting the cathode potential to be -300 volt, particle rate has been measured in different anode voltages as illustrated in Figure 4.39. It is evident from this plot; a proper operation potential is in the range of 1700-1800 volt.

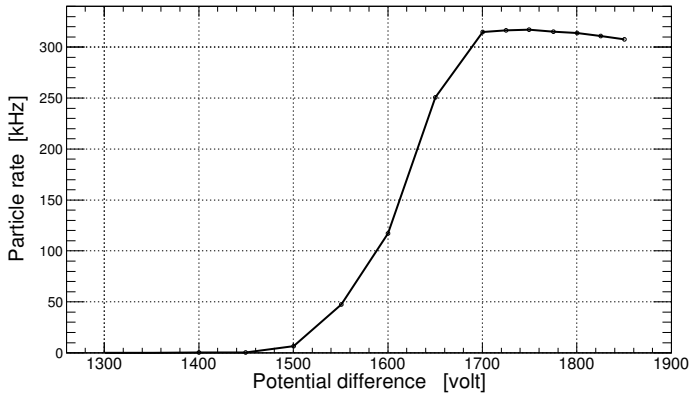

Figure 4.39: *Particle rate as a function of electrode potential difference*

4.2.5 Irradiation source

In ageing studies, calculation of the accumulated charge per unit length or area of detectors is a very important parameter. Based on this parameter, one can compare the detector performance in the lab and in real experiments. In this setup, the detector ir-

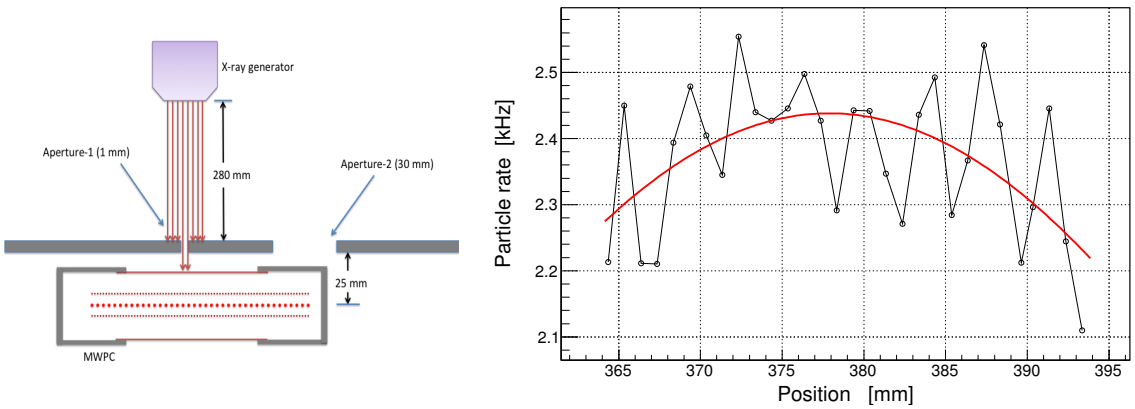

Figure 4.40: *left:Sketch of X-ray generator, collimator and chamber. right: Distribution of X-ray photons on the irradiation region of chambers.*

radiation approach is to use a copper based X-ray generator (described in Section 4.1.4) to irradiate a circular area, which has a diameter of 3 cm. Then, in the centre of this

irradiated area, the chamber performance will be diagnosed using the ^{55}Fe spectrum collimated with a 1 mm diameter pinhole or filtered X-ray. From the discussion above, it is important to irradiate the 3 cm region evenly, which makes it necessary to measure the X-ray distribution over this region. The left sketch in Figure 4.40 shows the distances between the detector and the X-ray generator, the irradiation and the measurement apertures. The X-ray distribution measurement has been done by measuring the particle rate while moving the aperture-1 (1 mm) horizontally in front of the entire active area of the detector, then the particle rate corresponding to the 3 cm diameter hole has been extrapolated. Results illustrated in Figure 4.40 (right) show the distribution of the X-ray rate onto the irradiated area with variation of about 6%. For gain measurement purposes, the characteristic peak of the spectrum of the X-ray generator can be filtered using a filter composed of brass and nickel foils. Figure 4.41 shows this spectrum with energy resolution ($\triangle E_{FWHM}/E$) of $\sim$15%. This combination of materials is used as a filter because it has higher mass attenuation coefficient for the k_β photons than for k_α of the spectrum coming from the copper anode X-ray generator, and has high attenuation of the bremsstrahlung spectrum.

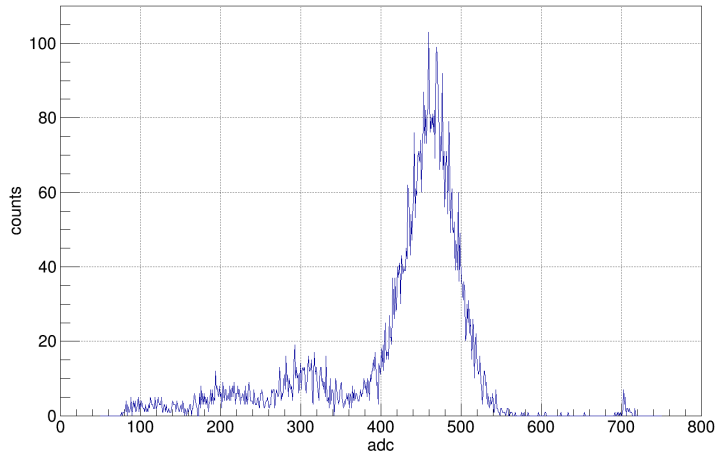

Figure 4.41: *Spectrum of X-ray generator using a brass and nickel filter.*

4.2.6 Cleaning procedures

In ageing studies, it is very important to build a setup that can be cleaned easily between the tests. It is a priority for the setup to be equipped with a simple and effective cleaning procedure. During the commissioning tests of the setup, two cleaning

processes have been used:

procedure-1: in this procedure, distilled water, iso-propanol and dry air are pumped through the pipes shown in Figure 4.42 in five steps, one hour each, as follows: distilled water, iso-propanol, distilled water, iso-propanol and dry air. This procedure is simple and does not require disassembling any part from the setup box, but it is untrusted to clean the flexible tubes completely, as will be discussed in the next section.

procedure-2: in this process, the rigid tubes are cleaned as in procedure-1, while

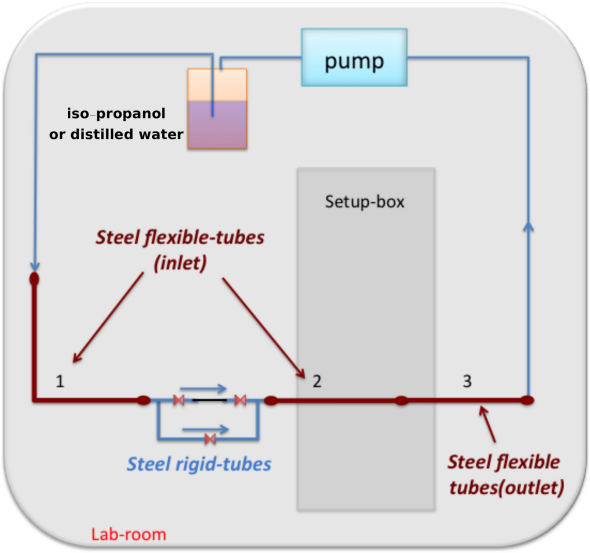

Figure 4.42: *Scheme of cleaning setup of procedure-1 using a pump*

the flexible tubes, which are numbered 1, 2 and 3 in Figure 4.42, are taken out to be cleaned following these steps: an hour in ultra-sonic bath using iso-propanol, an hour pumping iso-propanol through tubes 1, 2 and 3 in one line, an hour in ultra-sonic bath using iso-propanol, an hour pumping iso-propanol through tubes 1, 2 and 3 in one line and, finally, drying them with dry air. This procedure has resulted in a better cleaning of flexible tubes.

4.2.7 Commissioning test

There are many new components, such as chambers, cables, flexible tubes, motors and platforms had to be tested before utilising them in planned ageing tests. Firstly, because moving functions have been introduced into this setup, noise level had to be investigated before securing all the components. After that, optimisation of temperature measurements and investigation of setup cleanness have been implemented.

4.2.7.1 Noise measurements

After the previous test and installing the box contains the filter and the preamplifier close to chambers on the moving platform, as shown in Sketch 4.29, noise level along the movement range of the platform has been measured. In this test, rate and width of noise for the three chambers(CH-0, CH-1 and CH-2) have been measured along the platform, which is 50 cm. As shown in Figure 4.43, the rate does not change while the width increases as the platform moves away from the motor. In spite of that, noise remains at levels considered negligible on desired measurements. The red parts of the plots represent the positions of chambers when the mean of pulse height of iron-55 is measured.

4.2.7.2 Optimisation of temperature measurements

To achieve an accurate normalisation of gain (see Section 4.1.7), it is mandatory to measure precisely the gas pressure and temperature. Temperature measurement has been optimised with four different arrangements of the sensors to reach the required accuracy. Initially, one sensor was used at approximately 30 cm from the chambers, and it was not isolated from the air, as shown in Figure 4.44(1). Results obtained with this scheme revealed about a 1.5% variation of the ρ-corrected gain, which clearly correlated with the temperature variation. Figure 4.45(1) illustrates this correlation of the ρ-corrected gain (black curve) and the temperature (red curve) as a function of time. After that, two sensors were placed directly behind chambers CH-0 and Ch-2, which are not isolated from the air and not touching the metal body of the chambers, as illustrated in Figure 4.44(2). Figure 4.45(2) shows the ρ-corrected gain and the corresponding temperature obtained using the scheme (2). It is clear there was still about 1.5% variation of the normalised gain corresponding to the temperature variation. Due to that, it was necessary to add a third sensor and to fix them all in physical contact with the chamber body as illustrated in Figure 4.44, scheme (3). Significant improvement has been achieved using this scheme since only about 0.5% variation is still present in the normalised gain as shown in Figure 4.45(3). In the final step, an insulator has been inserted to restrict the sensor temperature variation with the gas temperature variation as much as possible, as in Scheme 4 in Figure 4.44. With this step, the normalised gain has no correlation with the temperature, as shown in Figure 4.45(4).

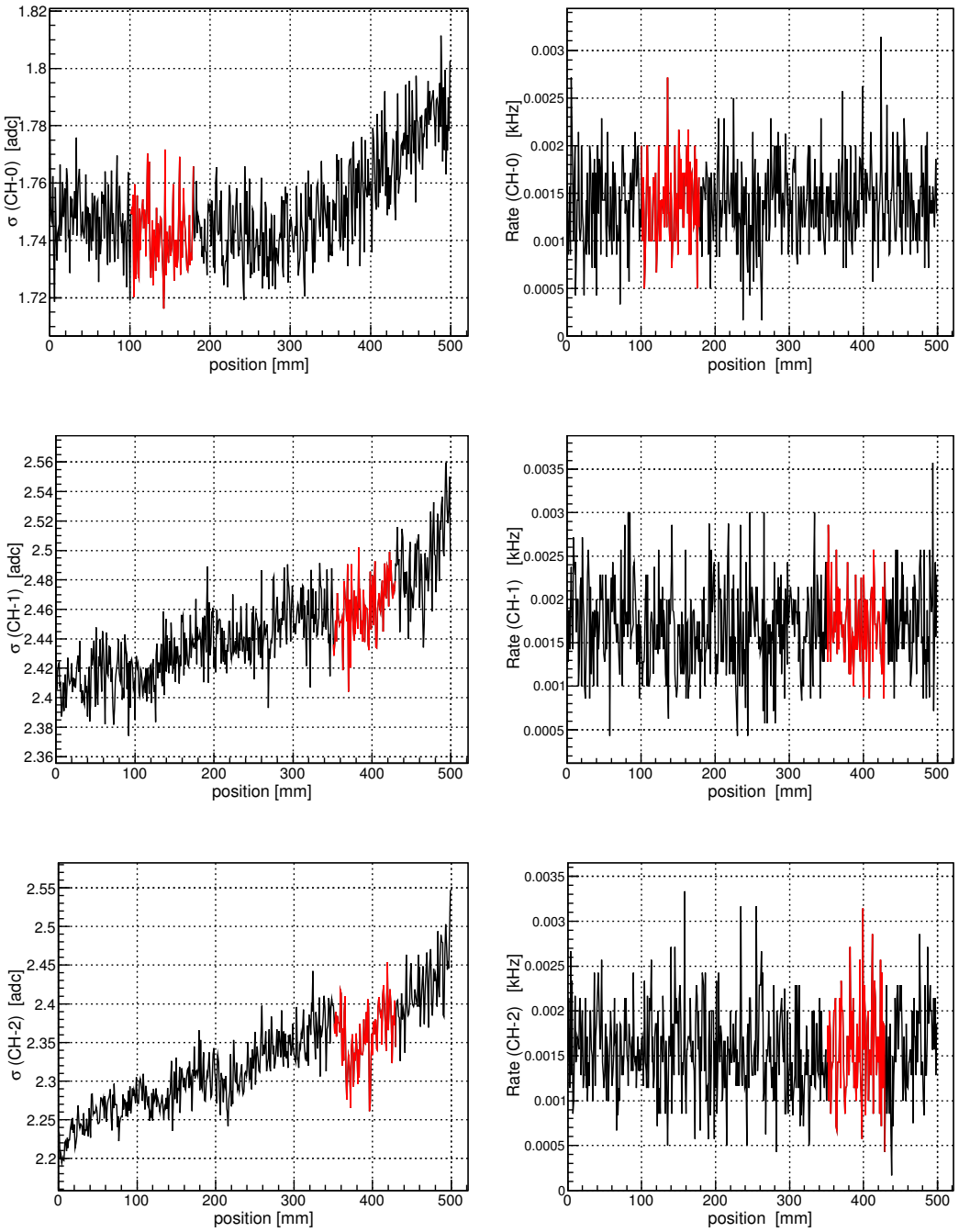

Figure 4.43: *RMS of noise (left) and rate (right) as a function of chamber position within platform movement range. Red regions are positions of CH-0(top), CH-1(middle) and CH-2(bottom) during gain measurements.*

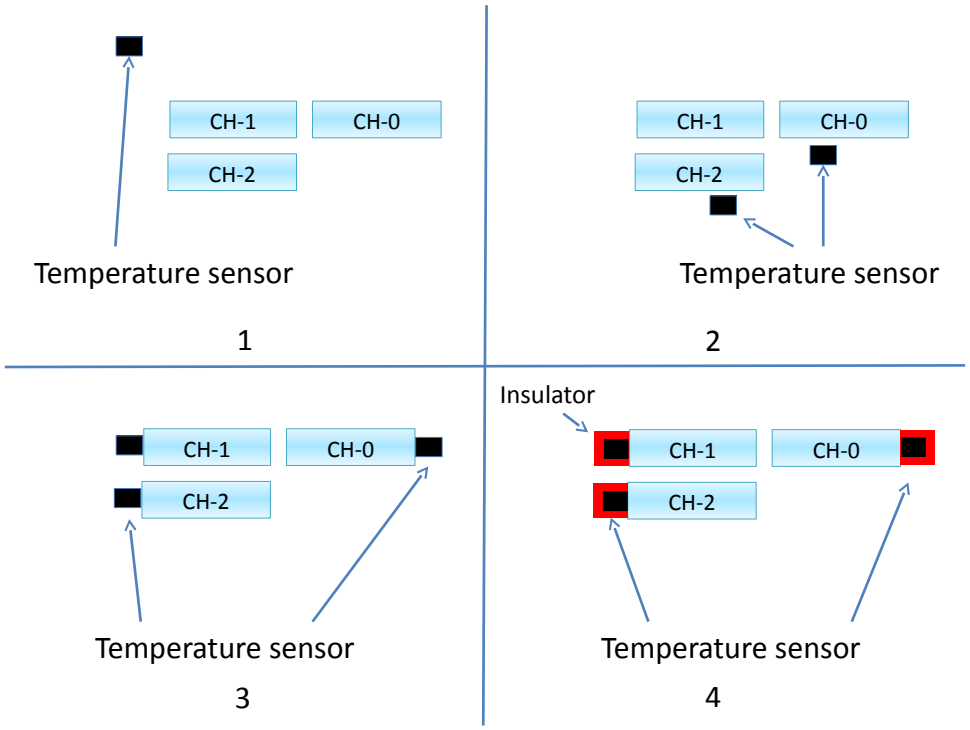

Figure 4.44: *Temperature sensor locations during optimisation of temperature measurement*

4.2.7.3 Investigation of setup cleanness

First commissioning test has revealed a clear ageing in two chambers out of the three caused by an unknown source of contamination which is somewhere in the gas system. In the context of seeking to reach a quite stable setup, systematic tests had to be implemented to know exactly where the contamination is coming from. These systematic investigations have been carried out using four schemes of gas system, see Figure 4.46. All detectors during these investigations have been exposed to an iron source only through 1 mm aperture. Below is a detailed presentation of these tests and the objective of each test.

1. **Setup cleaning by procedure-1**: After cleaning the setup by procedure-1 sketched in Figure 4.42, two new chambers have been inserted. Ch-0 is made of anode wires and foil cathodes while CH-1 is made of wires for both anodes and cathodes. Scheme-1 of the gas system has been used in this test. Then, the gain stability has been monitored to examine the effectiveness of the cleaning process during more than 18 days. A clear gain drop has been observed in both chambers with different rates. Another test aimed to measure ageing rate after exchanging

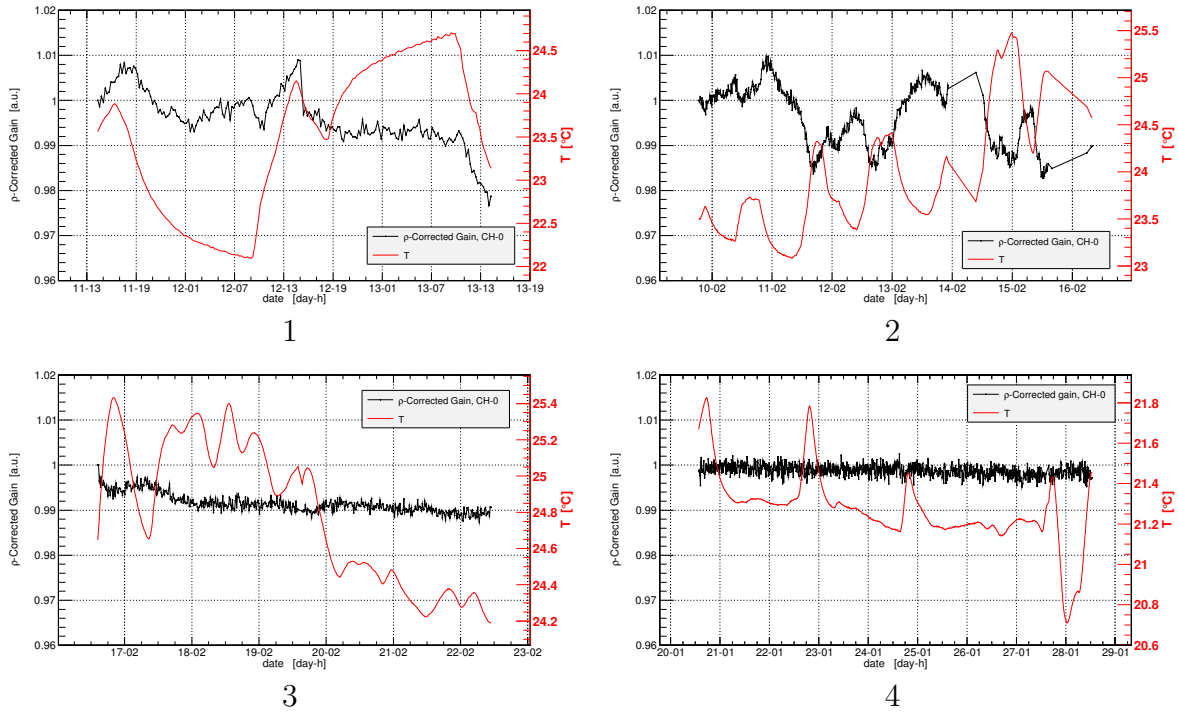

Figure 4.45: *Normalised gain (black) and temperature (red) as a function of time, using one temperature sensor for three chambers (1), two sensors (2), three sensors (3) and three isolated sensors (4).*

the gas lines revealed the same behaviour. The left plot of Figure 4.47 illustrates obviously the gain degradation of both chambers as a function of accumulated charge during the first test whereas the right plot shows a similar degradation behaviour after exchanging the gas lines. During the first test, chamber gain has been scanned horizontally along the active area of both chambers two times, before and after ageing as marked in Figure 4.47(left). With these two scans, a localised drop of gain is apparent in the irradiation spots as shown in Figure 4.48. After the end of this test, several probes of the anode wires, cathode wires and cathode foils have been analysed by an electron microscope. The upper pictures of Figure 4.49 compare anode wires before ageing (red) and after (black-line), while the lower spectrum shows an overlap of microanalysis of these two probes. Clear deposits of carbon could be read from this overlap. The upper right picture of Figure 4.50 shows a clear line in aged Al-Kapton foil compared to fresh foil (left) whereas the overlap of their microanalysis shows obvious etching of the aluminium layer. Analysis in figures 4.51 and 4.52 show traces of fluorine and

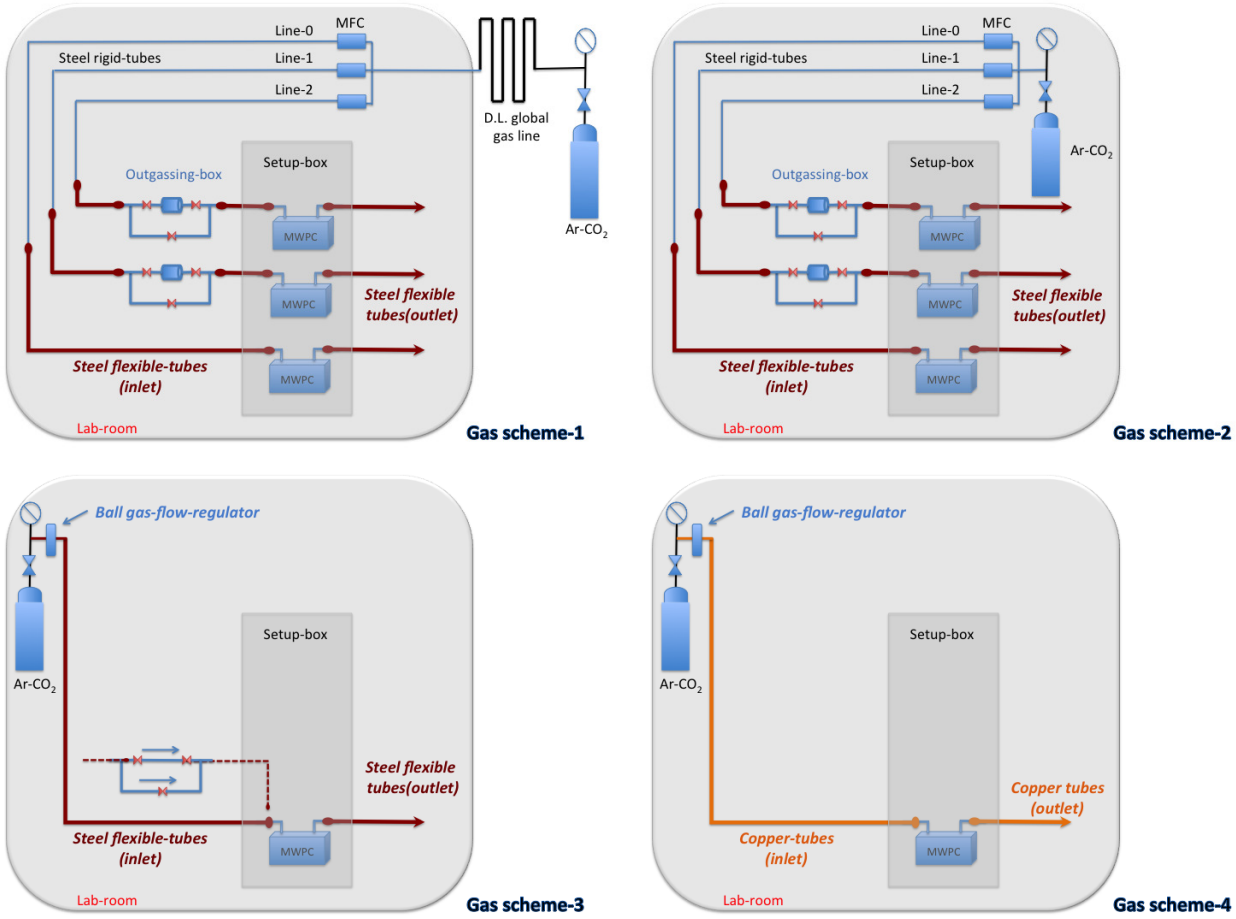

Figure 4.46: *Four schemes of gas lines used during the complete investigation of the setup cleanness*

carbon depositions on two probes of aged cathodes wires.

2. **Test with gas scheme-4**: The logical next step has been to test the gain stability of the new chamber using new, short and clean tubes. This test aimed to ensure there is no ageing effect of the chamber components. In the beginning of this test, scheme-4 of the gas system has been used. During 11 days of exposure to an iron source, it accumulated more than 80 μC. Stable gain has been obtained by this scheme, as seen in the black part of Figure 4.53. The small drop, about 1-2%, in the outset of gain measurement is always observed in the first 5μC of accumulated charge, which is considered as part of chamber conditioning in the beginning of test. To be sure that the ageing was ignited by the gas line and not by the chamber itself, the gas bottle was moved again to the outside of the lab and gas scheme-1 was used again. Again a clear gain drop has been observed as

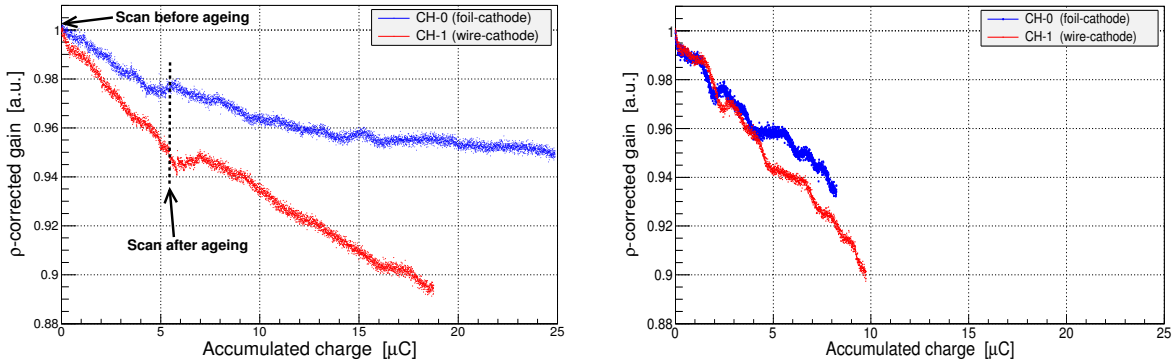

Figure 4.47: *Normalised gain (ρ-corrected gain) as a function of accumulated charge at CH-0 and CH-1 during two individual tests (left and right) after cleaning setup with procedure-1.*

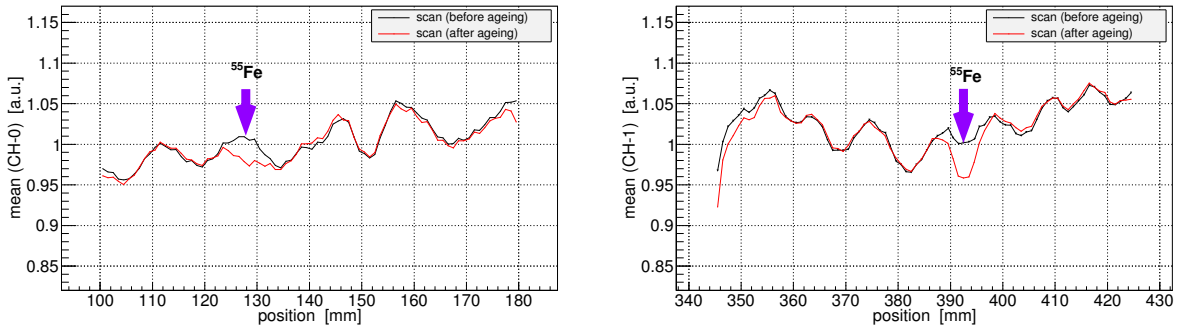

Figure 4.48: *Scan of mean of pulse height within the active area of CH-0 and CH-1 before (black) and after ageing (red).*

shown in the red part of Figure 4.53.

3. **Gas flow effect**: In this test, before changing the gas scheme used in the previous test, two tests with different gas flow rates have been implemented. The tests aimed to study if there is any effect of the gas flow rate to improve the gain behaviour, so the gas flow has been changed from 50 to 150 ml/min (from 2.5 chamber volume per hour (V/h) to 7.5 V/h). Figure 4.54 illustrates clear gain drop in both tests with small difference of ageing rate.

4. **Test with gas scheme-2**: From previous tests, it was clear that the contamination source should be followed point by point in the gas system. Due to that, this test aimed to use the gas scheme-2, which avoids the global gas lines of the lab. Therefore, the components in contact with the gas are: the mass flow controller,

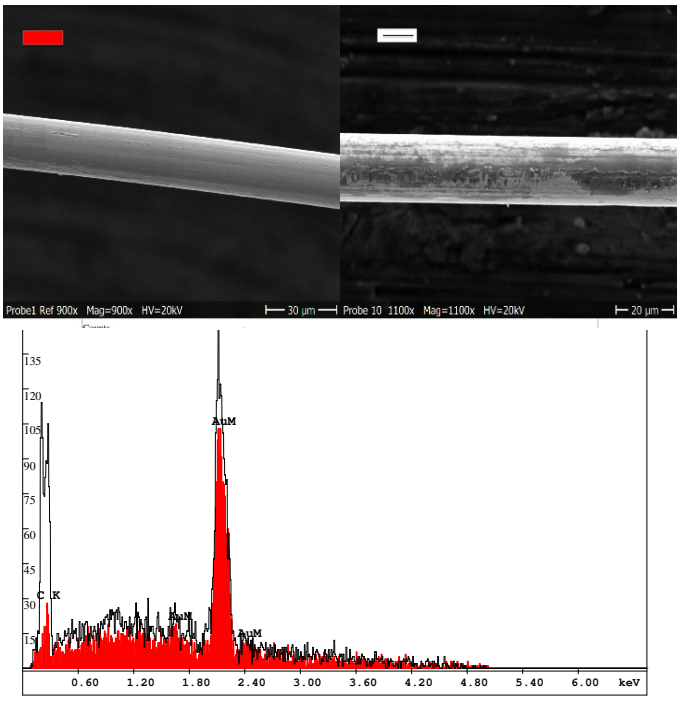

Figure 4.49: *upper: Pictures of fresh (red) and aged (line) anode wires. bottom: Overlap of microanalysis of fresh and aged anode wires.*

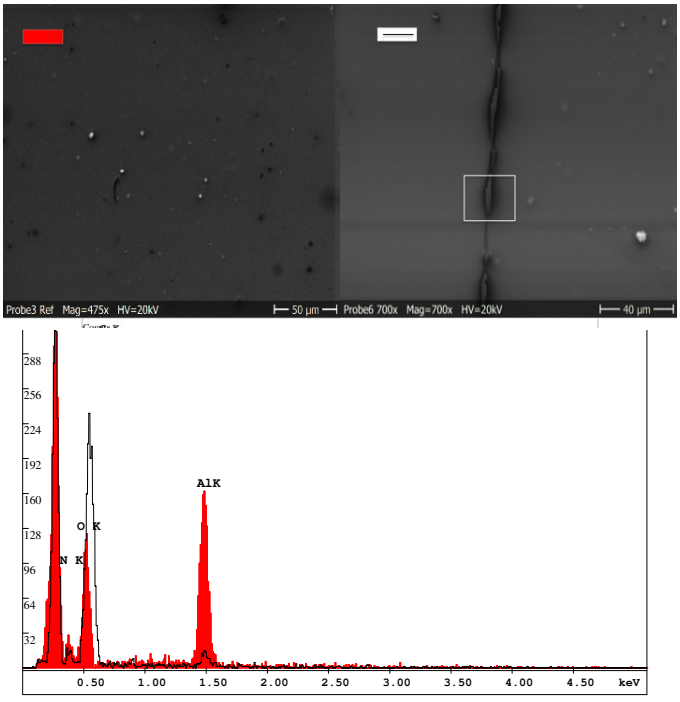

Figure 4.50: *upper: Pictures of fresh (red) and aged (line) cathode foils. bottom: Overlap of microanalysis of fresh and aged foils.*

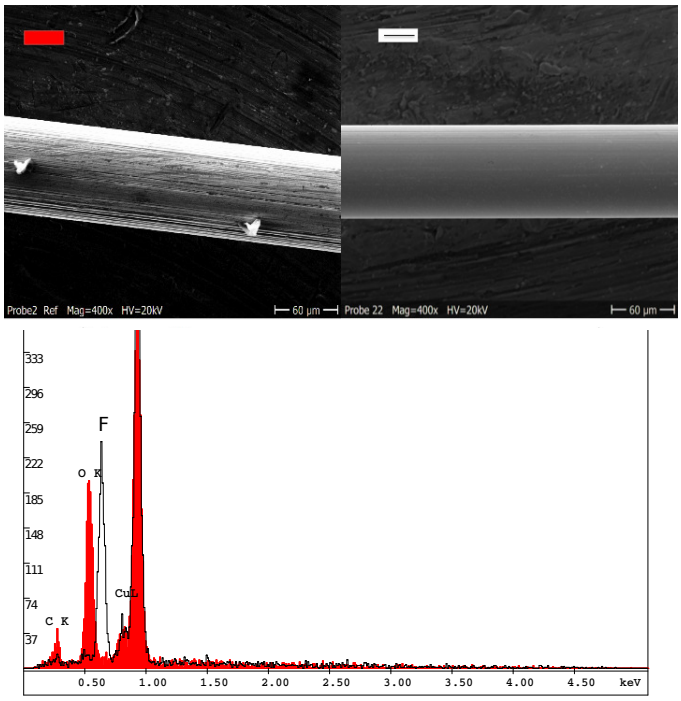

Figure 4.51: *upper: Pictures of fresh (red) and aged (line) cathode wires. bottom: Overlap of microanalysis of fresh and aged cathode wires.*

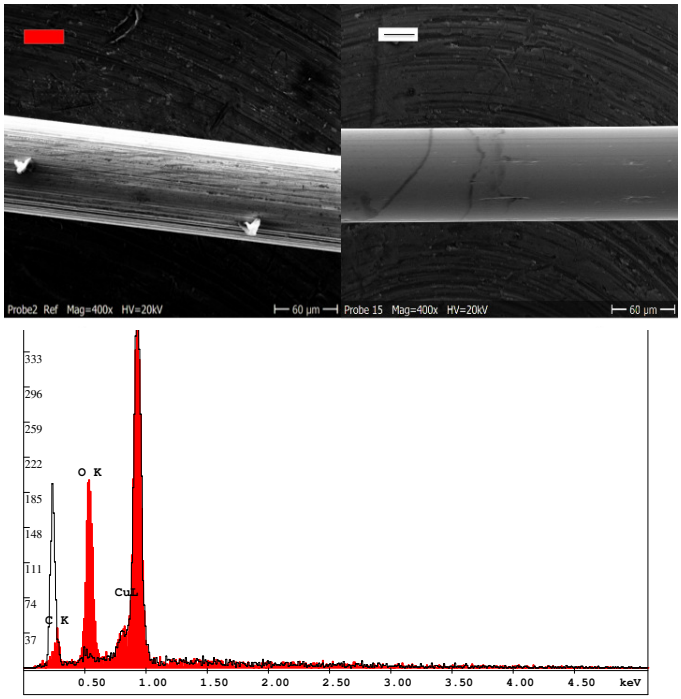

Figure 4.52: *upper: Pictures of fresh (red) and aged (line) cathode wires. bottom: Overlap of microanalysis of fresh and aged cathode wires.*

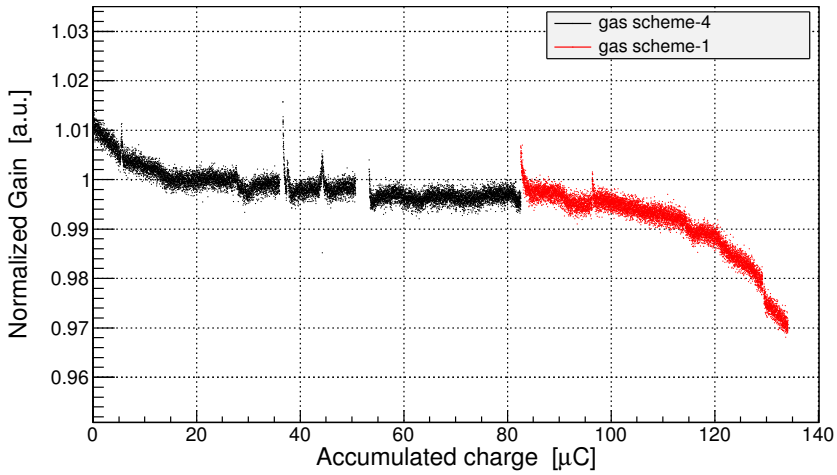

Figure 4.53: *Normalised gain (ρ-corrected gain) as a function of accumulated charge using gas scheme-4 (black) and scheme-1 (red).*

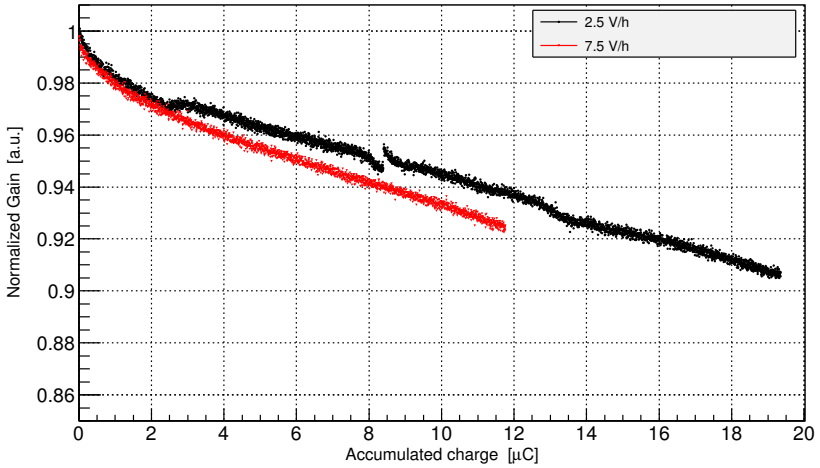

Figure 4.54: *Normalised gain (ρ-corrected gain) as a function of accumulated charge in two different rates of gas flow, using gas scheme-1.*

steel rigid tubes on the wall inside the lab, 3 flexible tubes and the chamber. Two tests have been carried out with this scheme. The left plot of Figure 4.55 shows clear gain drop after the chamber accumulated 27 μC. The right plot shows a higher ageing rate in the same chamber but in another iron spot.

5. **Test with scheme-3**: As was the result from previous tests, it is clear that the contamination source is still present in the rest of the components of the gas system. Consequently, another part of the system should be avoided, which

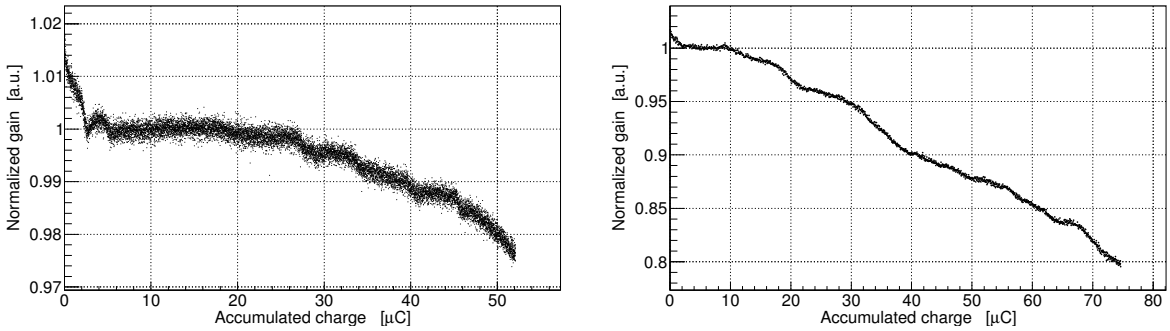

Figure 4.55: *Normalised gain (ρ-corrected gain) as a function of accumulated charge in two individual tests using gas scheme-2.*

resulted in scheme-3. In scheme-3, the gas is only in contact with flexible tubes and the chamber itself. Figure 4.56 shows clear ageing in this test, so the chamber lost about 5% after an accumulation of 37 μC of charge.

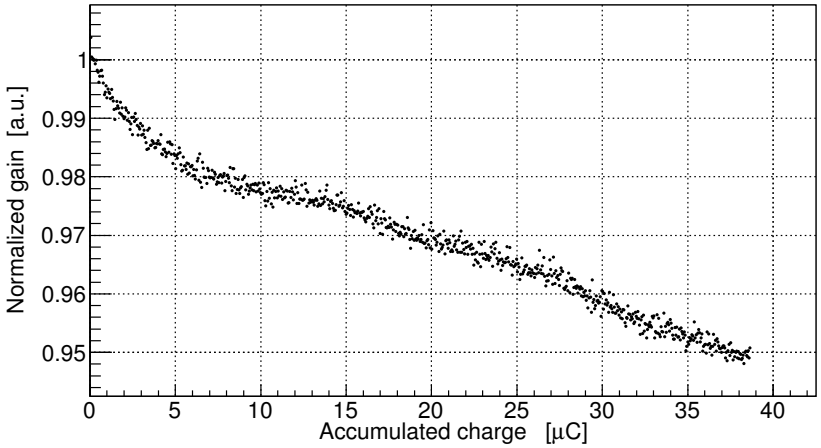

Figure 4.56: *Normalised gain (ρ-corrected gain) as a function of accumulated charge using gas scheme-3.*

6. **Test with scheme-4**: Using the same chamber as in the previous test, scheme-4 has been used in this step. This test aimed to determine whether the flexible tube is the contamination source. With these clean copper tubes, very stable behaviour has been achieved, as shown in Figure 4.57. So after an accumulation of about 80 μC, the gain variation is less than 1%. With returning to the flexible tube supplier, they were cleaned with a cleaning and degreasing agent is called commercially "A062-K21 hebro®lan TN" which contains: Phosphoric acid, Alkyl

alcohol, ethoxylate Methylethyl, ester, Amins, Alhkyldmiethyl and N-oxides. The ageing was attributed to exist of these materials in the gas lines.

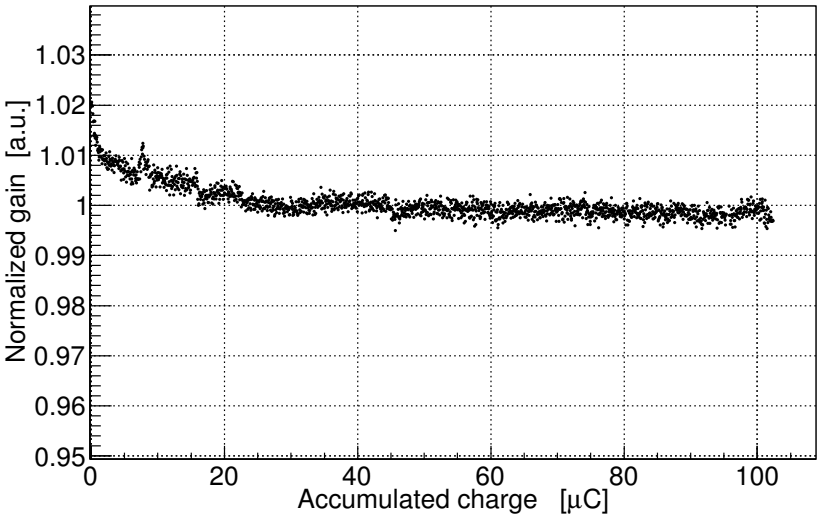

Figure 4.57: *Normalised gain (ρ-corrected gain) as a function of accumulated charge using gas scheme-4.*

7. **Setup cleaning by procedure-1**: Given that the flexible tubes are essential in a movable setup, they have been cleaned by cleaning procedure-1 and tested again. The result shown in Figure 4.58 presents that procedure-1 is not sufficient to clean the flexible tubes, which makes it necessary to look for an alternative effective method of cleaning. The picture in Figure 4.59 shows clear deposits on anode and cathode wires after this test.

8. **Setup cleaning by procedure-2**: A cleaning method has been proposed which includes an ultrasonic bath, named procedure-2. Utilising this second procedure, the flexible tubes, which caused ageing in the previous test, seemed to be clean and gave very stable results, as shown in Figure 4.60. Very stable normalised gain has been achieved, which was about 0.3% peak-to-peak as shown in Plots 1 and 2 as a function of accumulated charge and time respectively. While Plot 3 shows the RMS of the normalised gain is in the order of 0.06% after an accumulation of about 45μC. Figure 4.60(4) shows an ideal gain behaviour as a function of gas density as predicted in Figure 4.7.

Figure 4.61 summarises all investigations of setup cleanness during approximately eight months.

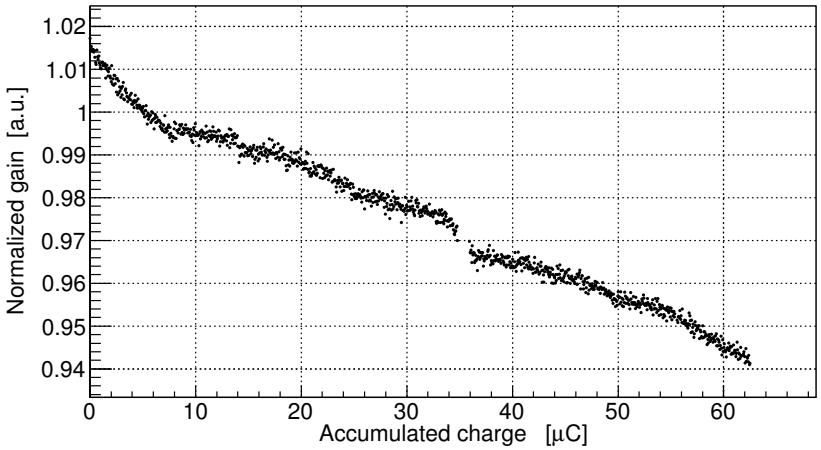

Figure 4.58: *Normalised gain (ρ-corrected gain) as a function of accumulated charge using gas scheme-3 after cleaning with procedure-1*

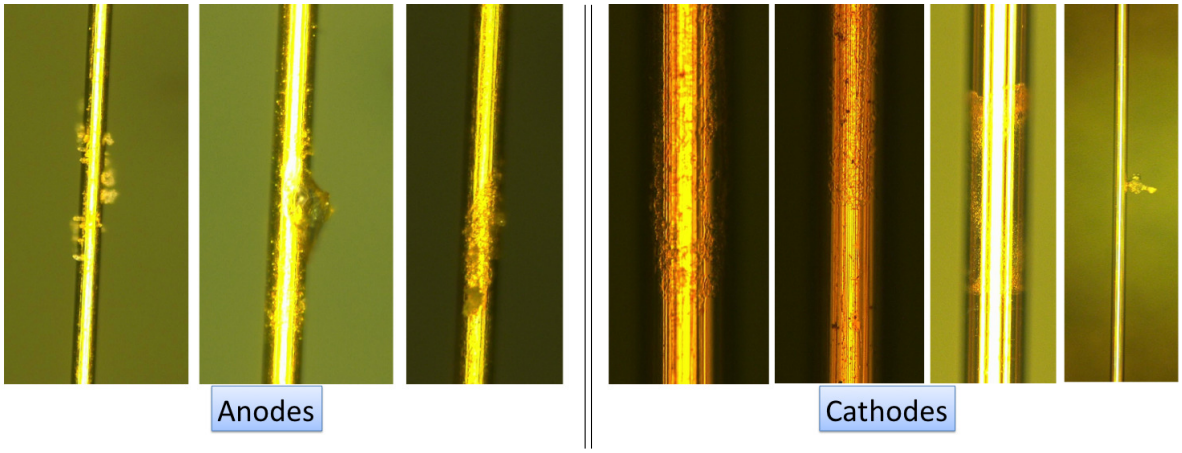

Figure 4.59: *Optical microscope pictures of aged anodes and cathodes using gas scheme-1 before cleaning.*

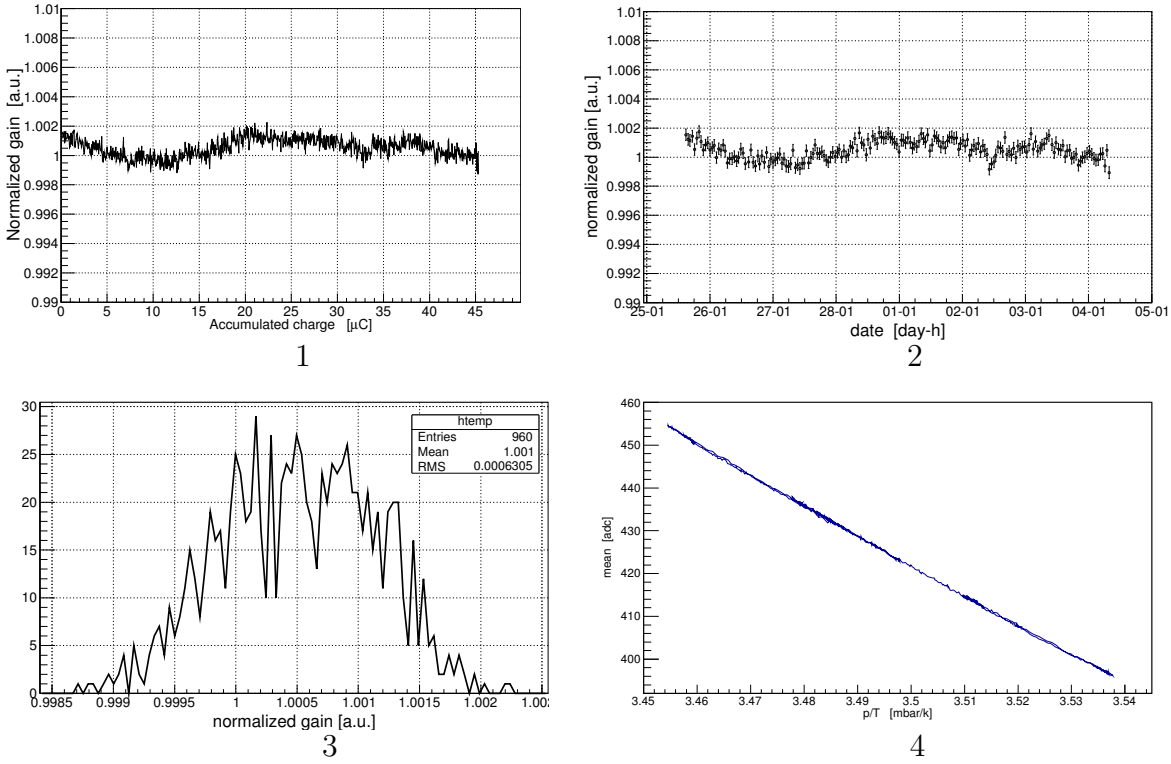

Figure 4.60: *(1) Normalised gain (ρ-corrected gain) as a function of accumulated charge. (2) Normalised gain (ρ-corrected gain) as a function of time. (3) Normalised gain deviation. (4) Mean of pulse height as a function of gas density.*

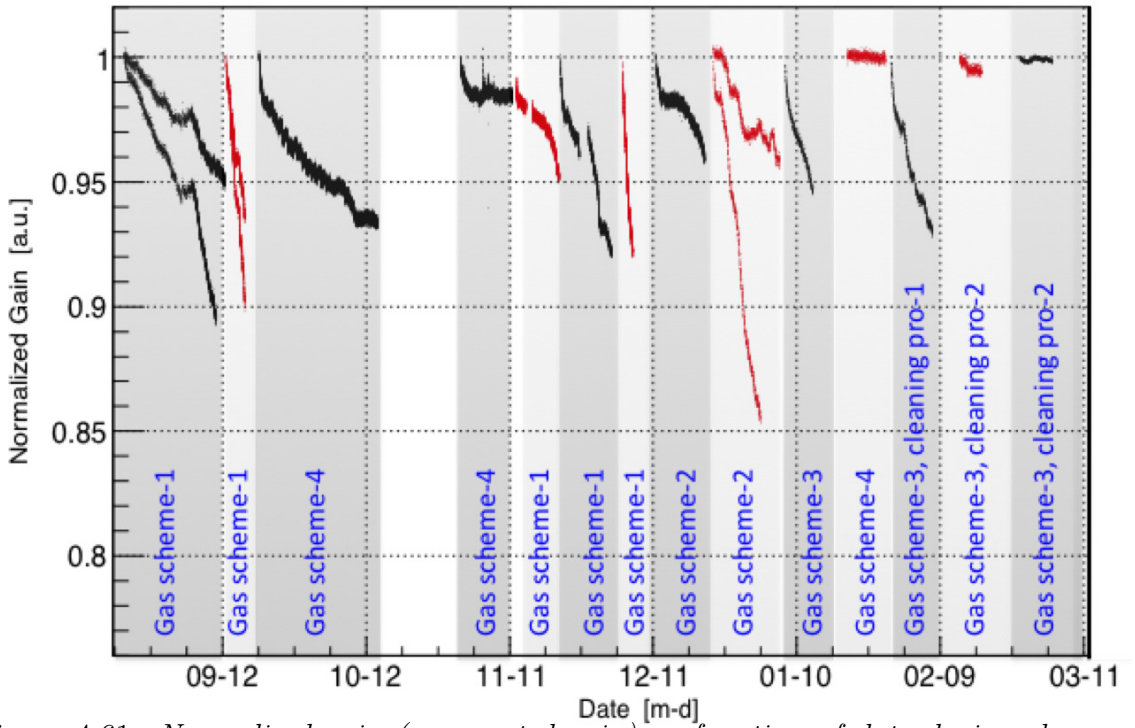

Figure 4.61: *Normalised gain (ρ-corrected gain) as function of date during cleanness investigations*

4.2.8 Full operation of the setup

According to the very stable normalised gain obtained after a successful cleaning of the flexible tubes, the setup was operated at full automatic function using three chambers in three clean parallel gas lines.

***Step-1**: Irradiation of the CH-1 and CH-2 with the X-ray generator through 3cm aperture*

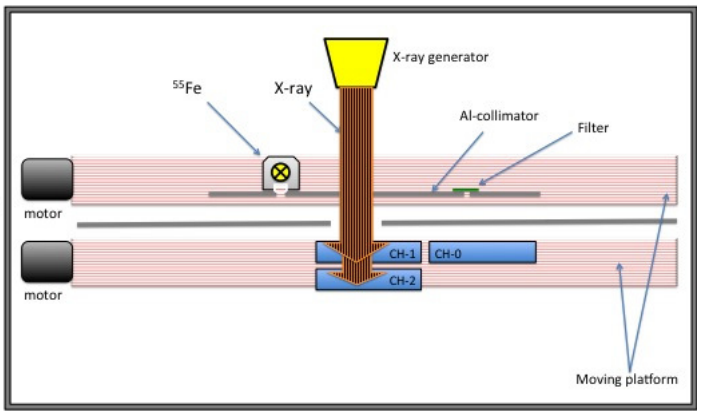

***Step-2 and 3**: Recording the mean of pulse height of ^{55}Fe for CH-1 and CH-2 in non-irradiated area*

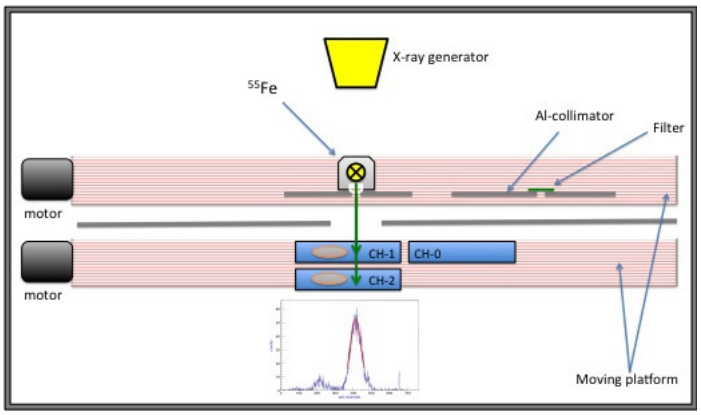

***Step-4**: Recording the mean of pulse height of ^{55}Fe for CH-0*

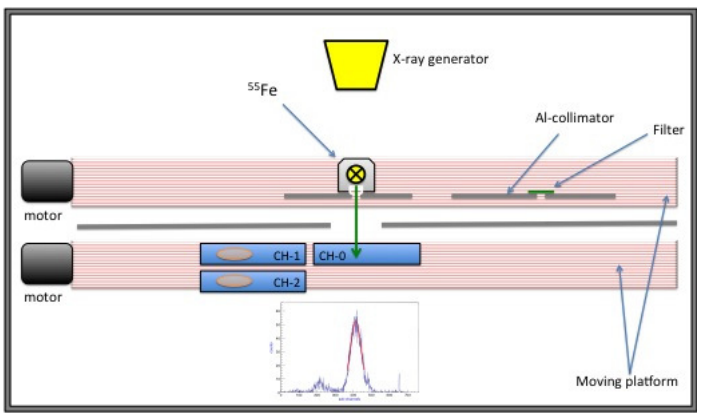

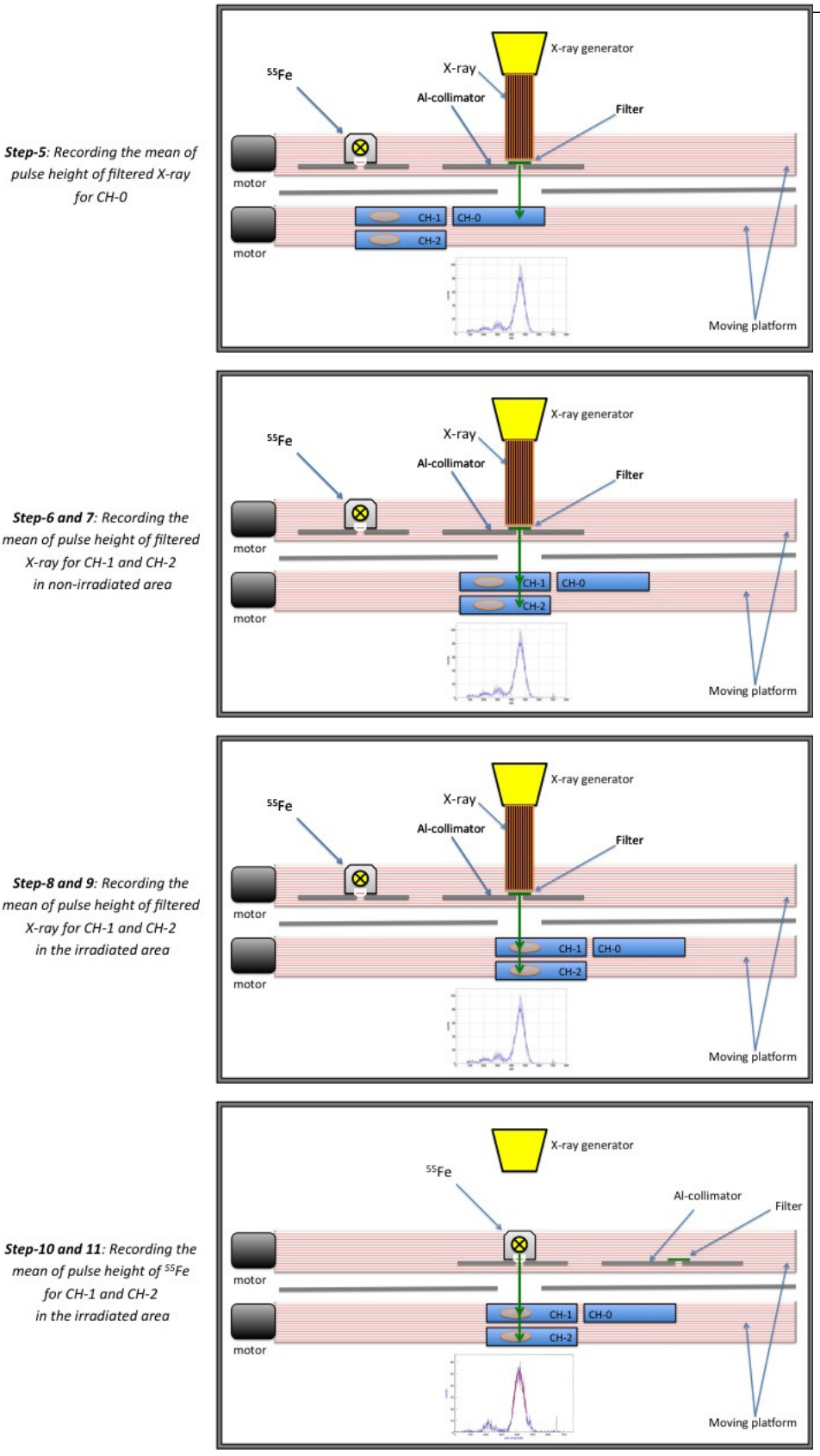

Figure 4.62: *Steps of the full operation of the automatic setup.*

The periodic steps of the full function of the setup, illustrated in the seven sketches in Figure 4.62, are respectively:

1. irradiation of CH-1 and CH-2 over 40 min through a 3 cm aperture by the X-ray generator.

2. recording the mean of pulse height of ^{55}Fe through a 1 mm aperture in a non-irradiated area of CH-1 and CH-2.

3. recording the mean of pulse height of ^{55}Fe through a 1 mm aperture in CH-0.

4. recording the mean of pulse height of the filtered X-ray through a 1 mm aperture in CH-0.

5. recording the mean of pulse height of the filtered X-ray through a 1 mm aperture in a non-irradiated area of CH-1 and CH-2.

6. recording the mean of pulse height of the filtered X-ray through a 1 mm aperture in the irradiated area of CH-1 and CH-2.

7. recording the mean of pulse height of ^{55}Fe through a 1 mm aperture in the irradiated area of CH-1 and CH-2.

According to these steps we have used the two main peaks of the ^{55}Fe spectrum and the filtered X-ray in separated spots for the gain diagnosis. Therefore, ten gain measurements were obtained: two in CH-0 as references, four in CH-1 (two for ageing measurement in the irradiated area and two as references in a non-irradiated area) and four in CH-2 (two for ageing measurement in the irradiated area and two as references in a non-irradiated area). Figures 4.63-4.67 illustrate the normalised gain (ρ-corrected gain) in all the ten spots as a function of time during nine days in clean conditions. The blue curve of Figure 4.63 shows very stable behaviour of the normalised gain in CH-0 over the ten days using ^{55}Fe, so it varies only $\sim$0.7% peak to peak. Whilst the black curve shows that the normalised gain, measured using the filtered X-ray, lost $\sim$3% of its initial value in the first five days, and it was stable in the last five days. This variety of the gain behaviour is attributed to the wire surface conditions since they used two different spots in the same chamber. The normalised gain in the non-irradiated area of CH-1 varies only $\sim$0.7% peak to peak for both spots that using ^{55}Fe (blue) and filter X-ray (black), as shown in In Figure 4.64. The normalised gain in the non-irradiated

area of CH-2 varies only ∼0.5% peak to peak in ^{55}Fe spot (blue) whilst it lost ∼1% in the first five days when using filter X-ray (black), as shown in In Figure 4.66. These six measurements reveals the ability to use the filtered X-ray for gain diagnosis in addition to the ^{55}Fe. Figure 4.65 and Figure 4.67 show the normalised gain in the irradiated area in CH-1 and CH-2 respectively. One can clearly see from both figures that the gain raised about 2% in the first four days which should be considered as conditioning irradiation period before starting ageing test with a specific material.
In the end of this test, the setup show high stability and ability to be used for precise ageing tests, as it will be discussed in Section 5.2.

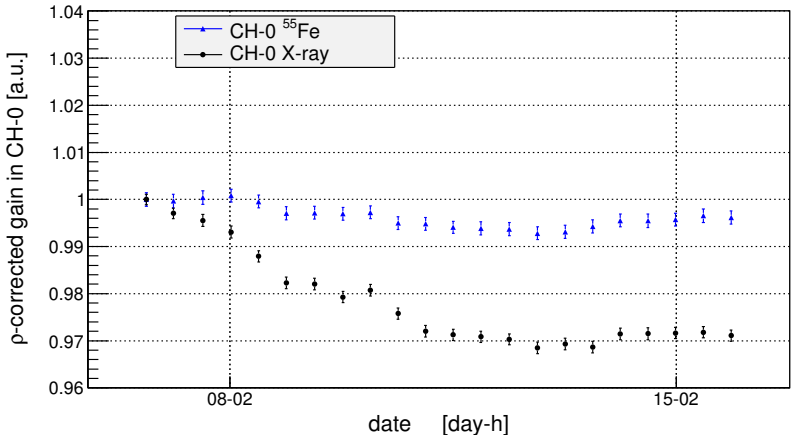

Figure 4.63: *The ρ-corrected gain of ^{55}Fe (blue) and the filtered X-ray (black) for CH-0 as a function of time.*

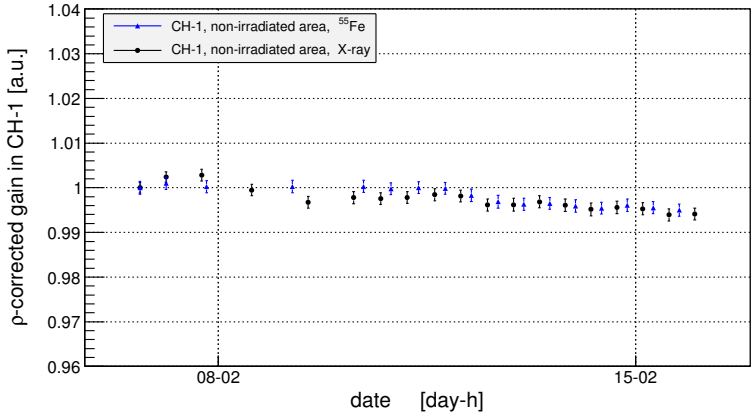

Figure 4.64: *The ρ-corrected gain of ^{55}Fe (blue) and the filtered X-ray (black) for the non-irradiated area of CH-1 as a function of time.*

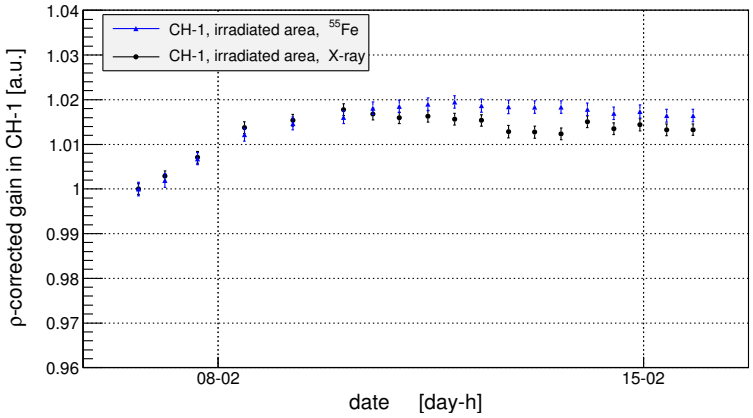

Figure 4.65: *The ρ-corrected gain of ^{55}Fe (blue) and the filtered X-ray (black) for the irradiated area of CH-1 as a function of time.*

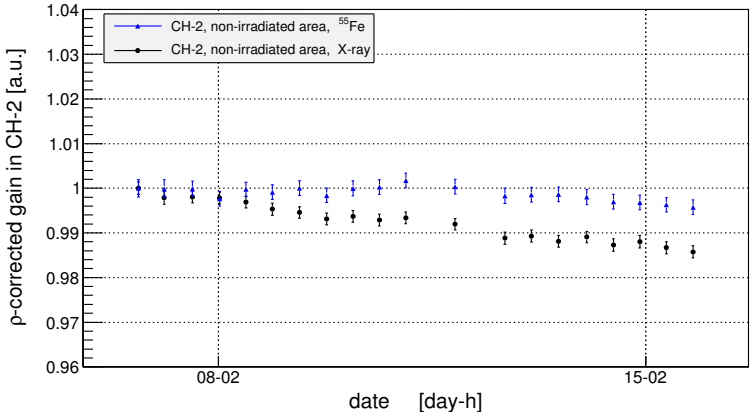

Figure 4.66: *The ρ-corrected gain of ^{55}Fe (blue) and the filtered X-ray (black) for the non-irradiated area of CH-2 as a function of time.*

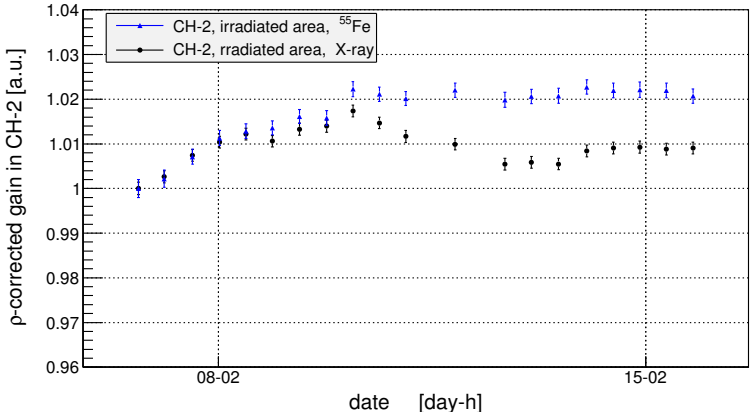

Figure 4.67: *The ρ-corrected gain of ^{55}Fe (blue) and the filtered X-ray (black) for the irradiated area of CH-2 as a function of time.*

Chapter 5

Ageing tests

5.1 Ageing test during the preparation tests

During the setup developments discussed in the previous chapter, several ageing tests were performed. Many goals were behind such tests, among them: developing the procedure of ageing investigations, obtaining the desired precise measurements of ambient conditions (e.g. temperature and pressure), reaching the appropriate approach of ageing acceleration, obtaining the suitable gas flow rate, controlling the contamination level at the setup, identifying the proper curing time of the ageing samples and testing the tolerance of the chamber components.

5.1.1 Ageing test of RTV-3145 using X-ray generator

In the very early stage of our setup construction, an ageing test of the glue Dow Corning RTV-3145 was performed. It was carried out with the procedure detailed in Section 4.1.7.1 utilising the old setup sketched in Figure 4.1. It was based on two wire chambers as shown in Figure 4.4, one of them as an ageing chamber and the other as a reference. Fresh counting gas (Ar-CO_2, 80/20) was flushed first through the reference chamber, then was exposed to the sample in the outguessing box and finally reached the ageing chamber, which in turn was exposed to 500 kHz of X-rays coming from the copper anode X-ray generator. While the ageing chamber received contaminant as well as X-ray exposure in a circle area of 3 cm diameter, the reference chamber was flushed with clean gas only and was exposed exclusively to a comparatively low intensity radioactive X-ray source ^{55}Fe for characterisation and diagnostic purposes. These 5.9 keV

single line X-rays entered the reference chamber, as well as simultaneously the ageing chamber, through a small pinhole, 1 mm in diameter, in their rear sides. The sample

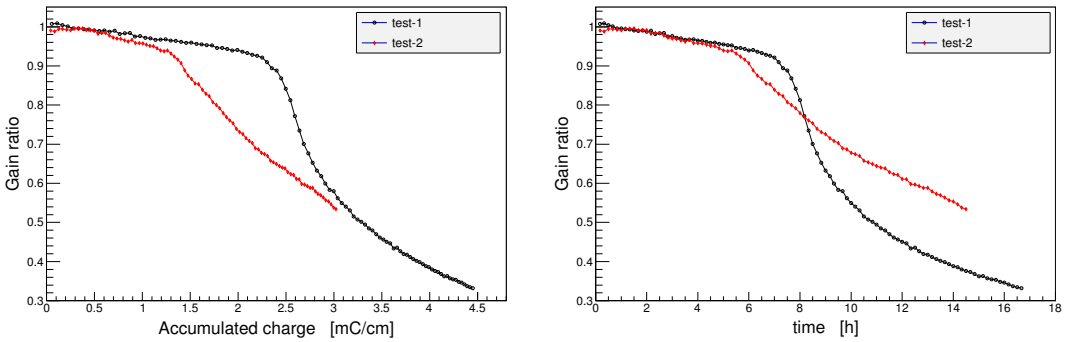

Figure 5.1: *Normalised gain as a function of accumulated charge (left) and as a function of time (right) during two ageing tests of RTV-3145 using X-ray generator.*

was prepared from a fresh tube of RTV-3145, which was applied to microscope glass sample holders and left to cure at ambient humidity for 24 h. The coatings had a size of about 100 cm^2 and a thickness of about 200 micrometers.
Immediately, a continuous drop of the gain ratio (gain of ageing chamber to reference) was observed, which after 8 hours became a steep drop, as the black curve in Figure 5.1. Therefore, the left plot in this figure represents the normalised gain as a function of the overall cumulated charge per 1 cm of wire length as determined through the continuous measurements of current in ageing chamber during exposure, whereas the right plot represents the normalised gain over the measurement period. The initially slower drop might be attributed to the anode wires being covered with deposits little by little. The steep fall of the gain after 8 hours of exposure could be attributed to the wires at that instant being fully covered with deposits, creating an insulating layer on the wires. With these enormous effects observed, doubts arose on whether the sample was left to cure sufficiently prior to the test. Thus, the ageing test was repeated with a new set of clean MWPCs. However, practically the same ageing effects were observed with these samples, which at the time of the second test had cured for about five days. Table 5.1 summarises the gain loss and the ageing rate calculated by Formula 4.6 during both tests (RTV-X_1, RTV-X_2).

A clear conclusion is that a silicon base glue RTV-3145 causes wire chambers to age at a disastrous rate of total failure within one day. Even though, in a real detector,

Table 5.1: *Gain loss and ageing rate obtained with RTV-3145 tests.*

test	Irradiation source	Sample curing time (day)	particle rate density (kHz/cm)	Gain loss (%)	Accumulated charge (mC/cm)	Ageing rate (%/mC/cm)
RTV-X_1	^{55}Fe+X-ray	1	0.8+ 21	67	4.4	15.2
RTV-X_2	^{55}Fe+X-ray	5	0.7+20.4	46	3	15.3
RTV-Fe	^{55}Fe	80	7	7.5	0.1	75

exposed surfaces may be held at much smaller areas, immediate and tremendous effects are to be expected.

5.1.2 Ageing test of RTV-3145 using ^{55}Fe

In this test, two fresh chambers were used in an identical scheme to that used in the previous test. The RTV-3145 sample had cured for two and half months at the beginning of this test. Ageing and reference chambers were being continuously exposed only to ^{55}Fe via 1 mm diameter aperture, unlike the ageing chamber in the previous test which was being exposed to ^{55}Fe and X-ray generator. During the 16 hour period of the test, the ageing chamber accumulated about 10 μC/mm, and it lost about 7.5% of its initial gain as shown in the upper plot of Figure 5.2. The lower plot shows a clear rise in ageing chamber resolution after 14 hours from the outset. As in the previous test, the same behaviour of slow gain drop was observed in the first six hours and a steep drop after that. Table 5.1 compares the gain loss and the ageing rate in this test (RTV-Fe) and the two tests in the previous section. From ageing rate values, it is clear that the ageing rate during exposure to the iron source only is greater than the ageing rate when it is exposed to iron source and X-ray generator. According to the inequality of the ageing rate in these three tests, deeper systematic studies had to be held to investigate the photon source effect on ageing rate.

5.1.3 Sample curing effect on ageing rate

During this test, the curing time of the material under test was studied by the setup sketched in Figure 4.24. The test was carried out over two intervals. In the first interval, five slices were painted with the glue Dow Corning RTV-3145 one year and four months prior and inserted in the outgassing box. The ageing chamber was exposed to the contaminated gas and 320 kHz of X-ray (emitting from the generator) over 210 hours. Meanwhile, in the second interval, the old curing sample was replaced

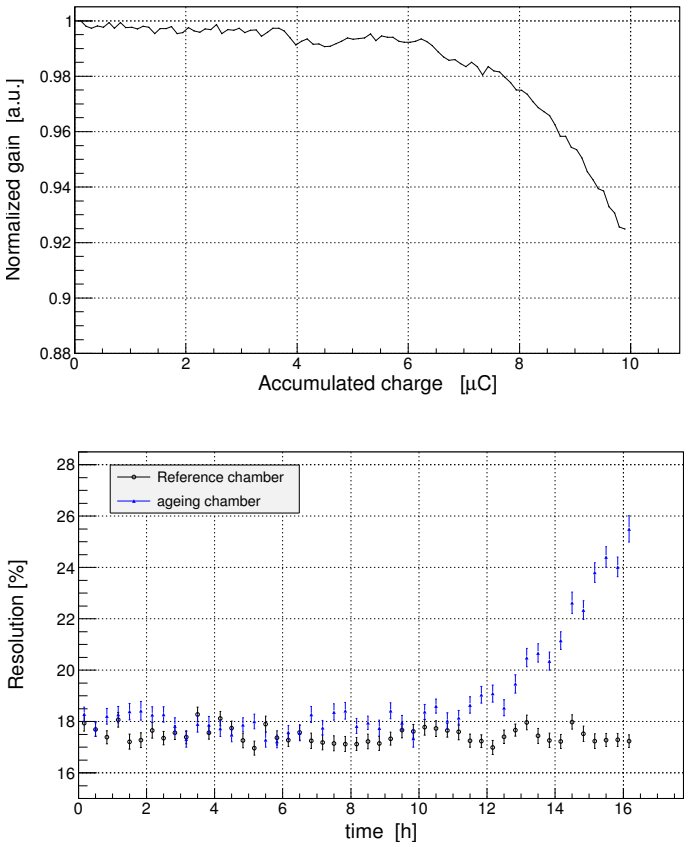

Figure 5.2: *Normalised gain (ρ-corrected gain) as a function of accumulated charge (upper) and resolution of ageing (blue) and reference (black) chambers as a function of time (lower) during an ageing test of RTV-3145 using iron source only.*

with one-day curing slices of the same material. Then the test was continued using the same chambers and the same approach. Figure 5.3 illustrates a clear drop of the normalised gain after inserting the short time curing sample. One can easily observe the importance of the curing time of the materials being tested, which means that the material under question should be cured over a comparable time to that in the real experiments.

5.1.4 Gas flow rate effect on ageing rate

Gas flow rate (GFR) is an important factor affecting ageing rate in gaseous detectors. Setup in Figure 4.24, equipped with two fresh chambers, was used to evaluate GFR effect in our setup. For that, one day curing slices painted with RTV-3145 were inserted in the outgassing box at the beginning of this test. The contaminated chamber (ageing)

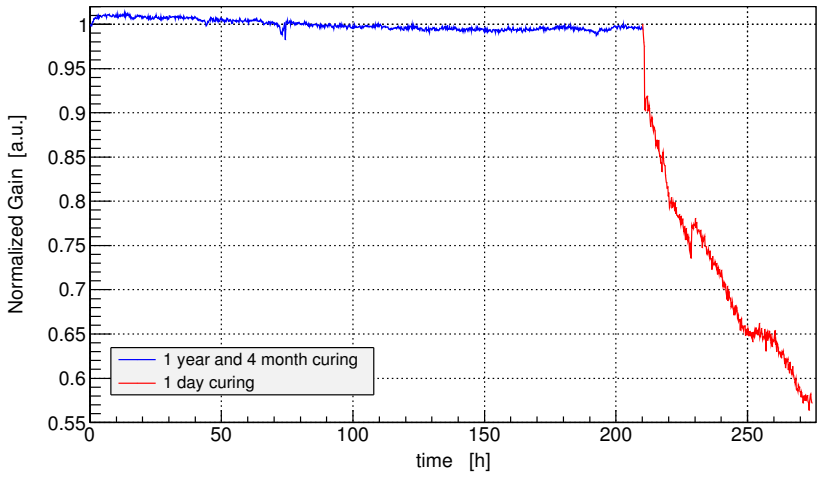

Figure 5.3: *blue: Normalised gain of a chamber contaminated with RTV-3145 cured for 1 year and 4 months. red: Normalised gain of a chamber contaminated with RTV-3145 cured for 1 day as a function of time.*

was irradiated over 10 min with X-ray, then ageing and reference gain were diagnosed by means of pulse height of the iron source in 1 min and so on. After 54 hours from the start, the gas flow rate was changed in the ageing chamber line from 25 ml/min to 50 ml/min. This resulted in a clear shift of the normalised gain gradient coinciding with the change of the gas flow rate as shown in Figure 5.4. This obvious correlation of ageing rate and gas flow rate proves the importance of this factor, which should be kept constant during the investigation of other factors.

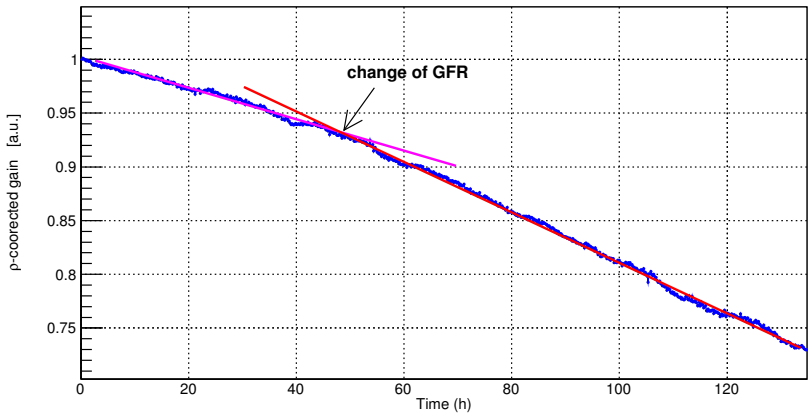

Figure 5.4: *Normalised gain of a contaminated chamber as a function of irradiation hours in two different gas flows.*

5.1.5 Ageing test of Durostone and Ar-Isobutane gas

A fibreglass material named "Durostone" is used to build frames or wire holders in gaseous detectors. Ageing effect of this material was investigated in a system filled with a gas composed of Argon and Isobutane with ratio of $(84\% - 16\%)$ respectively. This test was carried out with the system sketched in Figure 4.1. In total, five slides of the Durostone fibreglass were inserted in the outgassing box to be flushed with the Ar-Isobutane gas, which flowed afterwards to the ageing chamber. The irradiation process of the chambers was exactly like the process discussed in Section 5.1.1. After five days, the period of the test, the ageing chamber accumulated about 33 mC/cm of the wire length, resulting from the exposure to 523 kHz of X-ray generator photons. From Figure 5.5 (left), one can clearly see the high fluctuation of the normalised gain (gain ratio) which resulted from the fluctuation of the mean of pulse height in both chambers. This behaviour, for which we couldn't find any explanation, appeared in this test only when Isobutane was used. At the end of this test, the ageing chamber lost about 6% of its initial gain, with an ageing rate of about 0.18 %/mC/cm. This gain loss is attributed to polymer deposition on anode wires and cathode foils, as shown in Figure 5.5 (right). These polymers are resultant to polymerisation of the isobutane fragmentations, since this clear deposition had never been observed when Ar-CO_2 was used in all the tests.

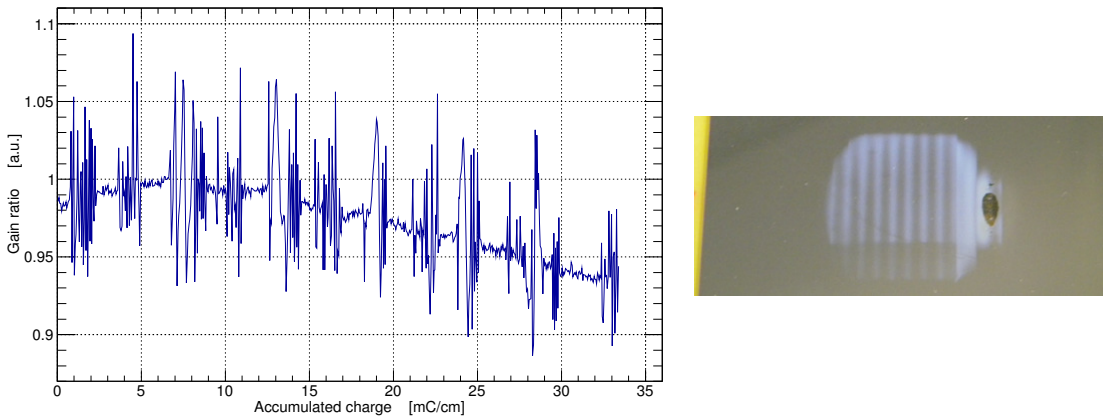

Figure 5.5: *The gain ratio of the ageing chamber to the reference as a function of the accumulated charge (left), the polymers deposited on the cathode foil using Ar-Isobutane gas mixture(right)*

5.1.6 Ageing test of Vetronit G11, Micro 3000 and Ar-CO_2 gas

Four ageing tests of the influence of a fibreglass material (Vetronit G11 produced by VonRoll Holding Ltd.) and sawing liquid (Micro 3000 produced by Microjet GmbH) were carried out. Six slides of G11 with a size of 6×2.5 cm^2 were inserted in the outgassing box. The first two tests ($G11_1$ and $G11_2$) were done with new and clean G11 slices, while the later two (G11+$Mi3000_1$ and G11+$Mi3000_2$) studied G11 slices painted with sawing liquid (Micro 3000 produced by Microjet GmbH) which consists of alcohol and synthetic ester. All were carried out with the old setup sketched in Figure 4.24, using the same test procedure used in the previous section. In all of them, the ageing chamber was irradiated by the X-ray generator over a circle area of 3 cm diameter . The four plots in Figure 5.6 illustrate the normalised gain (ρ-corrected gain) of the ageing chambers in all the tests as a function of accumulated charge per unit length of the anode wires. No loss of gain or resolution has been observed at all four tests after accumulation of 10.2, 7, 4.3 and 8 mC/cm. Table 5.2 summarises the conditions and the results of these tests.

Table 5.2: *Ageing rate of irradiated and non-irradiated chambers in ageing tests during four tests of Vetronit G11 and Micro 3000.*

test	photon source	particle rate density (kHz/cm)	Accumulated charge (mC/cm)	Ageing rate (%/mC/cm)	Resolution loss (%)
$G11_1$	^{55}Fe+X-ray	2.7+13	10.2	0	0
$G11_2$	^{55}Fe+X-ray	2.7+13	7	0	0
G11+$Mi3000_1$	^{55}Fe+X-ray	2.4+14	4.3	0	0
G11+$Mi3000_2$	^{55}Fe+X-ray	2.4+12.7	8	0	0

5.2 Ageing test for RTV-3145 and Gerband 705 with full automatic operation of the setup

After the stable automatic operation of the new setup, discussed in Section 4.2.8, two materials were tested in parallel over two weeks with same steps. Aluminium tape named Gerband 705 was inserted in the line-1 and RTV-3145 was inserted in the line-2. After about two weeks of material tests, ageing rate caused by Gerband 705 was about 0.3%/mC/cm while it was 3%/mC/cm for RTV-3145. The upper plot of Figure 5.7 illustrates the normalised gain of CH-1 (blue) and CH-2 (black) as a function of time. The chamber contaminated with Gerband 705 lost about 12% of its

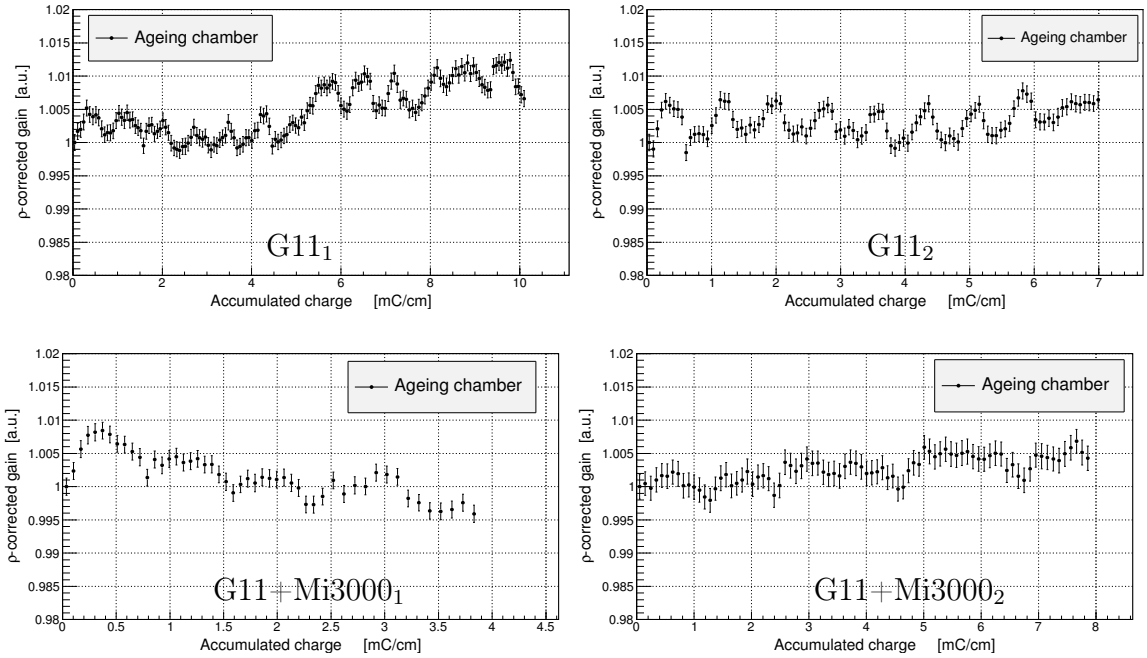

Figure 5.6: *Normalised gain of ageing chambers as a function of time during two tests of clean slides of G11 (upper) and two tests of G11 slides contaminated with Micro 3000 (lower).*

initial value after accumulating of 42 mC/cm. The chamber contaminated with RTV-3145 lost about 40% of its initial value after accumulating of 13 mC/cm as shown in the middle plot of Figure 5.7. The lower plot shows that the energy resolution of the chamber contaminated with Gerband 705 raised about 4% of its initial value while the chamber contaminated with RTV-3145 raised only 1.5%. Table 5.3 summarises the conditions of the particle rate during the test as well as the final accumulated charge and the ageing rates caused by the materials.

Table 5.3: *Ageing test conditions and results of RTV and Gebrand 705 ageing tests.*

Chamber	photon source	particle rate density (kHz/cm)	Accumulated charge (mC/cm)	Ageing rate (%/mC/cm)	Resolution loss (%)
CH-1 (Gerband 705)	^{55}Fe + X-ray	0.8 + 22	42	0.3	4
CH-2 (RTV)	^{55}Fe + X-ray	0.5 + 15	12	3	1.5

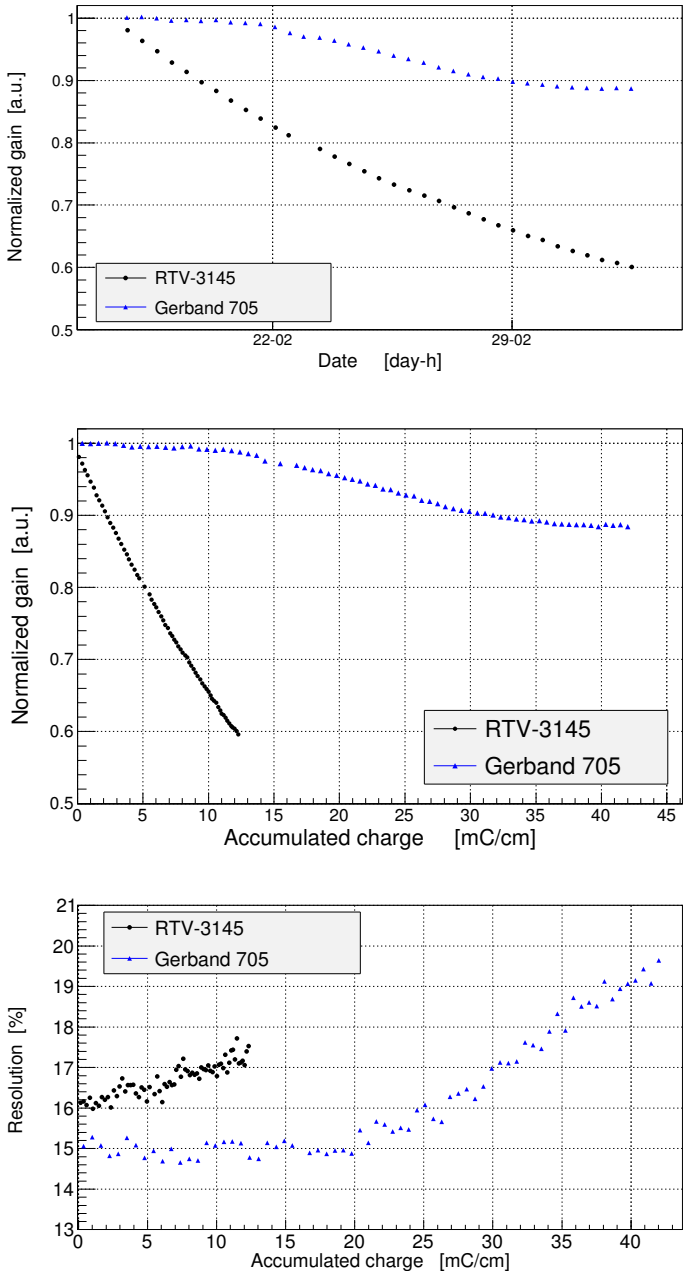

Figure 5.7: *upper: Normalised gain of chamber tested with Gerband 705 (blue) and chamber tested with RTV-3145 (black) as a function of time. middle: Normalised gain of chamber tested with Gerband 705 (blue) and chamber tested with RTV-3145 (black) as a function of accumulated charge per unit length of the anode wires . lower: Resolution of both chambers as a function of accumulated charge.*

Chapter 6

Summary and outlook

Employing gaseous detectors in high-rate particle or nuclear physics experiments requires to thoroughly test all detector construction materials in terms of ageing. For this reason, studies of detector ageing induced by construction materials have been conducted in many laboratories. Eventually, tolerable ageing behaviour had been concluded from laboratory tests employing intense radioactive sources. However, when used in actual experiments with particle beam different ageing rates had been observed. This difference is attributed to differences of detector conditions from the lab to the real experiments such as particle rates and types. Therefore, to avoid this ambiguities as much as possible it is mandatory to perform these ageing tests using a very precise setup. With accurate measurements, it is possible to carry out laboratory ageing tests using low irradiation rates which are comparable to those in the actual experiments in acceptable periods of measurement time. Within this thesis project, we have constructed and commissioned a setup which is sensitive to ageing effect in gaseous detectors, induced by the detector construction material or the chosen operating gas itself. Building of this setup has been done over two steps: 1) preparatory and characterisation tests and 2) commissioning a fully automated ageing setup.

6.1 Findings from the preparatory tests

At the beginning of this project, an existing setup in the detector laboratory of GSI has been utilised to identify all parameters and components relevant for ageing tests. Based on this, the properties and characteristics that must be met to build and operate a high precision ageing setup were selected. The existing setup consisted of two identical

Multi Wire Proportional Chambers (MWPCs), an X-ray generator with copper anode, an ^{55}Fe source and an outgassing box. The chamber design has been optimised using a combination of the gas simulation program (Magboltz) and the electric field simulation program (Garfield). An operating gas mixture of Argon (Ar) and CO_2 in the ratio of 80% to 20% respectively has been selected because this gas does not polymerise under irradiation such as hydrocarbon gases. For gain value measurement, a calibration of the ADC and the preamplifier has been performed. It is of utmost importance for our objectives to obtain stable gain measurements with the systematic variations of the normalised gain (i.e., pressure and temperature corrected gain) as low as possible. Thus, for the gain measurement several improvements of the setup have been implemented, which include the chamber design, chamber cathodes, schema of the gas lines and the gas mixing approach. The original chambers had a wire plane as anode and two aluminium-Kapton foils which served as cathodes and gas sealing windows, at the same time. With this design, the variation of the ambient pressure was causing a curvature of the windows that causes a variation of the electric field inside the chamber. This was solved with double foil windows which separated the gas sealing (outer foil) from the definition of the electrostatic geometry (inner foil). Clear signs of sputtering of the aluminium layer appeared on the cathode foils when the detector was exposed to the X-ray radiation over about one week. Therefore, the aluminium-Kapton foils were replaced with cathode wire planes. For better shielding and gas temperature measurement, the fibreglass housing of the chamber has been changed to aluminum. The lab temperature variation influenced the mass flow controllers (MFC) of the mixing station which causes a variation of the gas composition. Due to that, a premixed gas bottle of Ar/CO_2 (80/20) was used instead of the mixing station. Generally it was found that it is of paramount importance to ensure the cleanness of all components during the construction of the new setup.

6.2 Assembly and commissioning of the ageing setup

A new setup has been designed and built in the GSI detector laboratory. The setup consisted of three identical Multi Wire Proportional Chambers (MWPCs) mounted onto a moving platform, an X-ray generator and an ^{55}Fe source. A second moving platform holds an aluminium collimator plate which has three different apertures, thus allowing to vary the irradiated spot size. The new ageing setup has been equipped with

a data acquisition and control system enabling fully automated measurement during long term tests. Three gas lines with individual Mass Flow Controller (MFC) were used. Outgassing boxes are in two lines. Before fabrication of the chambers, simulations of their electric field and gain had been done using a combination of the gas simulation program (*Magboltz*) and the electric field simulation program (*Garfield*). The accuracy of the gas temperature measurement has been greatly improved which allows a very accurate gain normalisation. Over a period of eight months, cleaning procedures have been developed and all sources of contamination of the equipment have been eliminated. Thereafter, the setup has been operated with very stable behaviour, evidenced by the fact that around 0.3% peak-to-peak residual variation of the normalised gain has been achieved. Thus the setup shows the required high stability to be used for precise ageing studies.

6.3 Ageing tests

During the development of the setup, several ageing tests were performed. These tests aimed at the development of the procedure of ageing investigations, i.e., obtaining the desired precise measurements of ambient conditions (e.g. temperature and pressure), reaching the appropriate ageing acceleration, obtaining the proper gas flow rate, controlling the contamination level at the setup and identifying the suitable curing time of the ageing samples. The results can be summarised as follows:

1. RTV-3145 is poisonous and must avoided within the gas volume of MWPC detectors or anywhere in the gas supplying infrastructure.

2. The difference of the curing period of samples (e.g. glues) and gas flow rate were found to affect the ageing rate in our setup. These factors must be taken into account to obtain comparable results.

3. Ageing test with only the ^{55}Fe has shown faster ageing than when irradiated with X-ray generator at different particle rate densities. The difference of ageing rate due to the irradiation source and the particle rate density should be investigated in the future work.

The Al-tape (Gerband 705) has been tested. It reveals dangerous effect in terms of ageing on a MWPC during exposure to X-ray with particle rate density in order of

22 kHz/cm. It caused the MWPC to lose 0.3%/mC/cm of its primary gain. Ageing effect of a fibreglass material named "Durostone" was investigated in a system filled with a gas composed of Argon and Isobutane with ratio of (84%/16%) respectively. At the end of this test, the ageing chamber had lost about 6% of its initial gain, with an ageing rate of about 0.18 %/mC/cm. This gain loss is attributed to polymer deposition on electrodes, which are attributed to polymerisation of the isobutane fragmentations, since this clear deposition had never been observed while using the Ar-CO_2 mixture. Ageing tests of the influence of a fibreglass material (Vetronit G11 produced by VonRoll Holding Ltd.) and sawing liquid (Micro 3000 produced by Microjet GmbH) flushed with Ar/CO_2 have been carried out. No loss of gain or resolution has been observed at their tests.

6.4 Outlook for future work

After obtaining satisfactory operation of our apparatus, a number of systematic investigations should to be performed in the future tests. The impact of several factors on ageing rate should be studied systematically, such as the effect of particle density and type, irradiation area, gas flow rate, wire quality, gas gain and temperature of the tested sample. It might further be of advantage to upgrade the setup by adding more chambers and gas lines, which would be able to operate more than three chambers in parallel.

Zusammenfassung

Der Einsatz von Gasdetektoren in Teilchen- und Kernphysikexperimenten mit hohen Raten erfordert eine gründliche Untersuchung aller Komponenten im Hinblick auf Alterungsphänomene. Daher gehören die Untersuchung der Alterung von Detektoren aufgrund der bei ihrer Konstruktion verwendeten Materialien oder des Betriebsgases zu den Standardmessungen in vielen Detektorlaboratorien. Basierend auf Labortests mit radioaktiven Quellen hoher Intensität kann man das noch tolerierbare Alterungsverhalten von Detektoren bestimmen. Wenn sie jedoch in Experimenten mit Teilchenstrahlen eingesetzt werden, können abweichende Alterungsraten beobachtet werden. Dieses Verhalten ist unterschiedlichen Betriebsbedingungen von Labortests und realen Experimenten zuzuschreiben, wie z.B. unterschiedliche Teilchenraten und -arten. Daher ist es zwingend notwendig, Alterungstests unter Verwendung eines sehr präzisen Messaufbaus durchzuführen, um eine möglichst genaue Beurteilung des Alterungsverhalten treffen zu können. Mit genauen Messungen ist es in akzeptabler Messdauer möglich, schon mit geringen Bestrahlungsraten Alterungstests im Labor durchzuführen, die mit Experimentbedingungen vergleichbar sind. Im Rahmen dieser Dissertation wurde ein Messaufbau konstruiert und in Betrieb genommen, welcher sensitiv auf Alterungseffekte in Gasdetektoren ist, die durch die Detektorbaumaterialien oder das Betriebsgas hervorgerufen werden. Die Konstruktion des Aufbaus wurde in zwei Schritten durchgeführt: 1) Vorbereitungs- und Charakterisierungstests und 2) die Inbetriebnahme eines vollautomatischen Messaufbaus.

1. Erkenntnisse aus den Vorbereitungstests

Zu Beginn des Projektes wurde ein bereits vorhandener Messaufbau im Detektorlabor der GSI verwendet, um alle relevanten Parameter und Komponenten für Alterungstests

zu identifizieren. Auf dieser Grundlage wurden die Eigenschaften und Charakteristika ausgewählt, die bei Bau und Betrieb eines neuen Hochpräzisionsaufbaus erfüllt werden müssen. Der vorhandene Aufbau bestand aus zwei identischen Vieldrahtproportionalkammern (MWPCs), einem Röntgengenerator mit Kupferanode, einer ^{55}Fe-Quelle und einer Ausgasbox. Für Alterungstests werden MWPCs bevorzugt als Testdetektoren verwendet, da sie leicht zu konzipieren und relativ kosteneffizient zu bauen sind. Als erstem Schritt wurde das Detektordesign mit Hilfe der Simulationssoftware "Magboltz" (Gas) und "Garfield" (elektrisches Feld) optimiert. Als Betriebsgas wurde eine Mischung aus 80% Argon (Ar) und 20% Kohlendioxid (CO_2) ausgewählt, da dieses Gasgemisch unter Bestrahlung nicht polymerisiert, so wie es Kohlenwasserstoffgase tun. Für unsere Ziele ist es von größter Bedeutung stabile Verstärkungsmessungen zu gewährleisten, d.h. die systematischen Schwankungen des normierten Verstärkungsfaktors (d.h. druck- und temperaturkorrigiert) so niedrig wie möglich zu halten. Daher wurden für die Verstärkungsmessung mehrere Verbesserungen des Aufbaus vorgenommen. Die ursprünglich verwendeten Detektoren hatten eine Drahtebene als Anode, zwei einseitig mit Aluminium beschichtete Kaptonfolien, die gleichzeitig als Kathoden und Gasabdichtungsfenster dienten. Bei dieser Konstruktion verursachte der Umgebungsdruck eine Fensterkrümmung, die eine Veränderung des elektrischen Feldes in der Kammer bewirkte. Dieser Mangel wurde mit separaten Kaptonfenstern behoben, die die Gasdichtungsfolie (äußere Folie) von der elektrostatischen Geometrie (Innenfolie) trennen. Weiterhin wurden, wenn der Detektor Röntgenstrahlung über die Dauer von etwa einer Woche ausgesetzt war, Anzeichen von Abtragung der Aluminiumschicht der Kathodenfolie beobachtet. Aus diesem Grund wurde die Kathodenfolie durch Drahtebenen ersetzt. Für eine bessere Abschirmung und Gastemperaturmessung wurde das ursprüngliche Glasfasergehäuse des Detektors durch ein Aluminiumgehäuse ersetzt. Temperaturschwankungen im Labor beeinflussen die Massendurchflussregler (MFC) der Gasmischsation und verursachen Variationen in der Gaszusammensetzung. Aufgrund dessen wurde eine Gasflasche mit der Fertigmischung Ar / CO_2 (80/20) anstelle der Mis-

chstation benutzt. Im Allgemeinen konnte festgestellt werden, dass die Reinheit aller gasführenden Komponenten von ausschlaggebender Bedeutung für die Aussagekraft des verursachten Alterungsprozesses ist.

2. Montage und Inbetriebnahme der Messanordnung

Der neue Testaufbau wurde im Detektorlabor der GSI konstruiert und aufgebaut. Dieser besteht aus einem Röntgengenerator, einer ^{55}Fe-Quelle sowie aus drei identischen MWPCs, die auf einem beweglichen Schlitten montiert sind. Auf einem zweiten Schlitten befindet sich ein Kollimator, mit welchem der Bestrahlungsfleck auf drei unterschiedliche Durchmesser eingestellt werden kann. Die Anordnung wurde zusätzlich mit einem Datenerfassungs- und Steuerungssystem ausgestattet, welches vollautomatische Messungen und Langzeittests ermöglicht. Außerdem wurde der Aufbau mit separaten, getrennt gasflusskontrollierten Gasleitungen für jede MWPC ausgestattet. Für zwei Detektoren wurde das Gasgemisch durch jeweils eine Ausgasbox geleitet. Die präzise Normierung des Gasverstärkungsfaktors wurde durch die Verbesserung der Genauigkeit der Gastemperaturmessung ermöglicht. über einen Zeitraum von acht Monaten wurden Reinigungsverfahren entwickelt, um alle Verunreinigungen in der Anlage zu beseitigen. Danach konnte der Messaufbau sehr stabil betrieben werden. Der Spitze-Tal Wert der Variation des normierten Verstärkungsfaktor erreichte damit den sehr niedrigen Wert von 0,3%. Damit zeigte der Aufbau die erforderliche hohe Stabilität für präzise Alterungsstudien.

3. Alterungstests

Während der Entwicklung des Testaufbaus wurden mehrere Alterungstests durchgeführt. Das Ziel dieser Tests war die Verbesserung des Verfahrens zur Alterungsuntersuchung, um eine erhöhte Genauigkeit zu erreichen. Dazu gehörte z.B. die präzise Messung der Umgebungsbedingungen, wie Temperatur und Druck, die Einstellung der

optimalen Alterungsrate, der richtigen Gasflussrate, die Minimierung der Verunreinigungen in der Anlage und die Bestimmung der geeigneten Aushärtezeit für die Alterungsproben. Die Resultate können wie folgt zusammengefasst werden:

1. RTV-3145 beschleunigt die Alterung der MWPCs und muss deshalb im Gasvolumen und der sonstigen Gasversorgungsinfrastruktur vermieden werden.

2. Der Unterschied der Aushärtezeit von Proben (z.B. Klebstoffe) und die Gasdurchflussrate beeinflussen die Alterungsrate in der Messanordnung. Diese Faktoren müssen berücksichtigt werden, um vergleichbare Ergebnisse zu erhalten.

3. Alterungstests, die sowohl mit einer ^{55}Fe-Quelle als auch mit einem Röntgengenerator mit verschiedenen Intensitäten durchgeführt wurden, zeigten ein deutliche Abhängigkeit der Alterungsrate von der Stärke der Strahlungsquelle. Der Einfluss der Strahlungsquelle und deren Intensität auf die Alterungsrate sollte deshalb in Zukunft quantitativ untersucht werden.

Außerdem wurde der Alterungseinfluss eines gebräuchlichen Aluminiumklebebandes (Gerband 705) getestet. Es zeigte eine deutliche Wirkung im Hinblick auf die Alterung in einer MWPC, wenn sie einer Röntgenstrahlung mit der Teilchenratedichte 22 kHz/cm ausgesetzt ist. Das Aluminiumklebeband verursacht einen Verlust im Verstärkungsfaktor von 0,3%/mC/cm. Der Alterungseffekt durch das Glasfasermaterial "Durostone" wurde in einer Argon-Isobutan-Gasmischung (84%, 16%) studiert. Die Kammer verlor etwa 6% von ihrem Anfangsverstärkungsfaktor. Dies entspricht einer Alterungsrate von etwa 0,18%/mC/cm. Ein solcher Verlust wurde in einem Ar-CO_2-Gemisch nicht beobachtet. Dies ist der Polymerablagerung auf den Elektroden zuzuschreiben, die durch die Polymerisierung der organische Radikale verursacht wird. Alterungstests mit Glasfasermaterial (Vetronit G11 von VonRoll) und Sägeflüssigkeit (Micro 3000 von Microjet GmbH) in einem Ar-CO_2-Gemisch wurden ebenfalls durchgeführt. Es konnte hier keine Alterung nachgewiesen werden.

4. Ausblick für künftige Arbeiten

Nachdem die Anlage zufriedenstellend in Betrieb genommen wurde, sollten in der Zukunft eine Reihe von Untersuchungen angegangen werden. Der Einfluss verschiedener Faktoren auf die Alterungsrate, wie Teilchenart und -dichte, Bestrahlungsfläche, Gasflussrate, Drahtqualität, Gasverstärkung und Temperatur der Proben sollte systematisch bestimmt werden. Die Erweiterung der Messanordnung mit zusätzlichen Kammern und Gasleitungen könnte vorteilhaft sein, um mehr als zwei Proben gleichzeitig zu untersuchen.

List of Figures

List of Tables

Bibliography

[1] K Fukushima and T Hatsuda. The phase diagram of dense QCD. *Reports on Progress in Physics*, 74(1):014001, 2011.

[2] M Titov. Gaseous detectors. *Handbook of Particle Detection and Imaging, Springer*, 1:239–264, 2012.

[3] C Niebuhr. Aging effects in gas detectors. *NIM*, 566(1):118–122, 2006.

[4] M Binkley, RL Wagner, A Mukherjee, D Ambrose, G Bauer, DM Khazins, and M Atac. Aging in large CDF tracking chambers. *NIM*, 515(1-2):53 – 59, 2003.

[5] P Senger. The compressed baryonic matter experiment at FAIR. *Nuclear Physics A*, 862:139–145, 2011.

[6] Y Aoki, G Endrődi, Z Fodor, SD Katz, and KK Szabo. The order of the quantum chromodynamics transition predicted by the standard model of particle physics. *Nature*, 443(7112):675–678, 2006.

[7] Z Fodor and S Katz. Critical point of QCD at finite T and μ, lattice results for physical quark masses. *JHEP*, 2004(04):050, 2004.

[8] A Andronic, D Blaschke, P Braun-Munzinger, J Cleymans, K Fukushima, LD McLerran, H Oeschler, RD Pisarski, K Redlich, C Sasaki, et al. Hadron production in ultra-relativistic nuclear collisions: Quarkyonic matter and a triple point in the phase diagram of QCD. *Nuclear Physics A*, 837(1):65–86, 2010.

[9] JM Lattimer and M Prakash. Neutron star structure and the equation of state. *The Astrophysical Journal*, 550(1):426, 2001.

[10] S Chattopadhyay et al. Physics at high baryon density at FAIR. *Journal of Physics G: Nuclear and Particle Physics*, 35(10):104027, 2008.

[11] B Friman, C Höhne, J Knoll, S Leupold, J Randrup, and R Rapp. The CBM physics book: Compressed baryonic matter in laboratory experiments. *Springer*, 814, 2011.

[12] S Lebedev, C Hoehne, G Ososkov, et al. Ring recognition and electron identification in the RICH detector of the CBM experiment at FAIR. *Journal of Physics: Conference Series*, 219:032015, 2010.

[13] E Atkin, E Malankin, and V Shumikhin. CBM progress report 2013. pages 5–10, 2013.

[14] C A Dritsa. Design of the micro vertex detector of the CBM experiment: Development of a detector response model and feasibility studies of open charm measurement. *PhD thesis, Université de Strasbourg*, 2011.

[15] M Deveaux, S Amar-Youcef, I Fröhlich, M Koziel, Q Li, B Milanovic, C Müntz, B Neumann, T Tischler, C Schrader, et al. A first generation prototype for the CBM micro vertex detector. *NIM*, 718:305–306, 2013.

[16] J Heuser, W MŸller, V Pugatch, P Senger, C J Schmidt, C Sturm, and U Frankenfeld. Technical design report for the CBM, Silicon Tracking System (STS). *GSI-2013-05499, GSI Report 2013-4*, 2013.

[17] I Sorokin. The silicon tracking system of the CBM experiment at FAIR: overview and development progress. *NIM*, 718:366–368, 2013.

[18] C Höhne. Technical design report for the CBM Ring Imaging CHerenkov detector (RICH). *GSI-2014-00528*, 2013.

[19] S Biswas, DJ Schmidt, A Abuhoza, U Frankenfeld, C Garabatos, J Hehner, V Kleipa, T Morhardt, CJ Schmidt, HR Schmidt, et al. Development of a GEM based detector for the CBM Muon CHamber (MuCH). *Journal of Instrumentation*, 8(12):C12002, 2013.

[20] S Chattopadhyay. Technical design report for the CBM muon chamber (MuCH). *Technical report*, 2013.

[21] D Kresan and C Höhne. Event-by-event fluctuations of the k/π yield ratio in the CBM experiment. *CBM Progress Report*, 2008, 2009.

[22] I Deppner, N Herrmann, D Gonzalez-Diaz, V Ammosov, J Cheng, M Ciobanu, V Gapienko, KD Hildenbrand, A Kiseleva, M Kiš, et al. The CBM time-of-flight wall. *NIM*, 661:S121–S124, 2012.

[23] S Tavernier. Experimental techniques in nuclear and particle physics. *Springer*, 2010.

[24] V Palladino and B Sadoulet. Application of classical theory of electrons in gases to drift proportional chambers. *NIM*, 128(2):323–335, 1975.

[25] J Va'vra. Physics and chemistry of aging–early developments. *NIM*, 515(1):1–14, 2003.

[26] J Kadyk. Wire chamber aging. *NIM*, 300(3):436–479, 1991.

[27] HK Yasuda. Plasma polymerization. *Academic press*, 1985.

[28] M Capeans. Aging and materials: lessons for detectors and gas systems. *NIM*, 515(1):73–88, 2003.

[29] VE Blinov, IN Popkov, and AN Yushkov. Aging measurements in wire chambers. *NIM*, 515(1):95–107, 2003.

[30] A Schreiner, G Bohm, H Kolanoski, and M Walter. Humidity dependence of anode corrosion in HERA-B outer tracker chambers operated with $Ar/CF_4/CO_2$. *NIM*, 515(1):146–151, 2003.

[31] M Titov. Radiation damage and long-term aging in gas detectors. In *Proceedings of the 42nd Workshop of the INFN ELOISATRON Project Innovative Detector for Supercolliders*, pages 199–226, 2004.

[32] R Openshaw, R Henderson, W Faszer, D Murphy, M Salomon, and G Sheffer. Tests of wire chamber ageing with CF_4/isobutane (80:20), argon/ethane (50:50), and argon/ethane/CF_4 (48:48:4). *Nuclear Science, IEEE Transactions on*, 36(1):567–571, 1989.

[33] T Ferguson, G Gavrilov, A Korytov, A Krivchitch, E Kuznetsova, E Lobachev, G Mitselmakher, and L Schipunov. Aging studies of CMS muon chamber prototypes. *NIM*, 488(1):240–257, 2002.

[34] T Akesson, E Barberio, V Bondarenko, M Capeans, A Catinaccio, P Cwetanski, H Danielsson, F Dittus, B Dolgoshein, N Dressnandt, et al. Aging studies for the ATLAS transition radiation tracker (TRT). *NIM*, 515(1):166–179, 2003.

[35] LG Christophorou, PG Datskos, and JG Carter. Gases of possible interest to SSC muon detectors. *NIM*, 309(1):160–168, 1991.

[36] J Fischer, A Hrisoho, V Radeka, and P Rehak. Proportional chambers for very high counting rates based on gas mixtures of CF_4 with hydrocarbons. *NIM*, 238(2):249–264, 1985.

[37] WS Anderson, JC Armitage, E Dunn, JG Heinrich, C Lu, KT McDonald, J Weckel, and Y Zhu. Electron attachment, effective ionization coefficient, and electron drift velocity for CF_4 gas mixtures. *NIM*, 323(1):273–279, 1992.

[38] Lourdu M Yeddanapalli. The decomposition of methane in glow discharge at liquid-air temperature. *The Journal of Chemical Physics*, 10(5):249–260, 1942.

[39] M Capeans. Aging of gaseous detectors: assembly materials and procedures. *ICFA Instrum. Bull*, 24:85, 2002.

[40] A Andronic. The TRD of the CBM experiment. *NIM*, 563(2):349–354, 2006.

[41] F Sauli. Principles of operation of multiwire proportional and drift chambers. *CERN-77-09*, 1977.

[42] E Daubie, F Grard, I Boulogne, and F Defontaines. Aging tests of MSGC detectors. *NIM*, 515:196–201, 2003.

[43] MC Altunbas, K Dehmelt, S Kappler, B Ketzer, L Ropelewski, F Sauli, and F Simon. Aging measurements with the gas electron multiplier (GEM). *NIM*, 515(1):249–254, 2003.

[44] B Stephen. Magboltz: Transport of electrons in gas mixtures. *CERN program library*, 2009.

[45] R Veenhof. Garfield, a drift-chamber simulation program. http://garfield.web.cern.ch/garfield/.

[46] W Blum, W Riegler, and L Rolandi. Particle detection with drift chambers. *Springer*, 2008.

[47] K Katagiri, T Furukawa, E Takeshita, and K Noda. Numerical analysis of the space charge effect in a mwpc. *J. Plasma Fusion Res. SERIES*, 9:614–619, 2010.

[48] R Openshaw and R Henderson. Effects of materials on ageing rates in wire chambers operated with DME. *NIM*, 515(1):89–94, 2003.